Addis Ababa University
College of Natural and Computational Sciences
Department of Chemistry

Disposable Screen Printed Carbon Electrode Based Electrochemical Sensors for the Determination of Brucine, Chloramphenicol, Niclosamide and Nicotine.

By

Tesfu Hailu Halefom

Supervisor: Dr. Merid Tessema

September 2021

Abstract

In this study, various types of simple, scalable and low cost chemically modified electrodes were successfully developed for the sensitive and selective determination of niclosamide (NA), chloramphenicol (CAP), Nicotine (NIC) and Brucine (BRU). First, a simple and fast efficient activation of pristine bare screen printed carbon electrode (SPCE) was performed by linear sweep voltammetry using KOH solution and was used for the determination of NA and CAP. The activated-SPCE was characterized by cyclic voltammetry (CV), electrochemical impedance spectroscopy (EIS), electroactive surface area (ESA), Fourier transform infrared spectrometry (FTIR) and scanning electron microscope (SEM). The cyclic and square wave voltammetric (SWV) studies of NA in 30% DMF Britton-Robinson buffer (BRB) solution pH of 7.5 showed an electrocatalytic effects towards NA, which resulted in a higher current response and a negative shift in the peak potential at the activated-SPCE compared to the bare SPCE. Under the optimized conditions, a linear calibration curve was obtained using SWV in the range of 0.06 to 50 µM with a limit of detection and a limit of quantification of 0.0051 µM and 0.017 µM, respectively. Next, the same electrode material was used for the determination of CAP using SWV. The CV and SWV studies of CAP in 0.10 M phosphate buffer solution (PBS) pH 6.5 showed an electrocatalytic effect towards CAP, which resulted in a higher current response and a negative shift in the peak potential. The activated-electrode exhibited linear SWV responses towards the determination of CAP in the range of 0.05-100 µM with a limit of detection and a limit of quantification 0.02 and 0.067 µM, respectively. To the activated-SPCE, *para*-aminobenzene sulfonic acid (*p*-ABSA) was grafted electrochemically and SEM, EIS, CV, FTIR, and ultraviolet–visible spectroscopy (UV-Vis) were used for the characterization of the electrografted SPCE. The CV and EIS studies of the modified electrode showed that it has lower conductivity however; the grafted electrode has better electrocatalytic performance towards nicotine determination in BRB solution pH 8.0. The *p*-ABSA grafted SPCE exhibited excellent SWV responses towards NIC determination in the linear range of 0.5-300 µM with a limit of detection and a limit of quantification of 0.35 µM and 1.14 µM, respectively. Lastly, a new SPCE was prepared by electropolymerization of 3,4-Ethylenedioxythiophene (EDOT) on the surface of the *p*-ABSA grafted SPCE. The electrode was characterized by SEM, CV, ESA, EIS, FTIR and UV-Vis, and the formation of a highly conductive surface was confirmed by CV, ESA and EIS

studies. The polymer film modified SPCE was used for the determination of brucine (BRU). A significant enhancement in the peak current response for BRU was observed at the modified electrode compared to the unmodified electrode. The modified electrode demonstrated excellent SWV responses for the determination of BRU in the linear range of 0.03-5.0 μM with a limit of detection and a limit of quantification 0.012 μM and 0.042 μM, respectively. Generally, all the developed sensors were validated successfully for real sample analysis in pharmaceutical formulation and human urine samples with good recovery results. The proposed sensors also displayed good repeatability, reproducibility, long-term stability and selectivity towards potential interferents and are promising materials for the electrochemical sensing of these compounds in real samples.

Acknowledgments

First and foremost I would like to thank and praise the almighty God for giving me the strength and endurance throughout my PhD study to carry out my work.

I would like to express my deepest and sincere gratitude to my supervisor, Dr. Merid Tessema for his unreserved and continuous encouragement, excellent guidance, advice, invaluable suggestions and discussions throughout this endeavor, which nurtured a lot of confidence in me. His support in providing and facilitating the necessary materials for my research work were tremendous. I also thank him immensely for the critical comments during the courses, seminars, manuscript preparations and thesis write-up. I was privileged to enjoy his fatherly consultation, warm approach and treatment throughout my study.

My appreciation goes to Prof. Yaw-Kuen Li for hosting and supervising me in his lab as an exchange student and providing all the chemicals, apparatus and instrumentation required in addition to the financial support for the stay. I was lucky enough to spend some time at his Lab, Department of Chemistry, and National Chiao Tung University, Taiwan. I am very grateful for his cooperation and invaluable guidance during my stay. I am also thankful to YKL lab staff members and all PhD and MSc students.

I am highly indebted to Prof. B. S. Chandravanshi for his special treatment, continuous motivation and encouragement starting from my enrollment. I am also thankful for his support and constructive ideas.

My appreciation goes to Dr. Negussie Negash for providing me with lab materials and constructive criticism during seminar presentations and progress report. I would like to thank him for his unreserved constant encouragement and invaluable advice throughout my study. Moreover, I am very grateful for his critical comments and positive criticism. I owe my sincere gratitude to Dr. Weldegebriel Yohannes for his friendly approach, moral support and motivation and positive comments on my research work. I am thankful to all the academic and technical staff members of the Chemistry Department of Addis Ababa University.

My sincere gratitude goes to my previous lab mate and colleague Dr. Birhanu Mekassa whose genuine support and guidance at the beginning of the lab work was very critical and immense.

My appreciation also goes to Denekew Alemayehu for his continuous support and friendship. I express my sincere gratitude to Hailegebriel Mengesah and Henok Mekonnen for their friendship and invaluable discussions. I would like to show my gratitude to PhD students of the analytical chemistry stream whose discussions and friendships were socially invaluable in my study. All PhD students in the Department of Chemistry are kindly acknowledged for sharing resources and also for the discussions, affection and companionship we had together during this long journey. All my friends who have contributed in one way or another in my journey are kindheartedly acknowledged.

I am greatly indebted to my parents and families for boosting the whole spectrum of my life. Their guidance, support and unconditional love are a lot in my life career.

I am thankful to the Department of Chemistry, Addis Ababa University, for giving me the opportunity to pursue my PhD study.

Last but not least, I would like to acknowledge Addis Ababa Science and Technology University, Ethiopia, for sponsoring me and providing additional support for my study.

Table of Contents

List of Schemes

List of Figures

List of Tables

List of Abbreviations

ABS	Acetate Buffer Solution
AC	Alternating Current
BRB	Britton-Robinson Buffer
BRU	Brucine
ca.	Circa
CZE	Capillary Zone Electrophoresis
CAP	Chloramphenicol
CPs	Conducting Polymers
CSEM	Conventional Scanning Electron Microscope
CV	Cyclic Voltammetry
DMF	Dimethylformamide
DPV	Differential Pulse Voltammetry
DPASV	Differential-Pulse Anodic Stripping Voltammetry
DPSV	Differential Pulse Stripping Voltammetry
ESEM	Environmental Scanning Electron Microscope
E_g	Bandgap
EDOT	3,4-Ethylenedioxythiophene
EIS	Electrochemical Impedance Spectroscopy
FTIR	Fourier-Transform Infrared
GCE	Glassy Carbon Electrode
GC	Gas Chromatography
GC-MS	Gas Chromatography-Mass Spectrometry
HOMO	Highest Occupied Molecular Orbital
HPLC	High Performance Liquid Chromatography
HPTLC	High-performance thin-layer chromatography
IUPAC	International Union of Pure and Applied Chemistry
LSV	Linear Sweep Voltammetry
LoQ	Limit of Quantification
LoD	Limit of Detection

LSV	Linear Sweep Voltammetry
LC-MS/MS	Liquid Chromatography with tandem mass spectrometry
LSEM	Low-Vacuum Scanning Electron Microscope
LOMO	Lowest Unoccupied Molecular Orbital
NA	Niclosamide
NIC	Nicotine
p-ABSA	*para*-Aminobenzene Sulfonic Acid
PBS	Phosphate Buffer Solution
PEDOT	Poly(3,4-ethylenedioxythiophene)
RSD	Relative Standard Deviation
SDS	Sodium Dodecyl Sulfate
SEM	Scanning Electron Microscopy
SPEs	Screen Printed Electrodes
SPCE	Screen Printed Carbon Electrode
SWASV	Square-Wave Anodic Stripping Voltammetry
SWV	Square Wave Voltammetry
TLC	Thin Layer Chromatography
VPP	Vapor Phase Polymerization

1. Introduction

There are many problems which challenge the environmental and food safety organizations which are established with an aim of reducing the risks associated with numerous complex toxic chemicals, which are highly increasing and emerging as new variants. In the United States it is estimated that on average about 700 new chemicals are introduced to the market per annum [1]. Developing a new and sound method for environmental protection and for controlling the leachate of toxic chemical into the environment is the major concern of analytical research. These new methods are aimed at making the analysis outside the laboratory in the production areas. Because such methods solve the problems associated with sample collection, sample treatment, and sample transport to a central laboratory. Additionally, the on-site analysis also gives analytical data with minimum errors, the cost associated with the analysis is low and is fast results are obtained compared to the laboratory-based analyses [2]. Electroanalysis includes the wider area of electrochemistry, it involves in measuring electrical signal associated with transfer of charge in the solution. Electroanalysis can be classified as a special area of electrochemistry which focuses on the quantification of the analyte in a sample and also on qualitative characterization. Like the other instrumental method, electroanalysis also has an advantage and limitation. However, electroanalysis is compatible with the instrumental methods like detection in flow injection analysis (FIA), high-performance liquid chromatography (HPLC), and capillary electrophoresis (CE) [3]. For this reason, an electrochemical method that uses disposable electrodes which can perform an off-site analysis was selected.

1.2. Chemical Sensors

Devices that detect a given analyte and convert all the chemical information like concentration, pressure, activity of particles to an electrical signal are called chemical sensors. It is possible to obtain both qualitative and quantitative information beside the resolved structural information the chemical component investigated [3]. The chemical information is received by the receptor called the recognition system and is converted into chemical information by the transducer. The sensor receptor part works by using three different principles which are based on three different principles of stimuli. Physical stimuli is the first one in which there is no chemical reaction; the second one is based on chemical stimuli which the chemical reaction of the given analyte is the

basis for the analytical signal; and the third one is biochemical, in which the source of the analytical basis is biochemical process [4].

The International Union of Pure and Applied Chemistry (IUPAC) stated definition of chemical sensor is stated as "a device that transforms chemical information, originating from a chemical reaction of the analyte or from a physical property of the investigated system, ranging from the concentration of a specific sample component to total composition analysis, into an analytically useful signal [5]". Operation of chemical sensors rely on the generation of analytical signal generated that has a on with the concentration of the analyte to be determined. The signal recognition, reception and transduction efficiency in chemical sensors is the basis of chemical sensors [6, 7].

According to IUPAC, a chemical sensor is classified by their signal transduction in to the following category: Optical sensors based on the optical property of the analyte example absorbance, reflectance, luminescence, fluorescence, refractive index, optothermal effect and light scattering; Electrochemical sensors based on the electrochemical activity of the analyte example voltammetric, potentiometric devices, chemically sensitized field effect transistor (CHEMFET) and potentiometric solid electrolyte gas sensors; Electrical sensors based on measurement where no electrochemical process takes place example including those with metal oxide semiconductor sensors, organic semiconductors as sensors, electrolytic conductivity sensors and electric permittivity sensors; Mass sensitive sensors are based on the measurement on the mass change of the alnalyte example piezoelectric devices and surface acoustic waves; Magnetic sensors based on the paramagnetic properties of gas analyte example oxygen monitor; Thermometric sensors based on the measurement of the heat effect of chemical reaction or adsorption example thermistor; and other sensors, mainly based on emission or absorption of radiation [5].

1.3. Electrochemical Sensors

Electrochemical sensors are the largest and oldest group of chemical sensors. Some members of this group have reached commercial maturity while many are still at various stages of development. These sensors are notable because of several factors: the use of the electron for signal acquisition, which is considered a clean model for analytical applications, with no

generation of waste; miniaturization in portable; fast analysis; and low production cost. In addition, the development of electrochemical sensors aids in the improvement of other techniques, such as chromatography detectors. Associated with nanotechnology, electrochemical sensors are becoming increasingly precise, selective, specific, and highly sensitive [8].

Electrochemical are based on the transfer of charge from an electrode to another phase, which can be a liquid or gas sample. During this charge transfer process, chemical changes take place at the electrodes and charge is conducted through the electrolyte solution. Both the electrode reactions and/or the charge transport serve as a basis for the sensing process. Electrochemical methods have gained attention from the scientific community for their distinct property of high sensitivity and selectivity, a wide linear range, portable size, rapid response time, simple operation, minimal space and power requirements, and low-cost instrumentation. The rapid pace of development in the electronic miniaturization and their compatibility with advanced microfabrication technology in conjunction with advanced material in the field have culminated in the emergence of on-site monitoring of analytes [7].

Electrochemical sensors are based on transforming an electrical signal (current or potential) that is created due to the effect of the electrochemical interaction that takes place between the analyte and the electrode. The result due to the interaction may be stimulated electrically or it may result by a spontaneous interaction at zero-current conditions. Electrochemical sensors can be classified as voltammetric (including amperometric), potentiometric sensors, and impedimetric sensors [8].

Voltammetric sensors, including amperometric, are based on measuring the current produced by the electrochemical interaction of the analyte by direct or alternating current mode at a scanned or fixed potential. Amperometric, which is a voltammetric sensor, measures the current due to the oxidation or reduction of an electroactive species that is consumed or produced at the electrode surface at a constant applied potential while voltammetry is based on the measurement of current using a varying voltage. Cyclic voltammetry (CV), square wave and stripping voltammetry are some of the more common techniques [9].

Potentiometric sensors measure the potential across an interface, usually a membrane at zero-current. The signal is measured as the potential difference between the indicator electrode (ion-selective electrode, redox electrode, metal-meta1 oxide electrode) and the reference electrode.

The measured potential is then used to determine the analytical concentration of the analyte [10, 11].

In impedimetric sensors a sinusoidal voltage is applied and the resulting current is measured. The impedance is then calculated as the ratio of voltage to current in the frequency domain. The impedance transduction can be achieved by two ways: (1) faradaic mode using control of heterogeneous electron-transfer resistance in the presence of an electro active species or (2) non-faradaic mode using the capacitance of the equivalent circuit as a monitored parameter [9, 12].

1.4. Voltammetric Sensors

A voltammetric sensor is a class of electroanalytical techniques that depends on measuring the current by relating it to the voltage. This measurement is based on voltage-current-time relationship arising from the three electrodes, i.e., working electrode, reference electrode and auxiliary or counter electrode, system. This relationship is based on the measurement of current that is linearly dependent upon the concentration of the electroactive species (analyte) involved in a chemical or biological recognition process (at a scanned or fixed potential) [9, 12]. Specifically, voltammetry uses a varying voltage, and it includes the widely used linear, cyclic, square wave, differential pulse and stripping voltammetric techniques. Amperometric sensor is also a sub-class if voltammetry uses a potential that is held at a constant voltage [9].

Stripping analysis is one of the most sensitive voltammetric methods. These techniques enjoy the advantages of being less sensitive to matrix effects than other analytical techniques. It is mostly used for trace analysis of heavy metals for environmental analysis. Both cathodic and anodic stripping voltammetric techniques have been used for a highly sensitive determination of trace analytes [9]. The main advantages of using voltammetric methods over spectroscopic or chromatographic methods are their high sensitivity, precision, accuracy and cost effectiveness. In the past, voltammetric techniques were difficult to apply and were not nearly as useful as they are today. At present, voltammetric techniques are largely available due to the advent of computers and their key role in the control and measurement of the potentials and currents of potentiostats. Classical polargraphic techniques have advanced largely due to better instrumentation and improved electrode materials [13].

1.5. Electrode Substrate

In electrochemical sensor the transduction element is the working electrode and these electrodes should be chemically inert and conductive. Therefore material like platinum, gold, carbon (e.g. graphite) and silicon compounds are the widely used electrode depending on the analyte investigated [14].

Synergies between nanotechnology and bioelectronics present new possibilities for miniaturizing of electrode material and obtaining smaller devices at the nanoscale. It is become simpler to measure electrical responses using various electrode materials. The application of inorganic silicon nanowires and semiconductor nanowires shows electrical properties with lower the detection limit [15]. Since different functional groups on electrode substrate possess various physical and chemical properties, therefore choosing appropriate electrode substrate is crucial for successful electrochemical analysis. Researchers usually choose and predict the utility of a suitable substrate for specific application from the obtained experimental results [14]. For a material to function as an electrode, it must possess several characteristics: high electrical conductivity, hard and durable, homogeneous microstructure throughout the bulk, reproducible properties, good chemical inertness, low background current, stability over a wide potential range, rapid electron-transfer kinetics for a wide range of redox systems, easily-fabricated and inexpensive in cost [16].

1.6. Screen Printed Carbon Electrodes

Analytical research activity is devoted to the development of new analytical tools that are required for economic and real-time monitoring. Such progress enables the field of analytical chemistry to bring the analysis close to the production operations and real time field detection. Such advances offer improved analytical methods with reduced environmental impact. The limitation of sample collection and transport to a central laboratory could be solved by the development of portable devices with reduced sample volume [17].

Development of miniaturized electrochemical sensors for extracellular fluid measurement, clinical diagnosis and micro total analysis is among the advancement of science for real-time testing. In fact, electrochemical detection methods are fast, cheap and easy to perform, enabling the accurate quantification of the levels of several compounds in a wide range of samples [1].

However, screen printed electrodes (SPEs) based sensors have emerged as a major branch of miniaturization in electrochemical sensor. The main driving force for using screen printed electrochemical sensor is related to its affordable price, mass production, reproducibility and reliability beside the need for miniaturization [18, 19]. These SPEs can be drawn in various shapes, various materials can be incorporated and modification using various modifiers is possible [20].

The two main advantages of SPEs over the conventional ones are the versatility of the printing inks' composition that can be altered by adding a variety of substances to be incorporated with the carbon ink and the possible immobilization of substances by depositing on the electrodes surfaces. Additionally surface fouling can be eliminated by using a new electrode from the same batch [21, 22]. Screen-printed carbon electrodes (SPCEs) are one form of SPEs and have wide application in many areas of electrochemistry, mostly in sensing, energy conversion and storage, and microelectronics. They are also applied in flexible electronics, which is a technology for printing electronic devices directly onto flexible plastic substrates. Almost all forms of carbons have been deposited by screen printing. However, graphite, carbon black and activated carbon are the most widely used in screen-printed carbon electrode [23].

The production of SPEs involves a series of basic stages, specifically: i) selection of the screen or mesh, which will define the geometry and size of the screen printed electrode (SPE); ii) selection and preparation of the inks; iii) selection of the substrate material; iv) printing and v) drying and curing steps. The screen-printing technology involves the printing of a thixotropic fluid through the screen, which defines the shape and size of the desired electrode. A woven mesh supports an ink-blocking stencil, and a roller or squeegee moves across the screen stencil to promote the passage of the ink through the threads of the woven mesh. Usually, a series of woven meshes is prepared to print the different parts of the electrode. The inks applied in the production of the SPEs show high viscosity (from 3–10 Pa.s) and, between the print of two different ink layers on the substrate, the inks need to be dried and solidified through a thermal treatment. Finally, a protective ink coating is used to insulate the conductive track from the electrodes [18].

The advances in screen-printed technology resulted in mass production with various designs in SPEs. Generally, they are produced in the form of small strips, having dimensions in the range from 30 to 61 mm in length, up to 15 mm in width and up to 1 mm in height. Commercial companies that supply SPEs include; Pine Instrument Company (Grove City, Pennsylvania, USA), BI Technologies Corporation (Fullerton, California, USA), Dropsens, (Llanere (Asturias), Spain), Kanichi Research (Manchester, UK), BVT Technologies (Brno, Czech Republic), Gwent Electronic Materials (Pontypool, UK), Uniscan Instruments (Buxton, UK), Ecobioservices & Research (Firenze, Italy;), ALS Co. (Tokyo, Japan), Zensor R&D (Dali City, Taiwan). In addition, many research laboratories in the academic sphere possess screen-printing facilities for in-house production of SPEs [21, 22].

1.7. Electrode Modification

The performance of electrochemical sensor is highly influenced by the working-electrode material. The working electrode should provide high signal to-noise characteristics, as well as a reproducible response. A very wide range of materials have found application as working electrodes for electroanalysis and the popular ones are mercury, carbon, or noble metals (particularly platinum and gold) electrodes [7]. Most of compounds which are biologically and environmentally important do not show response within the potential window of the electrodes. The requirement of high potential and production of large back ground current during direct electrochemical detection results to small detection limits. Additionally the passivation or deactivation of the electrode surface due to the adsorption of reaction of products greatly affect the stability of electrode response [24].

The utilization of modified electrode for sensitive and selective application is the beauty of electrochemical techniques. The electrode itself can act as a reactant for the redox reaction, which cannot be expected in spectroscopic characterization methods. The term ‘chemically modified electrodes’ was introduced by Murray and co-workers to describe electrodes that had foreign molecules deliberately immobilized on their surfaces. The strong desire for obtaining a perfect electrode surface with required properties and quality together with the understanding of the process on the electrode surfaces have led to the development of chemically modified electrodes [25]. Electrode modification is a very popular technique used for improving both selectivity and sensitivity of electroanalytical detection. In general, the quality of electrode

materials are evaluated both on their ability to detect the target in complex media (selectivity), and to detect a very small amount of material (sensitivity), as reflected in a low limit of detection (LoD) [26]. Electrodes surfaces are modified in a quest to give an electrochemical function that are difficult to achieve using conventional electrodes. The improvements due to electrode modification include increased selectivity, sensitivity, chemical and electrochemical stability, as well as a larger usable potential window and improved resistance to fouling. Therefore, the need for improved electrode performance and logically designed interfaces is rapidly growing in many areas of science [18].

Commercially available conductive carbon ink consists of graphite, polymeric binders, additives, and solvent materials. The very presence of secondary components in the carbon ink reduces its conductivity and hinders the electrocatalytic activity of the electrode being used in electrochemical sensors. As the commercial ink formulation is generally unknown due to ownership concerns, and since the nature of screen-printed electrodes prevents any mechanical manipulation (polishing) for activation. In-situ electrochemical pretreatments of the fabricated SCPEs appear to be very promising for this task [27, 28]. Besides to the pretreatment of the fabricated electrodes there is numerous modification methods of this modification of the SPCEs with ionically conductive polymer and covalent attachment of tailored compounds are among the modification methods.

1.7.1. Electrode Pretreatment

The challenge of electrochemical measurements is controlling of the reproducibly of the electrode to achieve a low background current and a rapid rate of electron transfer for the target analyte. Electrodes exhibiting these properties are referred to as activated and it is accomplished by a process known as electrode pretreatment. This process involves conditioning the surface morphology, microstructure, and chemistry in a manner that promotes low background current and rapid reaction kinetics (both electron and proton transfer) with a redox analyte dissolved in solution or confined to the surface [29].

Electrochemical oxidation or reduction in various media has long been used to activate carbon electrodes. Polarization of a carbon electrode outside the electrochemical window yields significant current, which results from reactions of both the electrolyte and of the electrode itself.

Depending on the duration of anodization, the carbon surface can be disrupted significantly, to the point of forming a surface film of electrogenerated graphitic oxide. This film has an oxygen/carbon (O/C) ratio above 0.2, contains many anionic sites, and is permeable to solvent and small molecules [25]. It is also well known that electrochemical pretreatment introduces oxygen-containing functional groups on the electrode surface. The newly introduced functional groups exhibit like electron donor–acceptor, hydrogen bonding, electrostatic, dispersive or solvophobic interactions with various species [29].

The mechanism of edge plane active site formation during electrochemical pretreatment can be divided into two major steps. Firstly, graphene sheets get separated due to penetration of molecules and ions of solvents between the layers of the electrode structure then, due to intercalation of ions, microstructure strains start to increase to such an extent that fracture graphene sheet expose new edge planes [30]. In addition to the increase in surface roughness or functionalities electrode pretreatment is required for removing contaminants from organic ink in the Screen-printed carbon electrode (SPCE). There are various electrochemical techniques used to activate an electrode like anodizing the electrodes in phosphate buffer solution (PBS) [31], anodization in saturated Na_2CO_3 [32], in H_2O_2 [33], soaking using concentrated NaOH then anodizing it in dilute NaOH and polishing with fine emery paper followed by mechanical cleaning in an ultrasonic bath [34].

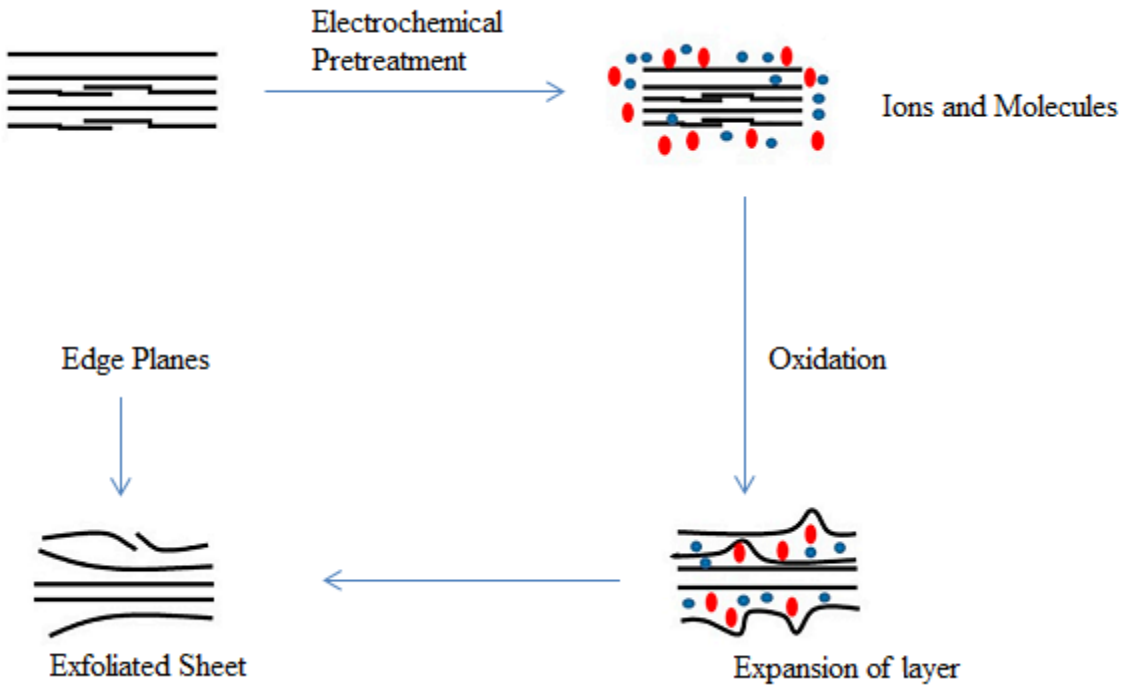

Scheme 1. Schematic representation for edge plane site formation during electrochemical treatment

1.7.2. Covalent Modification

Surface modifications with desired chemical functionalities at the molecular level are important processes to provide the surface with new, unique and special properties. Among the wide range of applications involved in surface functionalization, covalent modification of electrodes and their applications in electroanalysis holds a prominent place [27]. Covalent modification of the electrode surface that uses a specific functional group is also of particular interest in the preparation of chemically modified electrodes [8]. Covalent functionalization using the most common electrode materials has been widely explored [1]. Stronger attachment to the substrate surface can be accomplished by covalent linking of the desired component to surface groups present on, or formed on, the substrate. These covalent linking procedures frequently employ organosilanes and other linking agents. The substrate surface is usually activated, e.g., by an oxidative reaction, to form surface groups Scheme 2. The surface is then treated with the linking agent and the desired component [35].

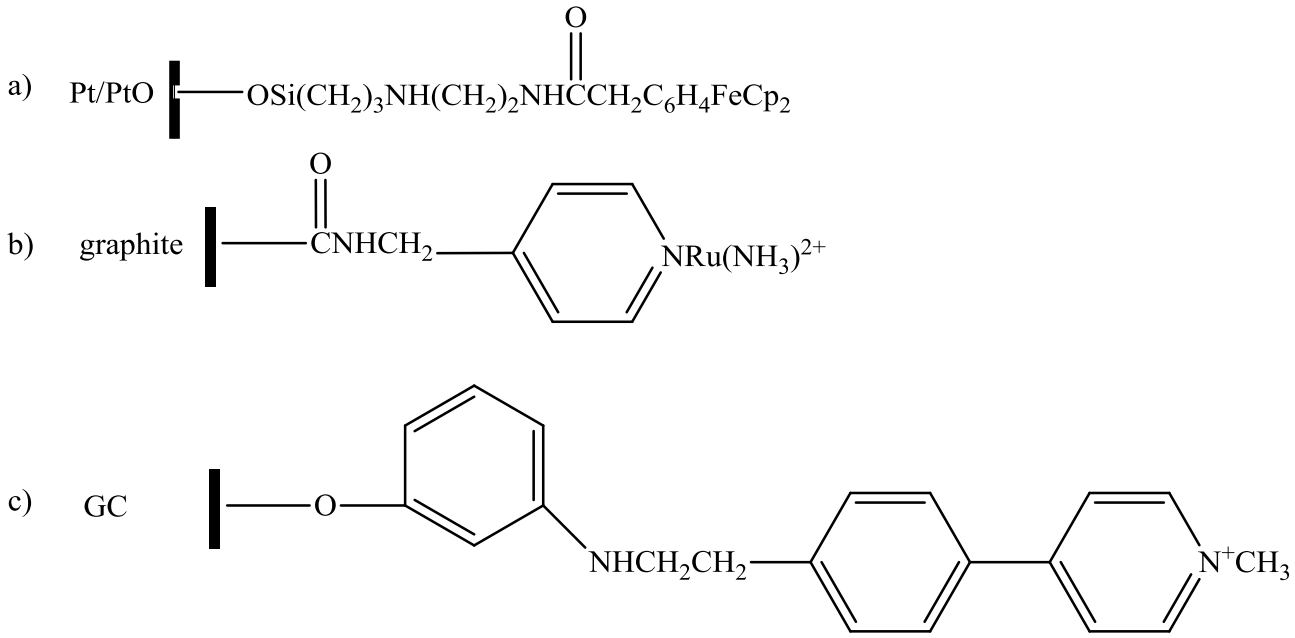

Scheme 2. Covalent attachment of (a) ferrocene containing group at Pt electrode (b) py-$Ru(NH_3)_5$ at graphite electrode (c) viologen at glassy carbon electrode

Grafting using aryl diazonium salts, pioneered by Pinson and co-workers in 1992, was the best method to introduce many types of functional groups onto a variety of surfaces (carbon, metals, silicon and indium tin oxide) with a reaction time scale of seconds to minutes [36, 37]. Aryl radicals generated from the reduction of diazonium salts have also been used to modify electrode surfaces. The reductive process of such salts results in the formation of aryl centered radicals covalently attached onto electrode surfaces after the spontaneous elimination of dinitrogen. The so-called grafting method has demonstrated to be an excellent strategy to be used for further immobilization of biomolecules because of the simple preparation and versatility. In fact, conductive and semiconductive surfaces can be modified with a wide range of functional groups in aqueous solution at room temperature and without sophisticated equipment [38].

Arenediazonium salts can be grafted by either chemical or electrochemical reduction method. But the electrochemical method is faster, and more controllable; thus homogeneous monolayer or two distinct over laid layers can be prepared. In the electrochemical method, the generation of phenyl radicals is localized at the electrode and the loss of diazonium salt by competing reactions in the bulk solution is minimal. This degree of control over the interfacial chemistry of

conducting polymers will greatly impact the ability to tailor conducting polymeric materials for specific tasks [39].

Electrografting of aryl diazonium salts is affected by many factors such as: i) the applied potential, ii) time, iii) concentration, iv) electronic nature of the salt, v) the type of electrode material used and vi) the type of solvent. Nonetheless, modification of surfaces by this method suffers from the high reactivity of aryl diazonium salts and so controlling the extent of reaction can be challenging [40]. To resolve this problem, since the past few years, the main approach developed was to avoid the formation of multilayers and obtain controlled organic films based on the use of sterically hindered aryldiazonium cations. In this way, the blocking of aryl-reactive positions by bulky substituents and the use of protected diazonium were reported to generate very thin films. By directly intervening on the electrografting mechanism using a radical scavenger it is also possible to control or prevent, the polymerization of the electrogenerated aryl radical on the electrode surface. The introduction of an appropriate amount of radical scavenger is expected to prevent the attack of grafted species by electrogenerated aryl radicals, without interfering with the direct grafting process [39].

1.7.3. Conducting Polymers

Polymers are macromolecules composed of many repeated sub units called monomers. The word 'Polymer' comes from the Greek word Poly meaning many and Meros meaning parts and, polymer means many parts [41]. Originally polymers have been thought of and used as insulators. Any electrical conduction in polymers usually due to loosely bound ions was regarded as an undesirable phenomenon. However the conductivity of polymer electrolytes and polyelectrolytes were utilized in electrochemical systems [42]. But the discovery of high electrical conductivity polyacetylene after dopped in 1977 and the further investigations in the field of conducting polymers (CPs) have expanded rapidly in number, scope of research, and importance. The Nobel committee in 2000 awarded the Nobel Prize for A. J. Heeger, A. McDiarmid, and H. Shirakawa for the discovery and development of electrically conductive polymers [43]. Now conducting polymers are coined as “synthetic metals” due to their electric, electronic, magnetic and optical properties inherent to/in metals or semiconductors [44].

In general, CPs possess alternating single (δ) and double (π) and this conjugated backbone is responsible for their unusual electronic properties such as electrical conductivity, low energy optical transitions, low ionization potential and high electron affinity. The inherent electrical conductivity, which is closely connected to the charge transfer rate and electrochemical redox efficiency, is the most notable property of CPs [45, 46]. The parameters that most affect the physical properties of CPs are their conjugation length, degree of crystallinity, and intra- and inter-chain interactions. The limitations of CPs in terms of solubility, conductivity and long term stability can be overcome by modifying the CPs or hybridizing it with other heterogeneous material components. The coupling of CPs with other materials can result in materials with attractive properties and new application [47].

To understand the differences among conductors, insulators, and semiconductors the energy band theory is a useful mechanism. There is an energy difference between the valence and conduction bands of a material called band gap. If the valence band overlaps that of the conduction band, the valence electrons are free to move and propagate in the conduction band. This is the intrinsic characteristic of conductors. But semiconductors possess small band gaps that electrons can cross upon excitation to reach the conduction band leaving a hole. This property allows both hole and electron charge transport, which allows the conduction of current. But in the case of insulators, the band gap is too large to be crossed by electrons, and therefore they do not conduct electricity [47]. However, the energy band theory does not clearly explain why CPs, being organic materials, conduct electricity. Many studies have addressed the transport properties of CPs at the molecular the conductivity that is explained by π-valence band and π*-conduction. Conjugated polymer possess delocalized π-electron structures in the π-valence band and π*-conduction band. The valence bands are filled by electrons but the conduction bands are all empty. The difference between the top of the valence band (the highest occupied molecular orbital, HOMO) and the bottom of the conduction band (the lowest unoccupied molecular orbital, LUMO) is called the bandgap (E_g) of the conjugated polymers. The E_g values of most conjugated polymers are in the range 1.5–3.0 eV. Therefore this E_g makes the conjugated polymers organic semiconductors [45]. To achieve high conductivity CPs has to be doped using different methods. Dopants in the polymer undergo redox processes in which charges are transferred with subsequent formation of charge carriers. The role of the dopant is not only to withdraw electrons from the conducting polymer (CP) but also to add electrons to the CP

backbone. During doping electrons are extracted from HOMO of the valence band (oxidation) or transferred to the LUMO of the conduction band (reduction). This oxidation/reduction process creates charge carriers in the form of polarons (radical ions), bipolarons (dications or dianions), or solitons in the polymer. CPs can be categorized into degenerate and non-degenerate systems based on their bond structures in the ground state. Solitons are known to be the charge carriers in degenerate systems such as polyacetylene [47]. Polyacetylene shows the simplest main chain structure composed of an alternate single bond and double bond carbon chain. According to the locations of the hydrogen atoms on the double bond carbons, there are two kinds of structures: trans-polyacetylene which possesses an equivalent structure after i.e degenerate conjugated polymer and cis-Polyacetylene which have non-equivalent i.e non degenerate structures after exchanging their double and single bonds [48]. The unique characteristic of CPs is due to the conjugated molecular structure of the polymer main chain where the π-electrons delocalize over the whole polymer chain. Scheme 3 shows the conjugation for poly(acetylene), a prototypical conducting polymer [49].

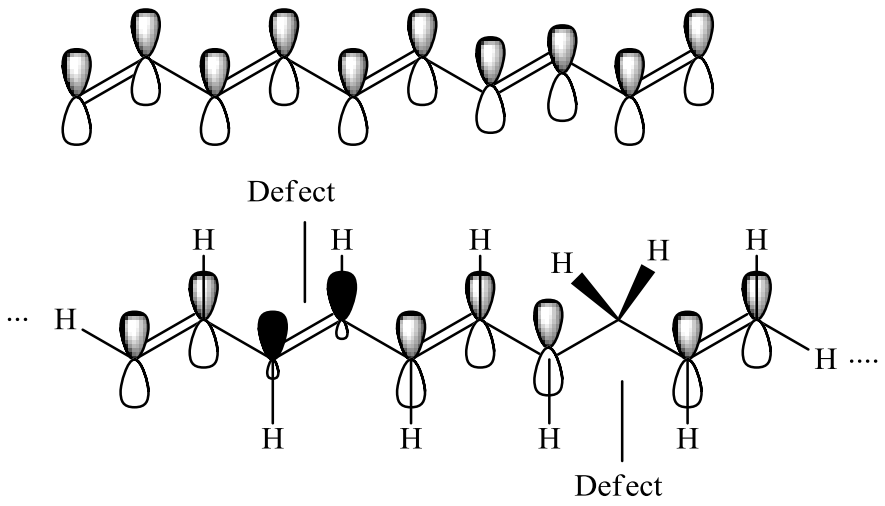

Scheme 3. Representation of π-conjugation in the conducting polymer poly(acetylene). Top: Basic scheme. Bottom: Three-dimensional, including defects.

Conducting polymers have a wide range of applications in the various fields of electronics, optics, energy devices, medicine, actuators, and composites as a viable alternative to metallic or inorganic semiconductor counterparts. Conducting polymers have also been used for sensor applications as a signal transducer. There are several important parameters in sensor technology,

such as sensitivity, selectivity, and response time. In most cases, a response time on the order of seconds is enough for human recognition. The sensing mechanisms of CPs can involve redox reactions, ion adsorption and desorption, volume and weight changes, chain conformational changes, or charge transfer and screening. Compared to the inorganic counterparts, conducting polymers have an advantage in achieving high sensitivity and selectivity by virtue of their chemical and structural diversity. Conducting polymers also shares the strengths of polymers over other materials, including low-temperature synthesis and processing, large-area manufacture, flexibility, and cost effectiveness. As a result, they can be competitive in sensor applications and sensors are therefore considered to be one of the most practical applications of conducting polymers [45].

1.7.3.1. PEDOT

Since its synthesis in 1980 by Bayer poly(3,4-ethylenedioxythiophene) (PEDOT) has been widely studied [50]. PEDOT is the most promising material due to the following unique properties: reversible doping state, improved chemical and thermal stability, regular structure due to the structure of the monomer, high electrical conductivity (up to 550 S/cm) in the doped state and films of PEDOT have a low redox potential and excellent stability in their doped state [51]. The processability, optical properties, and thermal properties make PEDOT an important transparent CP. Neutral PEDOT has a blue color with an absorption maximum at about 600 nm but the doped PEDOT is highly transparent in the visible range. The conformation and configuration of PEDOT change when it is changed from the neutral to the conductive state. Calculation on the geometry of PEDOT in neutral and doped states reveals that the thiophene ring has the benzoid structure for neutral PEDOT and it turns to the quinoid structure after being doped. Because the doping changes the charges on the CPs, the dielectric constant of PEDOT increases after it is doped [52].

1.7.3.2. Synthesis of PEDOT

The morphological, electrical and mechanical property of the polymer is related with its application and the preparation step plays a vital role in tuning these properties. In general polymerization begins via radical cations generated from 3,4-ethylenedioxythiophene (EDOT) monomer then radical-radical coupling reactions growing to ends with insoluble PEDOT chain

[53]. The EDOT monomers can be polymerized using different methods such as electrochemical polymerization, vapor phase polymerization (VPP) or chemical oxidative polymerization. Except the chemical oxidative polymerization the other methods usually give polymer films with very good properties such as surface quality, high conductivity and very stable redox chemistry. However chemical oxidative polymerization is a preferred route due to its ease to scale up production [54].

Electrochemical Polymerization

PEDOTs are prepared through the polymerization of its monomer EDOT through the radical cation polymerization. EDOT becomes a positively charged radical after it loses an electron. The radical structure makes the monomer chemically active, and the monomer molecules can connect into a polymer chain. The monomer can be oxidized by applying an electrochemical potential. The oxidation of EDOT in an acetonitrile solution of 0.1 M Bu_4NClO_4 starts at 1.04 V. Oxidation at this potential leads to the growth of PEDOT on the anode. A conductivity of about 200 S cm^{-1} was observed for the PEDOT doped with ClO_4^-. The electrochemical polymerization can also proceed in aqueous solution using surfactant to disperse the monomer in water. By carefully controlling the experimental conditions during the electrochemical polymerization, nanostructured PEDOT can be obtained [52, 55].

Chemical Synthesis

A mixture of persulfate salts, iron(III) salts, and bromine, were used as an oxidizing agent for the polymerization EDOT solution. Scheme 4 below shows the mechanism for the chemical polymerization of EDOT in aqueous solution of potassium persulfate [56].

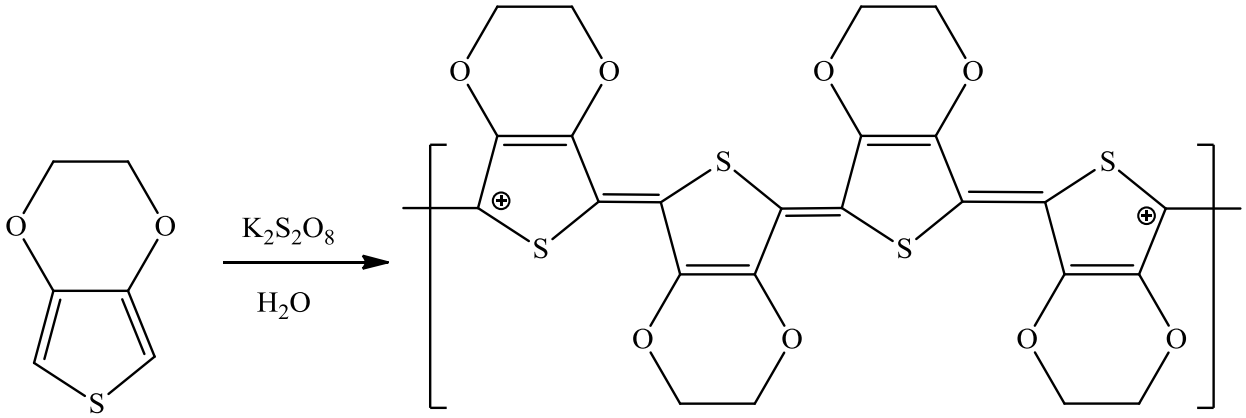

Scheme 4. Oxidative polymerization of EDOT with potassium persulfate

The polymerization and doping process take places in one step to yield conductive PEDOT polymer. The electrical conductivity and yield of PEDOT increased as the molar ratio of potassium persulfate to EDOT increased until the molar ratio reach unity and then decreased. The reaction rate for the oxidative polymerization is also affected by the acidity of the solution. It reaches the maximum yield when the pH of the solution is 2.7 [55].

Vapor-Phase Polymerization

The vapor-phase polymerization (VPP) is an alternative for polymerization of EDOT. In this method the monomer is initially deposited and then polymerization is carried out on the surface via thermal, photochemical, or other initiation process. The method gives a chance to produce a polymer with uniform, defect-free films [53, 57]. An oxidizing agent is coated onto the substrate to form a solid thin film on the substrate after drying. Exposure of this substrate to 3,4-ethylenedioxythiophene (EDOT) vapor produces a PEDOT film on the substrate. The VPP method combined with the electrospinning technique was used to fabricate PEDOT nanofibers. The produced nanofibers had average diameters of around 350 nm. The fibers are highly ordered at the molecular level, and the non-woven nanofiber mats had a high conductivity of ~60 S cm^{-1} [55].

2. Objective of the Study

2.1. Rationale and Motivation

Currently pharmaceutical products are recognized as emerging micropollutants. Unused pharmaceuticals end up in landfills from where they may be released in leachate which can contaminate surface water, groundwater and soil. These water resources could potentially lead to contamination of drinking water sources, dietary and plant products [58]. Thousands of studies have reported the existence and widespread distribution of pharmaceuticals and personal care products in marine, estuaries, rivers, lakes, and underground water around the world, with concentrations ranging from ng/L to µg/L, and even reaching mg/L [59]. Most of these substances are toxic to both humans and animals. Toxicity is the relative ability of a substance to cause adverse effects in living organisms and depends upon several conditions. The quantity or the dose of the substance determines whether the effects of the chemical are toxic, nontoxic or beneficial. In addition to dose, other factors may also influence the toxicity of the compound such as the route of entry, duration and frequency of exposure, variations between different species (interspecies) and variations among members of the same species (intraspecies) [60].

Many organic compounds with high therapeutic effects have the nitro group in their structure. Moreover, the nitro group is part of the chemical structure of veterinary drugs too. Nitro group contains nitrogen that bound to two oxygen atoms and connects the group to the rest of the molecule. On an aromatic ring, it has a strong electron withdrawing effect that deactivates the ring [61]. Nitro compounds require enzymatic reduction to induce the therapeutic and cytotoxic effects. A generalized sequence for the bio-reductive pathway involves the formation of a nitroso derivative, a nitro radical anion, a nitroxyl radical, hydroxylamine, and a primary amine. Toxicity issues associated with nitro compounds have been attributed to each of these intermediates, but the hydroxylamine derivatives are particularly responsible for methemoglobinemia, whereas the cumulative effects of the nitro radical anion, nitroso derivatives, or esterified hydroxylamine (e.g., sulfate derivatives) are held responsible for the mutagenic and carcinogenic activities [62].

Alkaloids are one of the largest groups of plant secondary metabolites present in several plant families and used for therapeutic. Alkaloids can act as defense compounds in plants, being

efficient against pathogens and predators due to their toxicity. Alkaloids affect different metabolic systems in animals, and the toxic mechanism of action of alkaloids may vary considerably. Toxicity may arise by enzymatic alterations affecting physiological processes, inhibition of DNA synthesis and repair mechanisms by intercalating with nucleic acids, or affecting the nervous system. Several alkaloids may affect multiple functions [63].

The conventional methods for drug quality monitoring and quantification in pharmaceutical formulations and biological fluids are quite expensive, require complicated and tedious sample preparation protocols, need skilled personnel and also not suited for field or onsite measurements. Therefore, the detection of these toxic drugs using simpler, faster and cheaper devices has great advantage than using the time-consuming and expensive laboratory-analysis. The motive for the current study was thus formulated considering these aspects.

There is an increasing demand for on-spot and point-of-care testing in biomedical, pharmaceutical, industrial and environmental analysis. Additionally, the analyses of biological samples such as blood, serum, urine, and so forth, often require small samples. Hence a technique that can solve such problems with a high degree of accuracy, precision, sensitivity, and selectivity is required.

One of the important factors in the fabrication of electrochemical sensor is the usage of cheap electrode material with improved performance. Screen printed carbon electrode is one of the cheapest electrode material used extensively for electrochemical sensor. This electrode gives a remarkable contribution in miniaturization of electrochemical sensor.

Using a simple procedure like electrochemical activation of SPCE oxygen-containing functional groups can be introduced in to the electrode surface. These functional groups exhibit electron donor–acceptor, hydrogen bonding, electrostatic or dispersive interactions with various analytes [29]. Using this simple techniques compounds containing nitro group can be determined electrochemically due to the electrostatic attraction.

Arenediazonium salts can be generated by using sodium nitrite and an aromatic amine in acidic solution. These salts can be attached to an electrode surface by using the faster and controllable electrochemical reduction method. The electrochemical method helps to localize the generated

phenyl radicals at the electrode and minimize the loss of diazonium salt [39]. Grafting of *p*-ABSA in the SPCE creates a negatively charged electrode surface and such type of modified electrode attracts cataionic analytes electrostatically.

PEDOT is the most promising polymer in electrode modification due to the reversible doping state, improved chemical and thermal stability, regular structure and high electrical conductivity [53]. Therefore, PEDOT, grafted *p*-ABSA with activated-SPCE were used in the fabrication of the sensor for it has a higher conductive surface.

2.2. Objectives

2.2.1. General Objective

The general objective of this research work was to develop simple and low cost electrochemical sensors for sensitive, selective and rapid determination of selected drugs (Niclosamide, Chloramphenicol, and Brucine) and biological molecule (Nicotine) in pharmaceutical formulations and biological fluids using screen printed carbon electrodes.

2.2.2. Specific Objectives

1. To fabricate activated screen printed carbon electrodes.

2. To modify conventional screen printed carbon electrode with *p*-amino benzene sulfonic acid (*p*-ABSA) by electrochemical grafting via in-situ generated arenediazonium salt.

3. To modify the *p*-ABSA grafted SPCE with PEDOT

4. To characterize the prepared electrode materials and the bare electrodes using high resolution scanning electron microscopy (HRSEM), Fourier-transform infrared (FTIR) spectroscopy, UV-Vis spectroscopy, cyclic voltammetry (CV) and electrochemical impedance spectroscopy (EIS).

5. To study the catalytic effects of the modified electrodes towards the electrochemical redox reaction of the selected drugs (Niclosamide, Chloramphenicol, Nicotine and Brucine).

6. To set the optimum working conditions for the determination of the selected drugs.

7. To establish the analytical performance characteristics (such as linear response range, method detection limit, repeatability, reproducibility, stability) of the developed sensors.

8. To investigate the selectivity of the method towards potentially interfering substances.

9. To investigate the analytical applications of the fabricated electrodes for the quantitative determination of the drugs in real samples such as pharmaceutical formulations and biological fluid (urine).

10. To compare the analytical performance of the developed methods with literature reports.

3. Methodology and Techniques Used in the Study

3.1. Electrode Materials

Screen printed electrodes (SPEs) which are used in environmental, industrial, and clinical analyses are designed for single use and are disposable. They have planar configurations and with various layers of machine-printed electrical conductive inks. SPEs represent one of the most interesting designs among electrochemical sensors [22]. The printing technology provides the production of large numbers of electrodes in a reproducible, low-cost, and disposable format. The incorporation of chemically functionalized materials in the printing process is straight forward. Almost all forms of carbon have been deposited by screen printing, with graphite, carbon black, and activated carbon being the most widely used [19].

A screen printed electrode comprises of a chemically inert substrate which is printed on the three electrodes (working, reference and counter) through screen printing methodology. The working electrode is the principal electrode on which electrochemical reactions are performed, while the reference electrode is used to measure the working electrode potential and counter electrode is a conductor that completes the electronic circuit. The chemical or biological event on the screen printed electrode is converted into a detectable signal with the integration of a transducer element. Among the different transduction techniques, the electrochemical method of detection has attracted high interest in the design of low cost devices [1].

A typical screen printed carbon electrode (SPCE) with three electrode systems form Zensor illustrated in Figure 1 was used in our study. It consists of a carbon working electrode, a silver pseudo reference electrode and a carbon counter electrode. With the screen printed technique, it is easy to achieve precise surface area and accurate relative position of three electrode system. In addition, comparing with the traditional three electrode system, the volume of analyte for SPCE is far less than the traditional system for electrochemical analysis.

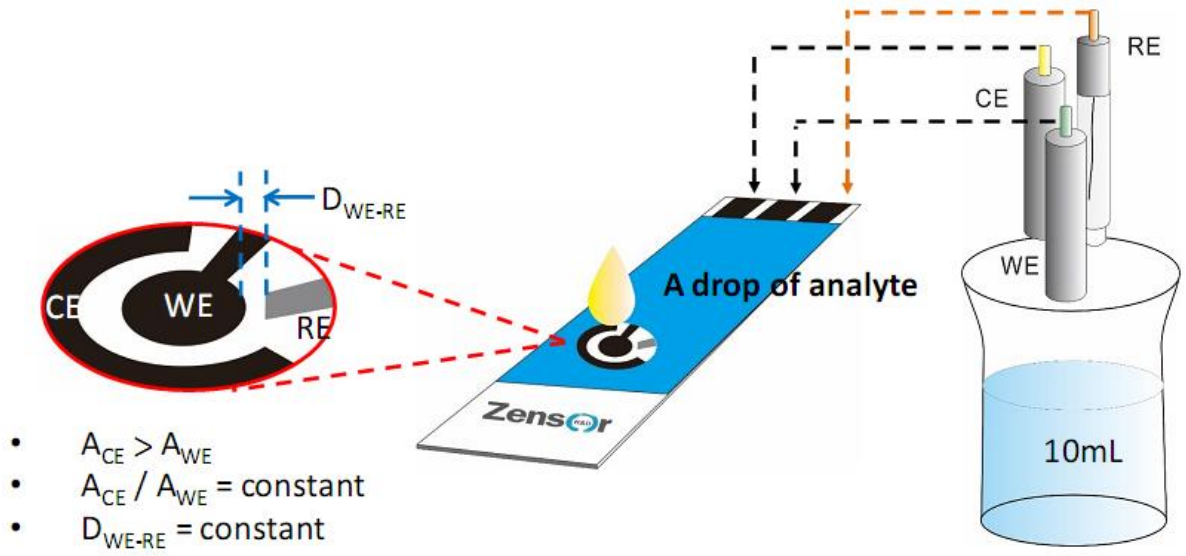

Figure 1. Design of a disposable and portable screen printed electrode (with reference, working and counter electrodes on the same substrate)

Where A_{CE} area of counter electrode, A_{WE} area of counter electrode and D_{CE-RE} distance between working and reference electrode

3.2. Voltammetry

Voltammetry is a class of electroanalytical method in which chemical information of the analyte is acquired by varying the potential and determining the resulted current. The potential variation method leads to different types of voltammetric methods in which CV is the main used method [64]. Voltammetry encompasses a large group of electrochemical techniques where nonspontaneous, interfacial charge transfer processes (electron or ion transfer across the electrode/electrolyte solution interface) are driven by externally applied electrical potential difference. The use of three electrodes (working, counter, and reference) together with the instrument allows accurate application of potential difference and the measurement of the resulting current. Voltammetric experiments are frequently conducted in a few milliliters of an electrolyte solution, using small electrodes with a surface area less than a square centimeter; alternatively, in more specific cases, electrodes are used with dimensions ranging from the micrometer to nanometer scale [64, 65]. A voltammetric measurement is organized in a specific way to provide information on the phenomena taking place at the working electrode only. The working electrode is the channel for the flow of current and it carries information solely from the

charge transfer across the electrode solution interface. To have a constant electric potential the reference electrode should be robust with a constant chemical composition. The potentiostat serves an electronic instrument that controls the voltage difference between a working electrode and a reference electrode while measuring the resulting current. The resulting electrochemical plot is then used to determine relation of the various parameters to the experiment. [66].

3.2.1. Linear Sweep and Cyclic Voltammetry

Linear sweep voltammetry (LSV) and cyclic voltammetry (CV) are potential sweep methods that are widely used for studying electrode processes. The LSV is performed by just a single sweep but in CV the potential sweep is reversed to form one complete cycle or multiple cycles. Both methods were first reported during 1938 and theoretically described in 1948 by Randles and Sevcik [67]. Of the two methods CV is more extensively used technique for acquiring qualitative information about electrochemical reactions. By using CV a rapid identification of redox potentials of the electroactive species under investigation can be obtained. The method also provides considerable information about the thermodynamics of a redox process, kinetics of heterogeneous electron-transfer reactions and analysis of coupled electrochemical reactions or adsorption processes. Cyclic voltammetry consists of scanning (linearly) the potential of the working electrode using a triangular potential wave form (Figure 2) [68].

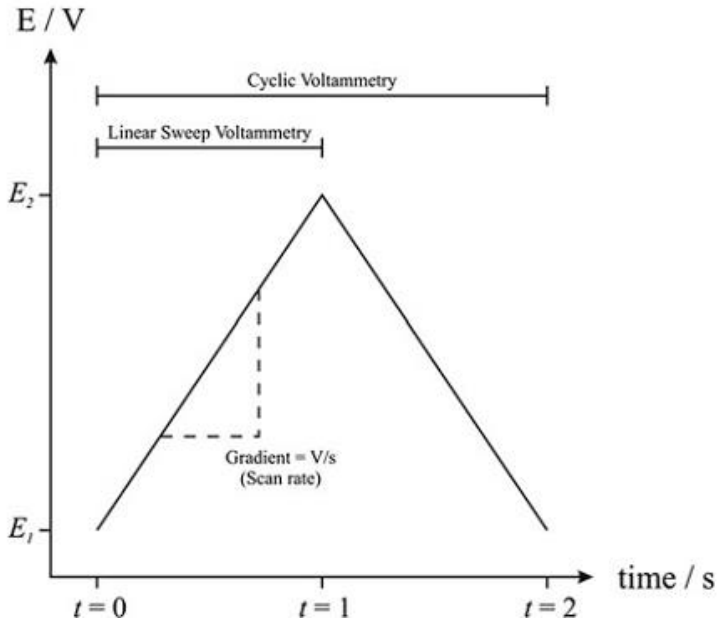

Figure 2. Potential—time profiles used to preform linear sweep and cyclic voltammetry

The potential is swept from E_1 to E_2 and the rate at which this sweep achieved is the scan rate as measured as mV s^{-1} or V s^{-1}. If the potential sweep is stopped at E_2 it is called a linear sweep voltammetry experiment but if the scan is returned back its initial potential i.e. a full potential cycle, this is called as cyclic voltammetry. Depending on the information required, either single or multiple cycles can be performed for both techniques [69].

Two conventions are used to report LSV and CV data which are classical and IUPAC convention [69]. In the case of classical convention, negative potentials are plotted in the positive "x" direction while the positive are in the opposite direction. In this convention cathodic currents due to reduction are positive and the anodic currents due to oxidation are negative. In the IUPAC convention the positive potentials are plotted in the positive ''x'' direction and the negative in the negative direction which is the opposite of the classical one. Therefore the anodic currents due to oxidations are positive and the cathodic currents due to reduction are negative Figure 3. It requires to become familiar with this concept as the literature presents voltammograms in mixed styles and to ensure clarification encountered in a voltammogram which potential sweep has been applied and which currents are anodic and which are cathodic have to be verified [68].

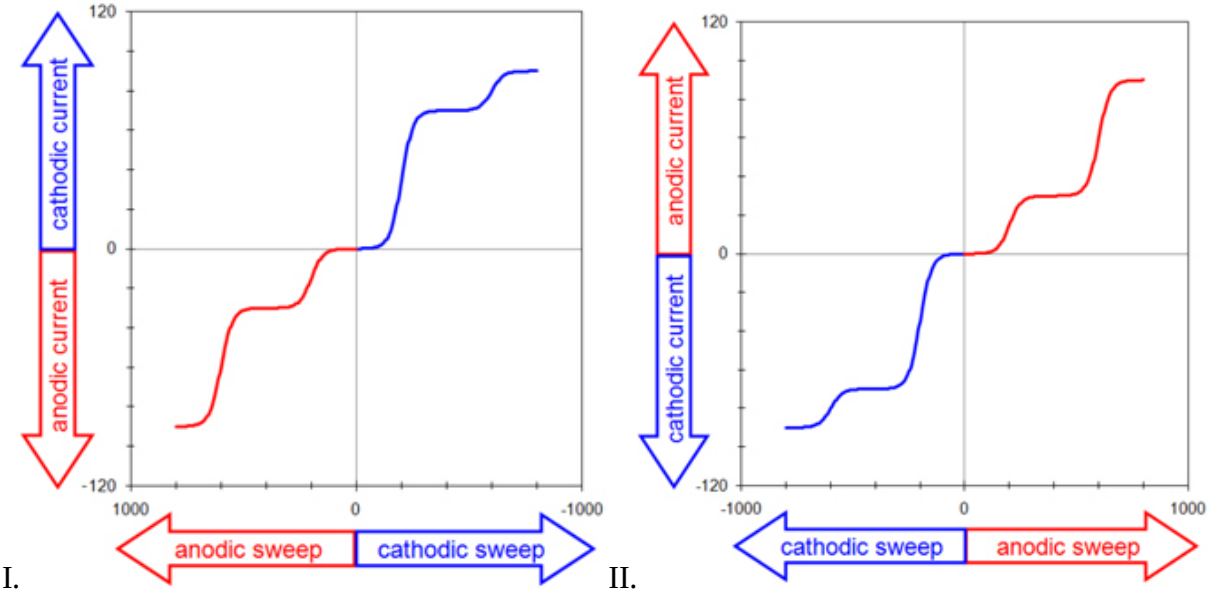

Figure 3. (I) Classical and **(II)** IUPAC voltammetry plotting conventions

Given a clear conventional representation quantitative information can be obtained in the kinetic parameters by performing qualitative experiments. This is done by observing how the peaks appear and disappear when the potential and scan rate are varied. Generally there are three types of reactions in which the shape of the cyclic voltammogram differs from one another, namely: (a) reversible, (b) quasi-reversible and (c) irreversible reactions [66]. An electrode process is defined as electrochemically reversible when the rate of the electron transfer is higher than the rate of the mass transport. But if the rate of the electron transfer is lower than that of the mass transport it is an irreversible processes. A quasi-reversible process occurs when the rate of the electron transfer is of the same order of magnitude as the mass transport [70]. The peak current for a reversible couple (at 278° K) is given by the Randles–Sevcik equation

$$i_P = (2.69 \times 10)^5 n^{3/2} A C D^{1/2} \nu^{1/2} \quad (1)$$

where n is the number of electrons, A the electrode area (in cm^2), C the concentration (in mol/cm^3), D the diffusion coefficient (in cm^2/s) and ν the potential scan rate (in $V\ s^{-1}$). Accordingly, the current is directly proportional to concentration and increases with the square root of the scan rate. The ratio between the forward to reverse peak currents, $|i_{Pr}/i_{Pf}|$, is equal to 1.0 for simple reversible couple.

The position of the peaks on the potential axis (Ep) is related to the formal potential of the redox process. The formal potential for a reversible couple is centered between $E_{p,a}$ and $E_{p,c}$:

$$\mathbf{E^{o}} = \frac{\mathbf{Ep,a + Ep,c}}{\mathbf{2}} \tag{2}$$

The separation between the peak potentials (for a reversible couple) is given by

$$\mathbf{\Delta E} = \frac{\mathbf{Ep,a - Ep,c}}{\mathbf{n}} \tag{3}$$

For an irreversible system the shift in the peak potential with scan rate is characterized by:

$$\mathbf{Ep,c = Ef^{o} - \frac{RT}{\alpha n' F}\left[0.780 + ln\frac{D^{1/2}}{K^{\circ}} + 0.5\ln\left(\frac{\alpha n' F v}{RT}\right)\right]} \tag{4}$$

where α is the transfer coefficient, n' is the number of electrons transferred per mole before the rate determining step and where E_f^o is the formal potential. For the case of a fully irreversible electron transfer process, the Randles–Ševc´ik equation is:

$$\boldsymbol{i_P^{irr} = \pm 0.496(\alpha n')^{\frac{1}{2}} nFAC\left(\frac{FDv}{RT}\right)^{\frac{1}{2}}} \tag{5}$$

where A is the geometric area of the electrode (cm^2), α is the transfer coefficient (usually assumed to be close to 0.5), n is the total number of electrons transferred per molecule in the electrochemical process and n' is the number of electrons transferred per mole before the rate determining step [7, 66].

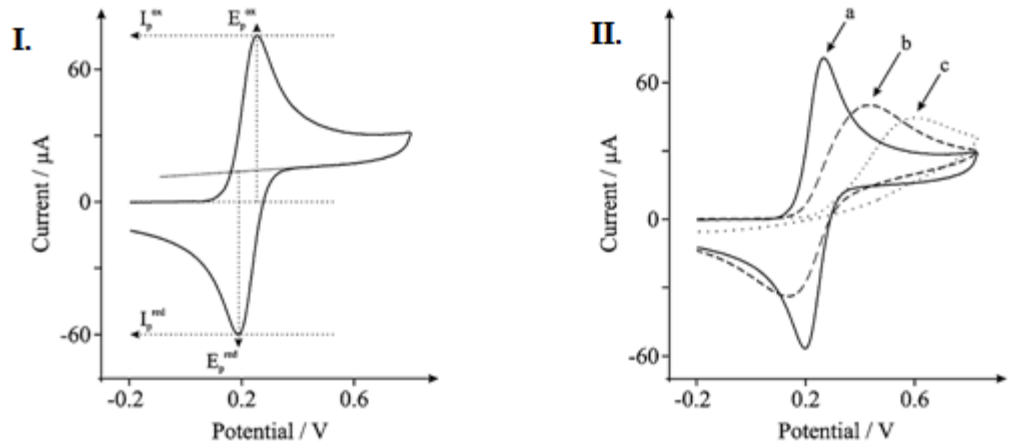

Figure 4. (I) Typical cyclic voltammogram depicting the peak position E_P and peak height I_P **(II)** cyclic voltammograms for reversible (a), quasi-reversible (b) and irreversible (c) electron transfer

3.2.2. Square Wave Voltammetry

The contemporary SWV originates from the Kalousek commutator and Barker's square-wave polarography. The Kalousek commutator switched the potential between a slowly varying ramp and a certain constant value to study the reversibility of electrode reactions. Barker employed a low-amplitude symmetrical square wave superimposed on a ramp and recorded the difference in currents measured at the ends of two successive half-cycles, with the objective to discriminate the capacitive current. SWV was developed by combining the high-amplitude, high-frequency square wave with the fast staircase waveform and by using computer-controlled instruments instead of analog hardware [71].

The potential modulation in SWV consists of a staircase potential ramp modified with square-shaped potential pulses Figure 5 (I). In each step of the potential ramp, two equal in height and oppositely directed potential pulses are imposed and the two potential pulses complete a single potential cycle in SWV Figure 5 (II). The potential cycle is repeated at each step of the staircase ramp in the course of the voltammetric experiment and due to historical reasons; the height of a single potential pulse is termed as amplitude. Relative to the direction of the staircase ramp, one recognizes forward and backward potential pulses. The potential pulses with odd serial number are forward pulses, whereas those with even serial numbers are assigned as backward (or reverse) pulses. In one single potential cycle, the electrode reaction is driven in both anodic and

cathodic directions. The critical time of the voltammetric experiment is represented by the duration of a single potential cycle (τ), or the duration of a single potential pulse, $t_p = \tau /2$. The voltammetric data can be interpreted in terms of τ, t_p, or the frequency of the potential modulation *f*, defined as $f = 1/\tau$. The physical meaning of the frequency can be understood as a number of potential cycles in a unit of time. The overall potential modulation can be attributed with scan rate defined as $\nu = f\,\Delta E$, where ΔE is the step of the staircase ramp Figure 5 (II). Therefor there is a certain analogy between the SW frequency and the scan rate in cyclic voltammetry. For example in an experiment SWV could be conducted at a very high frequency, i.e. a short potential cycle (e.g. f = 500 Hz; τ = 1 ms), but yet at a very slow scan rate, provided the scan increment is small (e.g. ΔE = 0.1 mV). For f = 500 Hz and ΔE = 0.1 mV the scan rate is moderate (ν = 50 mV s^{-1}) although the electrode reaction is driven in both anodic and cathodic directions over very short period of time (1 ms). But a corresponding experiment in CV, assuming a potential window of 300 mV, would require scan rate of 6000 mV s^{-1} [72].

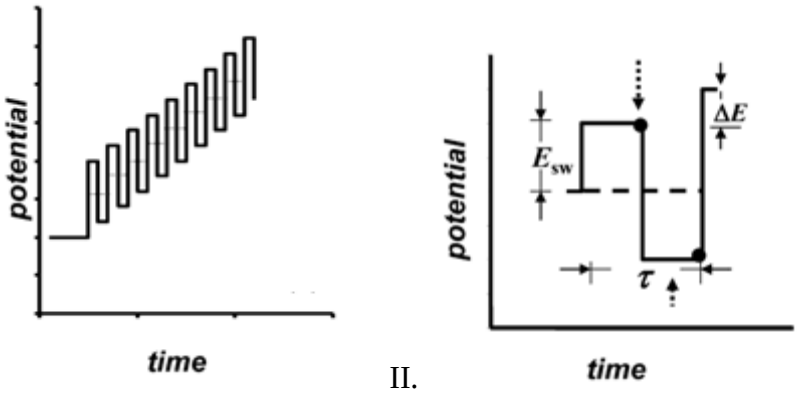

I. II.

Figure 5. (I) Potential waveform **(II)** One potential cycle for square wave voltammetry

Typical SW voltammogram encompasses three I-E curves two of them are experimentally measured (forward and reverse), and the third calculated net current Figure 6. Each voltammetric curve is discontinuous and depends on the scan increment. The forward and reverse currents are measured at the real potential of the corresponding pulses, $E_{for} = E_{step} + E_{sw}$, & $E_{rev} = E_{step} - E_{sw}$, for the forward and reverse pulses, respectively; they are, however, plotted versus the step potential E_{step}. The shape of the forward and reverse components resembles a cyclic voltammogram, and they provide analogous mechanistic information as CV does intrinsically. For all these reasons SWV unifies the advantages of cyclic voltammetry, as a tool for

mechanistic studies, with the advanced sensitivity, typical for pulse voltammetric techniques [69].

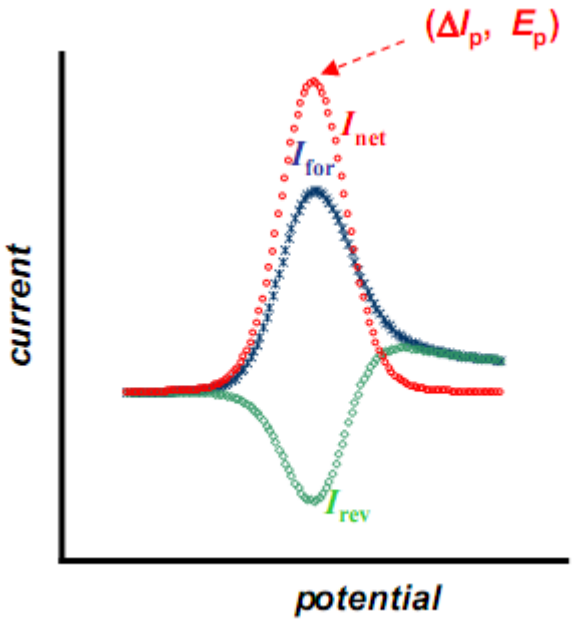

Figure 6. Typical square-wave voltammogram

The advantages of SWV over CV are faster scan rates are possible (faster reactions can be studied), higher sensitivity (lower concentrations can be detected) and a higher dynamic range (a larger range of concentrations can be investigated). By using SWV under optimum conditions a detection limits of *ca.*10^{-8} M or lower are achievable. Usually in electrochemistry, solutions are vigorously degassed with nitrogen to remove oxygen which is electrochemically reduced and can interfere with the voltammetric measurement under investigation. But the interference can be diminished by using a SWV at a high frequency without removing. Due to the irreversibility of oxygen reduction, the increase of its signal with frequency is small and at high frequencies becomes negligible [73].

3.3. Electrochemical Impedance Spectroscopy (EIS)

Originally the concept of electrical impedance was first introduced by Oliver Heaviside in the 1880s then after it is developed in terms of vector diagrams and complex number representation by A. E. Kennelly and C. P. Steinmetz [74]. Since then electrochemical impedance spectroscopy

(EIS) has been employed for studying electrochemical systems, including those involved in corrosion, electrodeposition, batteries and fuel cells [75].

EIS is a powerful method of characterizing many of the electrical properties of materials and their interfaces with electronically conducting electrodes. It is widely used to investigate the dynamics of mobile charge in the bulk or interfacial regions of any kind of solid or liquid material [74].

In principle, impedance is simply the opposition force to electrical current in a circuit and is measured in the same units as resistance, Ω. But resistance differs from impedance for it obeys Ohm's law and is observed in DC circuits. The concept of resistance can be applied in an alternating current (AC) circuit if only these criteria are met: (i) the voltage and current must be in phase with each other; (ii) the resistance is independent of the frequency; and (iii) the resistance is applied to all currents and voltages. However in the majority of cases the phase angle is not equal to zero, as capacitative and/or inductive effects are observed at almost all frequencies, therefore a more general principle must be used to account for frequency dependency. The concept of impedance essentially allows a quantitative representation of the opposition force to electrical current in these cases (as in AC circuits) [75].

Electrochemical reactions entail the transfer of electrons to or from a molecule, atom, or ion at an interface between an electronic conductor, the electrode and an ionic conductor example equation 6 [76].

$$\boldsymbol{O + ne \rightarrow R} \qquad (5)$$

where, n is the number of electrons transferred, O is the oxidant, and R is reductant.

As illustrated in Figure 7 (I), the charge transfer leads to both faradaic and non-faradaic components. The faradaic component is resulted from the electron transfer, according to equation 6, across the interface by overcoming an appropriate activation barrier, namely the polarization resistance (R_p), along with solution resistance (R_s). The non-faradaic currents results from charging the double-layer capacitor (C_d). When charge transfer takes place at the interface, the mass transport of the reactant and product takes on the roles in determining the rate of electron transfer, which depends on the consumption of the oxidants and the production of the reductant

near the electrode surface [76]. When impedance measurements are done they are whole cell impedance which includes contributions from the counter electrode's interface. The faradaic process at the working electrode is considered as general impedance, Z_f. The application of a current or potential input causes changes in concentration due the influence of mass transport and was introduced as Warburg impedance, Z_w [77].

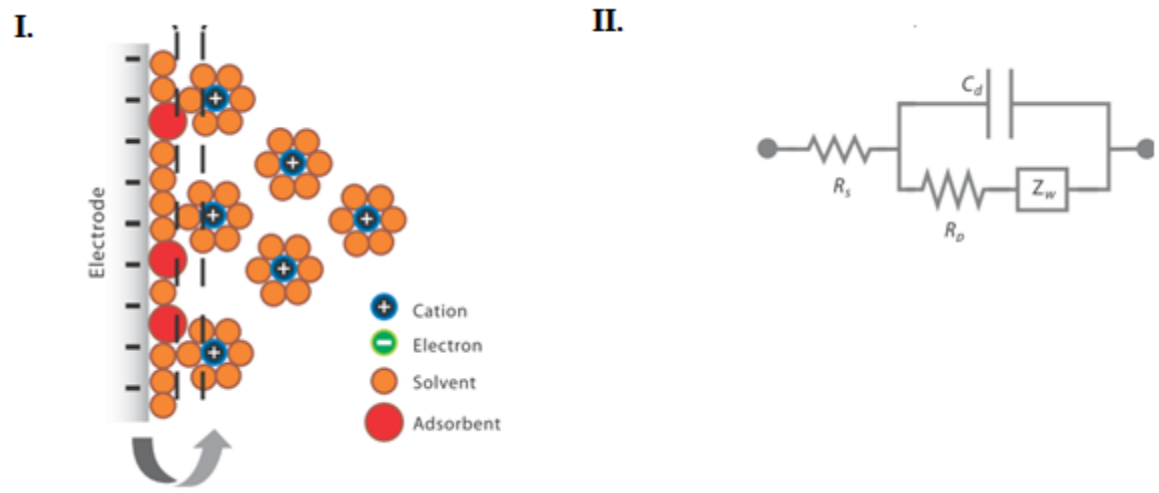

Figure 7. (I) An electrified interface in which the electrode is negatively charged; counter cations are aligned along the electrified surface. **(II)** An idealized Randles electrical equivalent circuit for the interface, shown with no specifically adsorbed anions.

EIS measurement is based on the excitation of an AC voltage (or current, in the case of galvanostatic EIS) to the system under study and on the analysis of the AC current (voltage) response as a function of the frequency. The amplitude of the AC should be as low as possible (small signal approximation) in order to consider the system under study as pseudo-linear. The frequency may span over a wide range, usually from some MHz down to few mHz. During the EIS measurements, the small signal sinusoidal voltage $V(\omega,t) = V_o \sin\omega t$ with amplitude V_o and variable frequency f ($f = \omega/2\pi$, where ω is the angular frequency) is applied to the system under study, and the response current $I(\omega,t)$ is measured at the same frequencies. The impedance $Z(\omega,t)$ related to the system can be calculated through Ohm's law as shown below

$$\boldsymbol{Z(\omega,t)} = \frac{\boldsymbol{V(\omega,t)}}{\boldsymbol{I(\omega,t)}} \quad (6)$$

For a given ω, the current response could be in-phase or out-of-phase with respect to the voltage applied, so that its general expression is given by $I(\omega,t) = I_o \sin(\omega t - \theta)$, where I_o is the current

signal amplitude and θ is the phase angle between voltage and current. By exploiting the complex number notation, the AC voltage and current signals can be expressed as $V(\omega,t) = V_o e^{j\omega t}$ and $I(\omega,t) = I_o e^{j(\omega t - \theta)}$, respectively, where j is the imaginary unit. With these notations, Equation 7 can be rewritten as:

$$Z(\omega,t) = \frac{V(\omega,t)}{I(\omega,t)} = \frac{V_o}{I_o} e^{j\theta} = |Z(\omega)| e^{j\theta} \quad (7)$$

where |Z| is the impedance modulus and θ is the impedance phase

Equation 8 is composed of a real and an imaginary part. The real part is plotted on the X-axis while the imaginary part is plotted on the Y-axis. EIS data are represented –Z'' as a function of Z' in the complex plane, and it is referred to as Nyquist plot [78]. The electrode process is controlled at both higher and lower frequency by electrochemical reactions and by mass-transfer, respectively. The intercept of the semi-circle at high frequency with the z' axis represents the ohmic resistance of the solution [79].

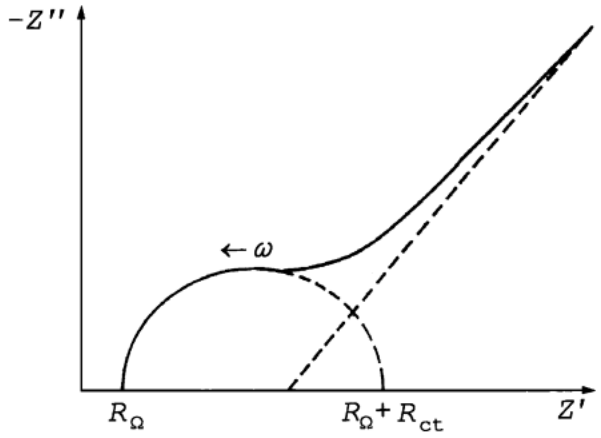

Figure 8. Randles equivalent circuit in the complex impedance plane (Nyquist plot)

3.4. Fourier-Transform Infrared Spectroscopy (FTIR)

Infrared radiation was discovered by Sir William Herschel in 1800 while he was investigating the energy levels associated with the wavelengths of light in the visible spectrum. He wanted to know how much heat was passed through the different colored filters and he noted that filters of different colors seemed to pass different amounts of heat. He directed sunlight to pass through a glass prism to create a spectrum of rainbow then he measured the temperature of each color. As

he measured the individual temperatures of the violet, blue, green, yellow, orange and red light, he noticed that all the colors had temperatures higher than the controls. While he continued to measure below the red he found that the temperature continued to become higher. Then he coined the rays below the red rays “non-colorific rays” or invisible rays, which were called later “infrared rays” or IR [80].

There are three well defined IR regions (near, mid and far). The boundaries between them are not clearly defined and debate still persists, but broadly they are defined as:

1. Near infrared (12820-4000 cm^{-1}): poor in specific absorptions, consists of overtones and combination bands resulting from vibrations in the mid-infrared region of the spectrum.

2. Mid-infrared (4000-400 cm^{-1}): provides structural information for most organic molecules.

3. Far Infrared (400-33 cm^{-1}): has been less investigated than the other two regions; however, it has been used with inorganic molecules [81].

Infrared spectroscopy provides direct information on the arrangement of atoms in a molecule under investigation, that is, on how the atoms are arranged relative to one another. The absorption of infrared radiation in a molecule arises from changes in its dipole moment. Generally if there is no polarity (dipole moment) in the molecule then the infrared interaction is inactive and the molecule does not produce any IR spectrum. The absorption 'bands' for structural information occur in the 4000-400 cm^{-1} region of the electromagnetic spectrum [80, 82].

Both classical IR spectrometers and modern Fourier-Transform Infrared Spectroscopy (FTIR) give the same information. And the main difference between them is FTIR uses a two beam interferometer, which split a beam of radiation into two paths. The original infrared spectroscopy instruments were of the dispersive type. These instruments separated the individual frequencies of energy emitted from the infrared source. This was accomplished by the use of a prism or grating. The infrared prism works in a similar fashion to that of a visible prism which separates visible light into its colors (frequencies). A grating is a more modern dispersive element which better separates the frequencies of infrared energy. The detector measures the amount of energy at each frequency that has passed through the sample and it results in intensity vs. frequency

spectrum plot. There are variety of approaches to achieve interaction between the radiation and the sample. The most common method is the transmission measurement. In this approach the sample is placed between two transparent plates then the transmitted intensity in the infrared region is recorded as a function of wavelength. In this approach having an appropriate sample thickness is crucial. Therefore, it is needless to say that the preparation of the sample is very important as even dust particles may have significant influence. The other approach is referred to as attenuated total reflection spectroscopy. In such approach the IR radiation is propagated in a transparent high-refractive-index material (often ZnSe or a diamond crystal), called the internal reflection element. The sample has a lower refractive index and is in contact with the surface of the crystal. The radiation undergoes total internal reflection at the angle at this surface, so that the evanescent field can interact with the sample. As a consequence, the reflected beam is attenuated and carries the spectroscopic information [80-83].

3.5. Ultraviolet-Visible Spectroscopy

Three types of electronic transitions occur as a result of excitation of outer electrons in the valence shell when molecules are exposed to ultraviolet or visible radiation. These are transitions involving π, σ, and *n* electrons (most organic molecules), transitions involving charge-transfer electrons (ligand and metal ion) and transitions involving *d* and *f* electrons (most transition metal ions) [84]. Ultraviolet-Visible (UV-Vis) spectroscopy is a mature and well established analytical technique used extensively in many industrial sectors including environmental analysis, pharmaceutical testing, food and beverage production, etc. UV-Vis spectroscopy involves the measurement of the absorbance of ultra-violet or visible radiation when light passes through an analayte. When radiation interacts with matter, a number of processes can occur, including reflection, scattering, absorbance, fluorescence/phosphorescence (absorption and emission), and photochemical reaction (absorbance and bond breaking). In general while recording UV-Vis spectra, the desire is for absorbance to occur only. Absorption of photons of light measures transitions from the ground state to the excited state. Molecules containing π-electrons or non-bonding electrons (n-electrons) can absorb energy in the form of ultraviolet or visible light to excite their electrons to higher anti-bonding molecular orbitals. The more easily excited the electrons (i.e. lower energy gap between the HOMO and the LUMO), the longer the wavelength of light it can absorb. UV-Vis spectroscopy is an effective technique for both

qualitative and quantitative analysis of organic and inorganic compounds. It is routinely used for the quantitative determination of solutions of transition metal ions and highly conjugated organic compounds based on Beer-Lambert law, equation (11), which states that the absorbance of a solution (A) is directly proportional to its concentration (c) and path length (l) when the wavelength of the incidence light remains fixed, and is summarized as [85, 86]:

$$A = \varepsilon cl \tag{8}$$

Where, Ɛ is the molar absorptivity coefficient.

3.6. Scanning Electron Microscope (SEM)

Generally two types of microscopy are available: optical microscope (OM) and scanning electron microscope (SEM). OM is the oldest type which is a form of simple device with limited capabilities and has been used for long time. It is also called light microscopy. OM differs from SEM in the following properties and features, the main working principle is based on using light unlike SEM and it has only one lens in simple OM or two lenses in compound OM. The magnification of modern OM reaches to the range between 400-1000 times the original sizes, which is very low compared to SEM. Scanning electron microscope has been used worldwide in many disciplines. It can be regarded as an effective method in the analysis of organic and inorganic materials on a nanometer to micrometer (μm) scale. SEM works at a high magnification reaching to 300,000 times and even 1,000,000 (in some modern models) in producing images very precisely of wide a range of materials [87].

The scanning electron microscope is one of the most versatile instruments available for the examination and analysis of the microstructure morphology. It is necessary to know the basic principles of light optics in order to understand the fundamentals of electron microscopy. Since the discovery that electrons can be deflected by the magnetic field in numerous experiments in the 1890s, electron microscopy has been developed by replacing the light source with high-energy electron beam. Scanning electron microscopy (SEM) is widely used for materials characterization. The microscopy images contain abundant information about the sample, because the brightness of a specific point depends on the spatial structure and physical properties [88, 89].

There are three types of SEM, conventional scanning electron microscope (CSEM), environmental scanning electron microscope (ESEM) and low vacuum scanning electron microscope (LVSEM). In a CSEM the interaction of electron beam with specimen occurs in a high vacuum at about 10^{-6} torr. Thus low energy secondary electrons will be emitted from the sample with minimum collisions with the gas molecules in the chamber. However, dehydration and cracking of concrete will occur due to this high vacuum, which will obstacle the ability to make direct observations on crack propagation. In the second type which is ESEM, the interaction between electron beam and specimen occurs at elevated pressures (0.2 to 20 torr). It lessens or eliminates dehydration, reduces the need for conductive coatings so an improved concrete imaging will be obtained and the ionization of gas molecules increases the strength of electron signal. The third type of scanning electron microscope LVSEM is similar to a CSEM but also adapted to operate at elevated pressures (0.2 to 2 torr). In such environment, any liquid water cannot be sustained and will dissipate very slowly in the vacuum. Effect of this type of SEM on cracking will be very slow and not seen during a typical analysis. Similar to CSEM, LVSEM eliminates surface charging and the need for coating [90, 91].

4. Experimental

4.1. Chemicals and Reagents

All the chemicals and reagents used in this study were of analytical grade and were used as received without any further purification. Double distilled water and/or ultrapure water from a Milli-pore Mill Q system was used throughout the preparation of solutions. Potassium hydroxide (Merck), potassium phosphate, dibasic (Joint work), ethylenedioxythiophene (AppliChem), tri(hydroxymethyl)-methylamine (PHARMACOS LTD), 37% hydrochloric acid (RDH), sodium dodecyl sulfate (AppliChem), potassium chloride (Joint work), potassium hexacyanoferrate(II)-3-hydrated (Acros), potassium hexacyanoferrate(III) (JANSSEN), acetic acid (Showa), sodium acetate (Panreac, Sigma, RDH, JT) were used in this experiments. Boric acid, phosphoric acid, potassium chloride, nicotine and N,N-dimethylformamide were from Riedel-de Haën. Lithium perchlorate, niclosamide, chloramphenicol, brucine, ascorbic acid (≥ 95%), uric acid (99%), urea, glucose, lactose, magnesium acetate, citric acid, sodium citrate, sodium nitrate, sodium nitrite, nickel nitrate, ferric nitrate, cobalt nitrate, copper nitrate, calcium nitrate, magnesium nitrate, hydrogen peroxide (30%), sulfuric acid (95-98%), hydrochloric acid (37%), and sodium hydroxide pellets (98%) were from Sigma-Aldrich. Standard buffer solution of pH 4.00 ± 0.02 (20 °C), pH 7.00 ± 0.02 (20 °C), pH 10.00 ± 0.02 (20 °C) from CARLO ERBA were used to calibrate the pH meter.

Acetate buffer solution (ABS) of 0.20 M was prepared from anhydrous sodium acetate and 99.8% acetic acid. Phosphate buffer solution (PBS) was prepared from of 0.1 M anhydrous Na_2HPO_4 and dihydrated NaH_2PO_4. Britton-Robinson buffer was prepared using 0.04 M boric acid, 85% phosphoric acid and 99.8% acetic acid and 0.2 M sodium hydroxide was used to adjust the pH of the supporting electrolyte to the desired value. Two different solvents 30% DMF and aqueous solution was used for Britton-Robinson buffer preparation. 1 mM $K_3Fe(CN)_6$ in 0.1 M KCl was used during measuring the electroactive surface area and 5 mM $Fe(CN)_6^{4-/3-}$ in 1 M KNO_3 solution was used as a probe for electrochemical impedance spectroscopic measurements (EIS).

4.2. Apparatus and Instruments

The electrochemical measurements: Cyclic Voltammetry (CV), Linear Sweep Voltammetry (LSV), Square Wave Voltammetry (SWV) and Electrochemical Impedance Spectroscopy for the determination of brucine were performed with a PC-integrated CHI660D (CH Instruments, USA) instrument controlled by software for data acquisition. All the other electrochemical experiments (CV, LSV, SWV and EIS) used for the determination of niclosamide, chloramphenicol and nicotine were performed using CHI760D electrochemical workstation (CH Instruments, USA). Disposable SPCEs with a 3 mm diameter carbon WE, a carbon CE and silver RE were purchased from Zensor (TE100-PF) Taiwan. The electrochemical measurements were performed with both bare (unmodified) and modified SPCE. All experiments were performed at room temperature.

SUNETX MICROPROCESSOR pH METER SP-2200 was used for measuring pH during the preparation of acetate buffer solution. The pH measurements in the preparation of PB and BRB solution were carried out using a pH meter (sensION, SHA Snilu Instruments CO. LTD, China). All electrochemical measurements were made at room temperature (22 ± 2 ^{o}C) under atmospheric conditions (without inert gas bubbling). JEOL JSM-7401F Field Emission Scanning Electron Microscope was used for imaging. IRTracer-100 Fourier-Transform Infrared Spectrophotometer (SHIMADZU) was used for FTIR spectra recoding.

4.3. Preparation of Stock Solutions

Stock solutions of all the analytes in this study were freshly prepared prior to the experiments. Stock solutions of niclosamide standards were prepared initially by dissolving the standard in dimethylformamide. Then subsequent dilution and all the other working standard solutions were prepared using Britton-Robinson buffer 30% DMF. Similarly aqueous Britton-Robinson buffer solution was used for the nicotine working standard sample preparation from stock solution prepared by double distilled water. Similarly, stock solution of brucine was prepared using double distilled water. The working standard for brucine was prepared by dilution in 0.2 M ABS (pH 4.0). Chloramphenicol solutions were prepared in double distilled water by ultrasonication for 30 min followed by dilution to get the final working standard solutions. The working standard for chloramphenicol was prepared by dilution in 0.1 M PBS of pH 6.50.

4.4. Preparation of Real Samples

4.4.1. Preparation of Milk Sample

Pasteurized milk Lame Dairy *(*Shola) was purchased from a local super market and prior to determination, milk was processed as suggested by Zarei and coworker [92]. In brief, 5 mL of sample were transferred into a 10 mL centrifuge tube and spiked with different concentrations of CAP standard solution. Next, 5 mL ethyl acetate was added and the sample shaken vigorously and sonicated for 5 min. The mixture was centrifuged at 4000 rpm for 5 min and the supernatant was collected and evaporated. This extraction was repeated two times. Then residue was dissolved in 10 mL 0.1 M PBS (pH = 6.5).

4.4.2. Preparation of Vegetable Sample

The vegetable sample (spinach) was collected from a local market near to Akaki River, Akaki Kality sub city, Addis Ababa, Ethiopia. The vegetable was prepared according to the procedure described in [93] with some modification. The sample was chopped into small pieces with a knife and then blended. Then, 10 g of the vegetable sample was immersed in 60 mL of dimethylformamide, and the possible NA residues were enriched by ultra-sonication for 30 min. The extract was filtered and the solvent was allowed to evaporate to dryness by gentle heating in an over at 40 ^{o}C. The residues was dissolved in DMF and then after diluted to 10 mL with BRB pH 7.5, which and was stored in a refrigerator until analysis.

4.4.3. Preparation of Urine Sample

Human urine sample was collected from a healthy volunteer in sterilized plastic containers. Then the protein that can passivate the electrode was removed according to the procedure reported in [94]. The urine sample was diluted with acetone in 1:1 ratio then it was stirred for 5 min using a magnetic stirrer followed by filtering using Whatman filter paper (0.45 µm pore size) and the residual acetone was removed by drying at room temperature. Then, an appropriate quantity of the standard drug solutions was added and diluted to the mark with the appropriate working buffer solutions to make the final concentration. The solutions were drop casted on the surface of the electrode to be analyzed without any further pretreatment. The standard addition method was used for the determination of drugs in the urine samples.

4.5. Pharmaceutical Formulations

4.5.1. Chloramphenicol Formulation

Commercial pharmaceutical eye drop of 5% chloramphenicol formulation (MBL Pharma, Pakistan) was purchased from a local drug store from Addis Ababa, Ethiopia. Then, 50 µL of the eye drop was pipetted out and poured in to a 50 mL volumetric flask then it is filled with the supporting electrolyte (PBS pH 6.5) to obtain the final concentration of 15.5 µM the range of the calibration curve. Then, solution was taken and transferred to 25 mL volumetric flasks and spiked with different concentrations of the CAP standard to get the desired concentration. The peak current response was measured using SWV under the optimized conditions and the standard addition method was used to determine CAP in the real sample. All solutions were kept in a refrigerator at 4 ^{o}C in the dark.

4.5.2. Nicotine Formulation

Nyala cigarette containing 20 cigarettes per pack from Nyala, National Tobacco Enterprise, Ethiopia, was bought from a shop in Addis Ababa. The cigarette samples were prepared for analysis according to the procedure reported [95]. The rolling paper was peeled off from the cigarettes to obtain the tobacco sample. The tobacco was dried at 40 °C under vacuum for 2 h. Then, 0.20 g of each sample was soaked in 40 mL water and ultra-sonicated for 3 h. The brown mixture was filtered and the filtrate was diluted to 50 mL and stored at 4 °C for later use in experiments.

4.6. Preparation of Solution

4.6.1. Preparation of KOH

Potassium hydroxide solution was prepared freshly by dissolving appropriate amount of KOH in distilled water to get a final concentration of 0.5 M and was kept in closed plastic container.

4.6.2. Preparation of *p*-Aminobenzene Sulfonic Acid

The *p*-aminobenzene sulfonic acid (5 mM) for electrografting was prepared freshly by dissolving the appropriate quantity of the acid in 0.5 M HCl and was kept in an ice bath. The $NaNO_2$ that

was used to generate diazoinium ion was prepared by dissolving in water to get a final concentration of 10 mM then dropped in to the ice cold *p*-ABSA solution with stirring for 15 min [96].

4.6.3. Preparation of EDOT Solution

10 mM 3,4-ethylenedioxythiophene (EDOT) was prepared in a solution containing 0.1 M $LiClO_4$ with 0.05M sodium dodecyl sulfate (SDS) as a surfactant to dissolve the EDOT in aqueous media and it was kept in the dark area after flushed with N_2 [97].

4.7. Preparation of Modified Electrodes

4.7.1. Electrochemical Activation of SPCE

Electrochemical activation of a carbon electrode helps to the formation of an edge plane carbon surface. Edge plane pyrolytic graphite electrodes are advantageous for use as electrode substrates in electrochemical sensor development owing the highly reactive edge plane site which allow low detection limit, high sensitivity and improved signal to noise ratio with low over-potentials. The electrochemical activation of SPCE was performed according to literature report [98]. In brief 0.5 M KOH was dropped on the surface of the SPCE covering the working, reference and counter electrode then the potential was scanned in the range of −1.5 to 1.0 V at a scan rate of 100 mV s^{-1} for 10 cycles by LSV. Thereafter, it was cleaned with deionized water and flushed with N_2 until it was dry.

4.7.2. Electrografting of Activated-SPCE

The electrografting was done on SPCE that was activated by KOH according to procedure 4.7.1. The diazonium cation was produced by dropping 10 mM $NaNO_2$ to an ice cold 5 mM *p*-ABSA in 0.5 M HCl with stirring for 15 min according to procedure [96]. After waiting for extra 5 min then 100 µL of the cold solution was pipetted out and dropped on the surface of activated-SPCE covering the electrodes. And the grafting was done by cycling the potential in the range of 0.0 to −1.V using LSV for 15 cycles at 100 mV s^{-1}. After modification, the electrode was rinsed with distilled water and flushed with N_2 until it was dry.

4.7.3. Electropolymerization of EDOT on Electrografted Activated-SPCE

First the screen printed carbon electrode was activated using KOH according to the procedure 4.7.1 followed by electrografting using *p*-ABSA according to the procedure 4.7.2. Then electropolymerization was done using 10 mM EDOT prepared in 0.1 M $LiClO_4$ solution having 0.05M sodium dodecyl sulfate (SDS) as a surfactant according to the literature report [97] with some modification. 100 μM of the EDOT solution was dropped to the surface of the electrografted activated-SPCE surface covering the reference, counter, and working electrodes and then the potential was cycled for 10 cycles in the potential range of 0.4 to 1.5 V with a scan rate of 100 mV s^{-1}.

5. Results and Discussion

5.1. Square Wave Voltammetric Determination of Niclosamide at Activated-SPCE

5.1.1. Background

A major part of analytical research activity is devoted to the development of new and robust methodologies. New analytical tools are required for economical and real time monitoring of environmental pollutants, and for the prevention of toxic materials in the environment [1]. Niclosamide (2,5-dicloro-4-nitrosalicylanilide, NA) is an effective anthelmintic medicine that is widely used in public health, veterinary and aquaculture. The World Health Organization has recognized it as the only molluscicide to be commercially available in large-scale for schistosomisasis control. However, many researchers identified that NA has high toxicity to some aquatic snails and organisms [99]. The increased use of pharmaceutical drugs, in order to meet the world-wide growing demand, require firm regulations regarding quantitative analysis associated with the drug processing stages. Such strict measures not only ensure the quality and stability but also assure the appropriate formulation of the designed drug [100].

NA is an antihelminthic drug that is approved by the U.S. Food and Drug Administration and that belongs to the salicylanilide structural family which is especially effective against cestodes [101, 102]. The antiparasitic activity of niclosamide is thought to be mediated through disruption of mitochondrial oxidative phosphorylation and inhibition of adenosine triphosphate production, a hypothesis based on a number of studies that identified uncoupling activity of niclosamide in isolated mitochondria and invertebrates. Beyond its traditional use in public health and veterinary medicine, niclosamide has recently received attention as a promising drug adapted to be used for different purposes for the potential treatment of cancer, bacterial infections, endometriosis, and Zika virus [101]. NA is used as lampricide and molluscicide, in agriculture as a pesticide, as well as in human and veterinary practices. Niclosamide, along with oxyclozanide, was found to display "strong in vivo and in vitro activity against methicillin-resistant *Staphylococcus aureus*", and it was suggested that it may inhibit Zika virus replication in vitro. A number of studies have established the anticancer activities of niclosamide and have identified it as a potential anticancer agent [102]. Despite to its wide applications in agriculture, veterinary, and public health, it is not only toxic to target snails but also to non-target aquatic organisms, and

caused problems to terrestrial and aquatic plants over long-time administration. Therefore, a sensitive and selective method for the determination of NA, especially in monitoring of NA concentration levels in pharmaceuticals, environmental samples or food control is very important [103].

Drug analysis mainly considers the testing of raw materials and drug formulation, but it also includes the analysis of complex matrices such as foods, drinks, biological fluids and tissues. Drug analysis also involves the determination of not only active components but also the degradation intermediates of the drug [104]. A number of analytical techniques have been reported for the determination of NA drug including determination in pure form or in combination with other drugs by using spectrophotometric methods [105, 106]. fluorometric method [107] and various chromatographic methods including high performance liquid chromatography (HPLC) [108], reversed phase HPLC [109], high-performance thin-layer chromatography (HPTLC) [110] and liquid chromatography with tandem mass spectrometry (LC-MS/MS) [110, 111]. But the advantages of low instrumental cost, simple sample preparation and fast analysis, make electrochemical methods attractive choice for the analysis of pharmaceutical samples [112, 113]. The biological and electrochemical reactions (oxidation/reduction) can be assumed as they undergo similar mechanisms at the electrode surface and in the body. Important biological molecules can be investigated in different ways using an electrochemical method. The applications of electrochemistry include the determination of analyte mechanisms at the electrode surface. These redox mechanisms of the analyte give us an insight to their metabolic fate in redox processes or pharmacological activity [114].

The development of point-of-care testing requires simple, applicable and user-friendly electrochemical sensors. In order to satisfy comply with these requirements, SPCEs are among the suitable alternative [115]. SPCEs have been widely used in environmental, biomedical and industrial monitoring owing to the fact that they have low cost of production, easy operation and replacement. However, SPCEs alone do not meet our demands due to their low sensitivity and poor selectivity [116]. In the application of electrochemically activated-SPCE for the electrochemical determination of some biological molecules like dopamine by activating the SPCE potentiostatically using NaOH [117], a direct electron transfer to glucose oxidase [118], has been reported. These reports indicated that the activation of SPCE improved electrochemical

response and may be attributed to increases in the hydrophilicity surface, increased quantity of carbon-oxygen functional groups on surfaces, augmented surface roughness and/or the removal of the organic ink constituents or contaminants introduced into the printing stage [119-120].

5.1.2. Electrochemical Activation of SPCE

The solid graphite electrodes used in the printing inks of SPCEs contain some mineral insulating polymers to improve the adhesion onto the substrate. These polymers in the inks might block the electrochemically active carbon particles and increase the electron transfer resistance that will result in slower kinetics of heterogeneous reaction, and hence quasi-reversible or irreversible redox processes might occur at SPCEs. It is well known that the activation of carbon electrodes have a dramatic effect on improving the electron transfer properties of the electrodes [29]. In this work the electrochemical activation of SPCE electrode was performed by cycling 0.5 M KOH in the potential range of −1.5-1.0 V for 10 cycles at a scan rate of 100 mV s^{-1}. After activation, the electrochemical and physical properties such as peak to peak separation (ΔEp), electroactive surface areas (ESA) of the electrodes and electron transfer resistance, for $Fe(CN)_6^{4-/3-}$ couple were greatly changed. Meanwhile, the electrochemical response of NA has also been enhanced dramatically.

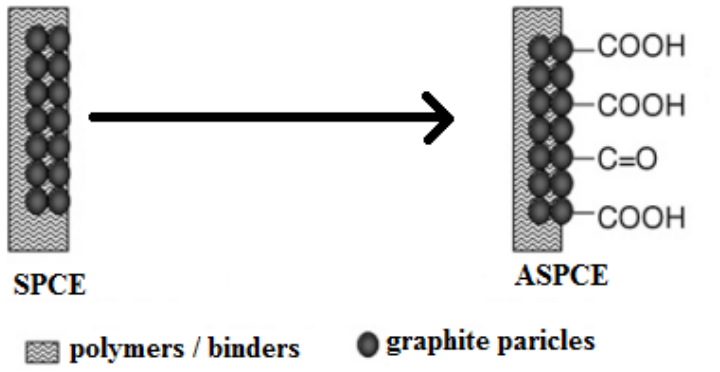

Scheme 5. Mechanism for the activation of SPCE

5.1.3. Surface Characterization

The activated-SPCE was investigated using FTIR. Figure 9 displays the FTIR spectra of bare SPCE and activated-SPCE. For the activated-SPCE, the absorption band observed at 3500 cm^{-1} is attributed to the O-H stretching and the absorption peaks at around 1600 cm^{-1} was due to

C=O group. The FTIR result indicates that during the activation of SPCE there is and incorporation of acidic and carbonyl groups [121]. Additionally, the band at around 1200 cm^{-1} can be ascribed to the C-OH stretching vibration. These results further confirm the existence of O-H groups in the activated-SPCE, which were not present in the bare SPCE [122].

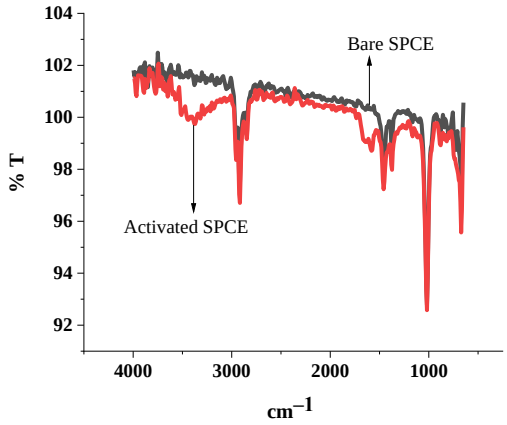

Figure 9. FTIR spectra of bare and activated-SPCE

The surface morphology of the electrode was investigated by the SEM technique. The SEM image of activated-SPCE exhibits the more cracked surface along with large defects compared to the bare SPCE. It is confirmed that the electrochemical activation greatly affects the surface morphology of SPCE. It can be seen that the small ball like structures were distributed over the activated-SPCE surface with the average size range of 56.4 to 86 nm Figure 10.

I. 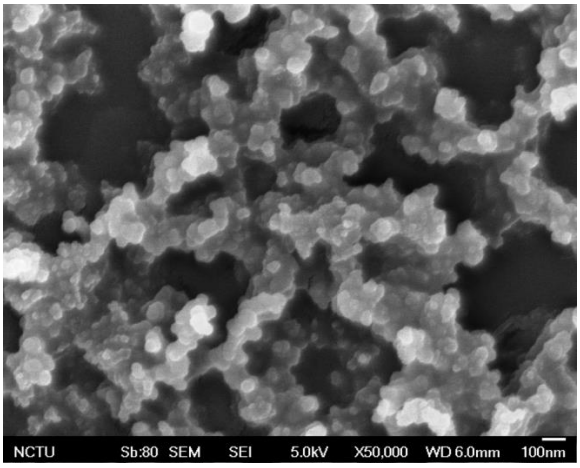

II. 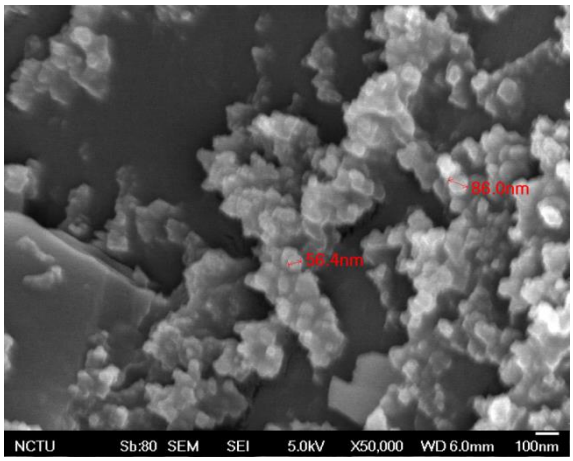

Figure 10. SEM images of bare SPCE **(I)** activated-SPCE **(II)**

5.1.4. Estimation of the Electroactive Surface Area

Electrode reaction rates and most double layer parameters are extensive quantities and have to be referred to the unit area of the surface. Knowledge of the real surface area of electrodes is therefore needed. Obviously, the electroactive surface area of an electrode is related with its geometric surface area. Accordingly, the higher the exposed surface, the higher currents are measured across the electrode–solution interface. Nevertheless, the importance of the electroactive surface area is that it reveals which portion of the surface remains available to species in solution for the transfer of charge. Strictly speaking, it measures the efficiency of the exposed surface towards the electrocatalytic reaction [123, 124].

In order to investigate whether the activated-SPCE film could increase the surface area and hence the conductivity of the sensor, the electroactive surface area of the bare SPCE and activated-SPCE were determined by cyclic voltammetry (CV) using 1 mM $K_3Fe(CN)_6$ as a probe at different scan rates. For a reversible process, the Randles-Sevcik formula equation 1 [124, 125], was used to calculate the electroactive surface area. For 1 mM $K_3Fe(CN)_6$ in 0.1 M KCl electrolyte, n = 1, $D_R = 7.6\times10^{-6}$ cm^2 s^{-1} [126]. Both the anodic and cathodic peak currents of the bare SPCE and activated-SPCE were proportional to the square root of the scan rate. Therefore, with the constant parameters of D_R, C_o, n, and the slope of the plot of I_p versus $\nu^{½}$, the electroactive surface area was calculated. For the bare SPCE, the electroactive surface area of the electrode was found to be 3.36–3.58 mm^2 and, for the activated-SPCE, the electroactive surface area was 4.6–5.3 mm^2. Thus, the electroactive surface area after modification, which measures the efficiency of the exposed surface towards the catalytic reaction, was increased by about 37–47% compared to the bare SPCE, providing an evidence for the superior conductivity of activated-SPCE film.

5.1.5. Electrochemical Impedance Analysis of Activated-SPCE

Electrochemical impedance spectroscopy (EIS) was employed to investigate the impedance changes and also the interfacial characterization of the electrode surface during the modification processes. It is a powerful method of characterizing many of the electrical properties of electrode material and their interfaces. It is widely used to investigate the electron-transfer ability of an electrode surface in a given interfacial region [74]. A semi-circle is located in the range of high

frequencies and corresponded to the electron-transfer process. The linear part at low frequency corresponded to the diffusion process [78].

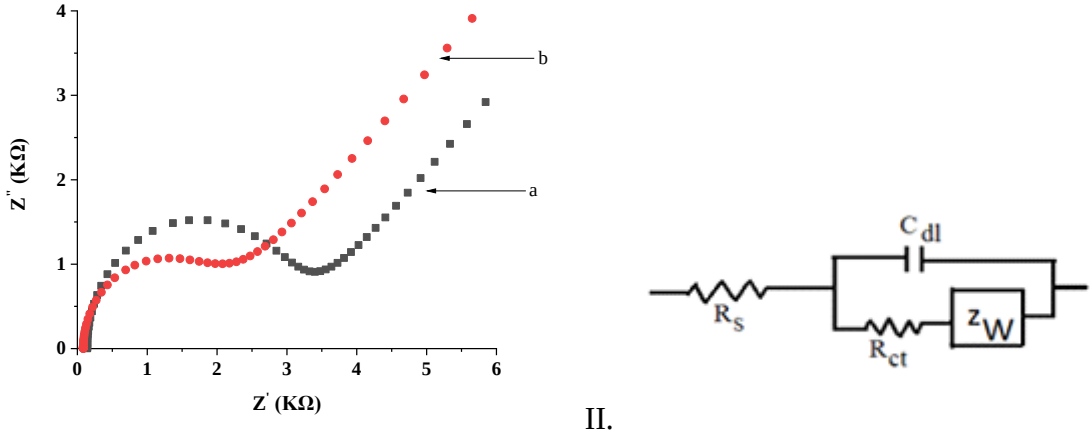

I. II.

Figure 11. (I) Nyquist plots of EIS obtained at bare SPCE (a) and activated-SPCE (b) in 5 mM $Fe(CN)_6^{-4/-3}$ (supporting electrolyte 0.1 M KCl). **(II)** Randles equivalent circuit used for data evaluation

Figure 11(I) displays the EIS Nyquist spectra of 5 mM $Fe(CN)_6^{-4/-3}$ at bare SPCE and activated-SPCE in 0.1 M KCl. The EIS results were fitted based on the Randles equivalent circuit shown in Figure 11(II). This equivalent circuit consists of the ohmic resistance of the electrolyte solution (R_s), the charge transfer resistance (R_{ct}), the Warburg impedance (Z_w) and the double layer capacitance (C_{dl}). As shown in Figure 11(I), the semicircle diameter of the Nyquist plot of the activated-SPCE, which represents the charge transfer resistance (R_{ct}) is about 462 Ω, less than that of the bare SPCE 501.6 Ω. The higher R_{ct} value of the bare SPCE shows a slow charge transfer rate. A lower charge transfer resistance observed for the activated electrode could be due to the increase of the roughness and the accumulation of the redox probe on the pinholes of the attached film. Hence, the electron transfer process of the redox probe is easier and occurs at longer distances when the film is activated. These results are also in good agreement with the CV and electroactive surface area measurements and provide evidence for the successful activation of the SPCE film.

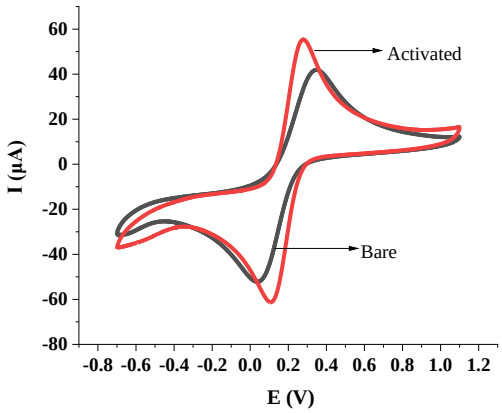

Figure 12. Cyclic voltammogram of 5 mM $[Fe(CN)_6]^{4-/3-}$ for bare and activated-SPCE at a scan rate of 100 mV s^{-1}

5.1.6. Electrochemical Behavior of NA

Figure 13 shows the characteristic cyclic voltammograms of 20 μM NA in BRB-30% DMF (pH 7.50) recorded at bare SPCE (b) and activated-SPCE (c) in the potential range of 0.3 to −1.0 V. The electrochemical behavior of 20 μM NA at the modified electrode shows a well-defined cathodic peaks (I_c) and (II_c) with peaks at −633 mV and −151 mV, respectively, and in the reverse sweep an anodic peak (II_a) appeared at −91 mV. The cathodic peak current (I_c) was related to the irreversible reduction of the nitro group in the NA to form a hydroxylamine group equation 10. And both the anodic I_a and the cathodic peak currents II_c are due to the reversible redox behavior of the hydroxylamine group as shown in equation 11 [127].

$$\mathbf{RNO_2 + 4e^- + 4H^+ \rightarrow RNHOH + H_2O} \quad (9)$$

$$\mathbf{RNHOH \leftrightarrow RNO + 2H^+ + 2e^-} \quad (10)$$

The electrocatalytic activities of bare SPCE and activated-SPCE towards NA were examined by CV and SWV methods Figure 13 and 14. The response for NA at the bare SPCE showed weak and broad (curve b) due to sluggish electron transfer, while the response was considerably improved at the activated-SPCE (curve c). The remarkable enhancement in the peak current indicate catalytic role of activated-SPCE film in the electro-reduction of NA. The interaction

between the modified electrode and NA contributed to the enhancement of the peak current which causes higher sensitivity and electrocatalytic activity [126].

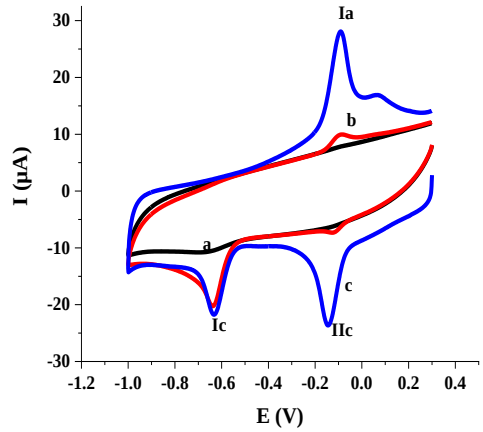

Figure 13. CVs of the supporting electrolyte (a) and 20 µ M NA (b, c) at bare SPCE (b) and activated-SPCE (c) in BRB-30%DMF (pH 7.50) at scan rate of 100 mV s^{-1}

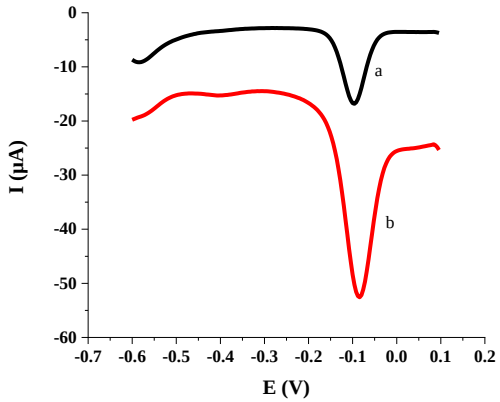

Figure 14. SWVs of 20 µM NA in BRB-30%DMF (pH 7.50) at bare SPCE (a) and activated-SPCE (b)

According to the described electrochemical redox reaction of nitro compounds in equations 12 and 13, the peak I_c can be related to the irreversible reduction of the nitro group in NA, and peaks I_a and II_c are related to the reversible redox behavior as shown in Scheme 6 [128].

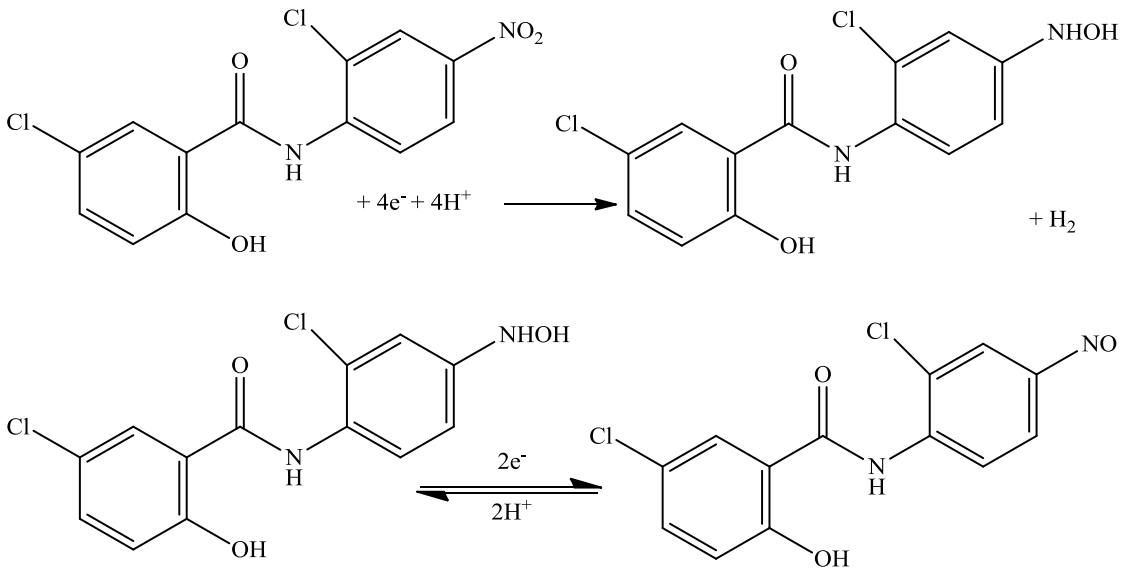

Scheme 6. The proposed electrochemical reaction mechanism for the reduction of NA on activated-SPCE

5.1.7. The Effect of pH

The effect of pH on the determination of NA at activated-SPCE Figure 15, was investigated over the range of pH 5.0–9.0 using CV. The results indicated that the peak currents of NA at the activated-SPCE increased gradually with increasing pH until it attained the maximum at pH 7.50, then decreased gradually when the pH increased further. This is probably related to the fact that NA is unstable in acidic media [129]. Therefore, a slightly alkaline environment is good for the determination of NA and pH 7.50 was chosen for the voltammetric determination at the activated-SPCE.

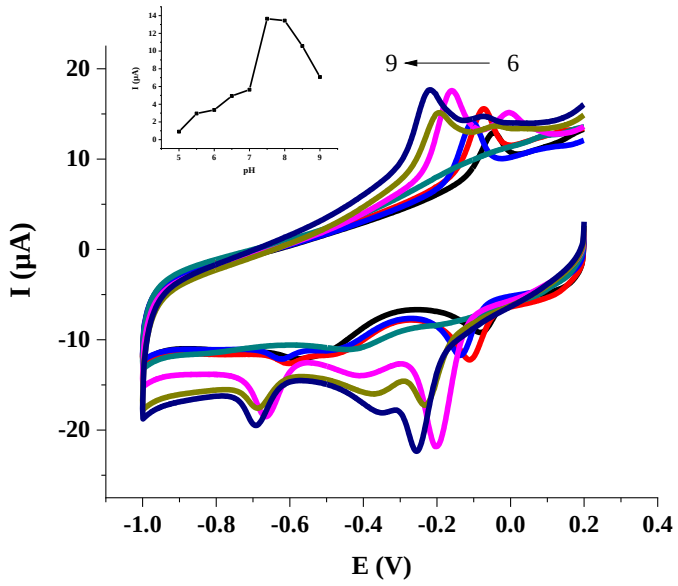

Figure 15. CVs of 20 µM NA on activated-SPCE in BRB-30% DMF (pH 6.0-9.0) at a scan rate of 100 mV s^{-1}. Inset: The plot of peak currents vs pH

The relationship between peak potentials of NA (E) and pH at activated-SPCE was demonstrated in Figure 16. The peak potential (E) is shifted negatively with the increase in pH values and the potential (E) increased linearly with rising pH. The equation and correlation coefficient obtained from the plot was E(V) = –0.05543pH + 0.24534 (R^2 = 0.99262), according to the following formula of equation 12:

$$\frac{dE_p}{dpH} = \frac{(-2.303mRT)}{nF} \quad (11)$$

Where n is the number of electron transferred in the electrochemical reaction, m is the number of protons participating in the electrochemical reaction. The ratios of m/n at the modified electrodes were all approximately to 1, suggesting that the number of electrons and protons was equal. Therefore, the electrochemical redox reaction of NA at the modified electrode is a two-electron and two-proton transfer process, which is consistent with previously reported results [130].

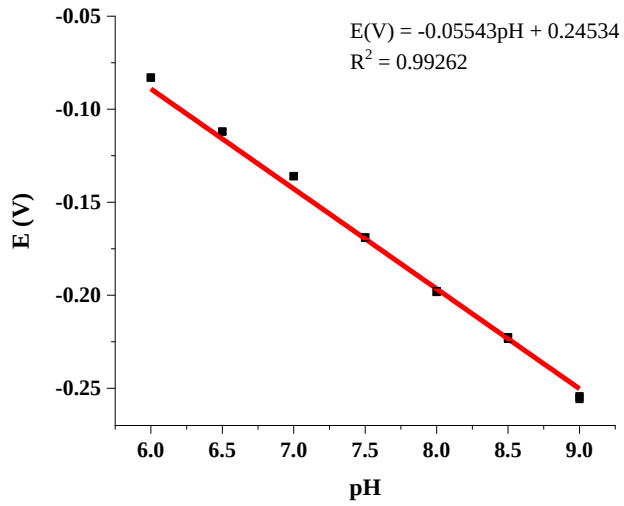

Figure 16. Plot of peak potential vs pH for 20 µM NA in BRB-30% DMF

5.1.8. The Effect of Scan Rate

In order to see the effect of scan rate on the peak currents of NA, cyclic voltammograms of 20 µM NA in 0.1 M BRB-30% DMF solution pH 7.50 were recorded at various scan rates using the activated-SPCE. The cyclic voltammogram shows a pair of reversible redox peak with symetrical shape due to the redox reaction of N-phenylhydroxyamine/nitroso derivative (equation 13) resulted from the reduction of nitro group of NA. A linear dependence found for the anodic peak current and cathodic peak current versus the scan rate v (mV s^{-1}) confirmed adsorption behavior. Moreover, the logarithm of oxidation peak currents (log I_{pa}) and reduction peak currents (log I_{pc}) show a better linear relationship with the logarithm of scan rates (log v) in mV s^{-1}, yielding the regression equation log I_{pa} (µA) = 0.998 log(v) – 6.773 (R^2 = 0.982) and log I_{pc} (µA) = 0.93 log(v) +6.66 (R^2 = 0.993), respectively. From this we could infer that the reaction of NA was controlled by adsorption process according to the data from the slopes of two linear equations ranging from 0.5 to 1 [131].

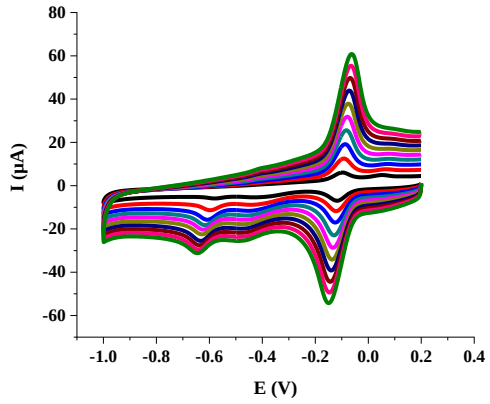

I.

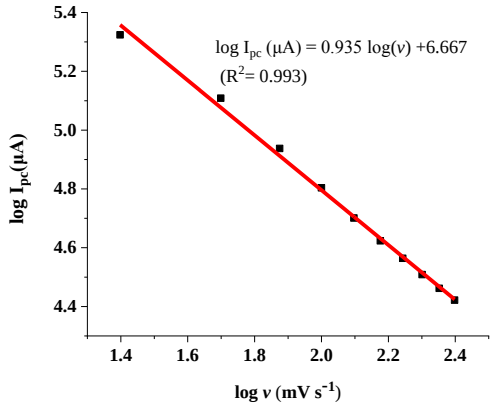

II.

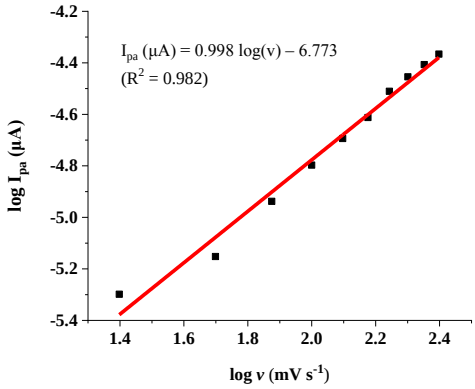

III.

Figure 17. (I) CVs of 20 µM NA on activated-SPCE at scan rates of 25-250 mV s^{-1} in BRB-30% DMF (pH 7.50). **(II)** Plot of log of I_{pc} vs scan rate **(III)** Plot of log of I_{pa} vs scan rate

5.1.9. The Effect of Accumulation Potential and Time

Since the reduction of NA at the surface of activated-SPCE is an adsorption controlled process, the effect of accumulation potential and time were studied using SWV. The effect of accumulation potential at the modified electrode on the peak current for 20 µM NA was examined in the range of −0.3 to −1.0 V at 15 s accumulation time. The peak current for NA increased sharply with the potential up to −0.50 V, and then reached a plateau over the range −0.5 to −0.70 V Figure 18 (I). Thus, the optimum accumulation potential was set at −0.5 V for the subsequent experiments.

The effect of accumulation time was also studied in the range of 0 to 120 s a −0.5 V accumulation potential. The peak current increased with accumulation time from 0 to 60 s and reached a maximum value around 60, Figure 18 (II). Upon increasing the accumulation time beyond 60 s the oxidation peak current of NA remains almost constant. Therefore, 60 s was chosen as the optimal accumulation time for the determination of NA.

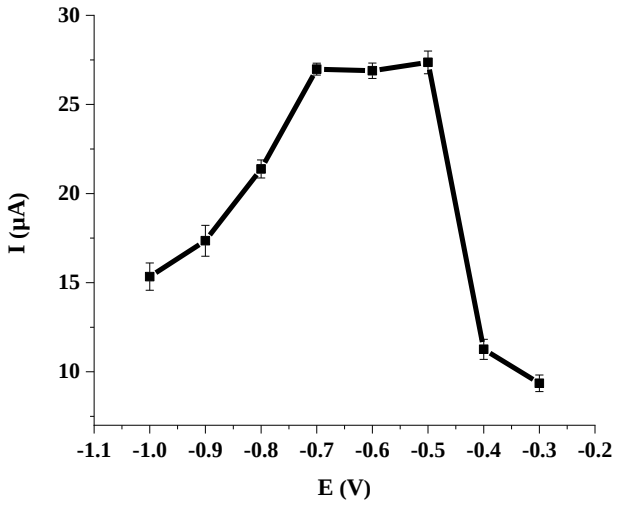

I.

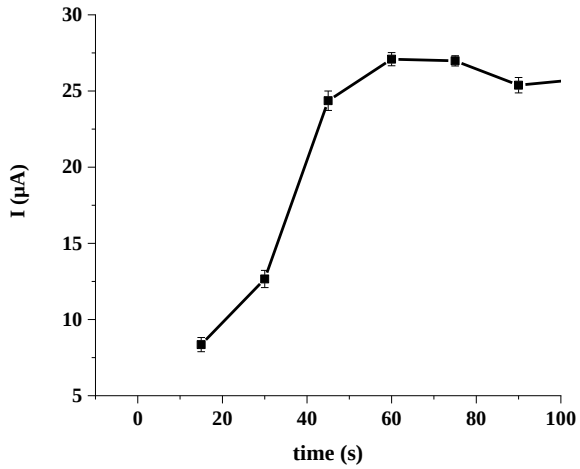

II.

Figure 18. (I) Effects of accumulation potential and **(II)** accumulation time on the peak current

5.1.10. Optimization of SWV Parameters

Square wave parameters were evaluated in order to obtain the highest signal for NA determination. The dependence of the peak current on SW parameters was studied in the range of: step potential (1–15 mV); amplitude (10–120 mV) and frequency (10–100 Hz) by keeping two of these parameters at constant value while measuring the other. By considering the optimum signal and good square wave voltammetric peak shape for NA, the optimized parameters were 4 mV step potential; 25 mV amplitude and 15 Hz frequency.

5.1.11. Determination of NA by Square Wave Voltammetric Technique

Under the optimum conditions, the square wave voltammetric responses for different concentrations of NA were recorded in BRB-30% DMF (pH 7.50) Figure 19. The cathodic peak current is linearly related to NA concentration in the range of 0.06 to 50 µM with a regression equation of: I µA = 1.74485[NA] µM − 9.37313 and R^2 = 0.99256 Figure 20. The limit of detection (LoD, $3s_b/m$) and limit of quantification, (LoQ, $10s_b/m$) was found to be 0.0051 µM and 0.017 µM, respectively; where s_b is the standard deviation of the blank and m is the slope of the calibration curve. These values were compared with similar studies reported in the literature, Table 1. As shown in the table, the analytical performance of the presently modified electrode shows promising results in terms of providing higher sensitivity and wider linear range when compared to most of the chemically modified electrodes reported for the determination of NA (Table 1).

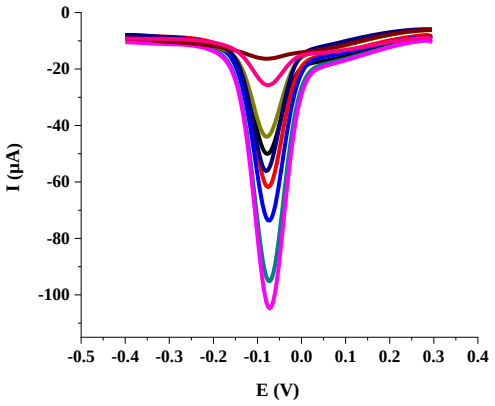

Figure 19. SWVs for varying concentrations of NA (background subtracted): 0.06, 1.5, 6, 12, 17, 22, 28, 37 and 50 µM in BRB-30% DMF (pH 7.50) at activated-SPCE

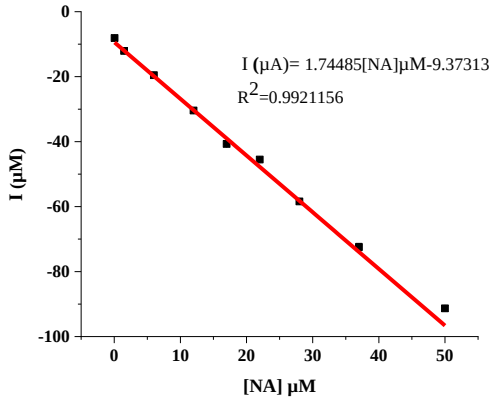

Figure 20. The plot of peak current vs. NA concentration

Table 1. Comparison of the proposed method with other electrochemical methods used for the determination of NA

Electrodes	Method	Linear Range (µM)	LoD (nM)	Reference
[a]PEDOT/GCE	DPASV	0.075–7.50	10.9	[132]
[b]ER-GO/GCE	DPV	0.020 to 23.1	6.6	[133]
[c]MWCNTs/GCE	DPV	0.023-3.3 and 5.4-26.3	7.7	[134]
[d]SWCNTs/GCE	DPV	0.023-5.4 and 6.5-19	15	[135]
[e]Pal-Gr-COOH/GCE	DPASV	0.02-0.99	4.6	[136]
[f]CNP/CS/GCE	SWASV	0.01-2	7.7	[131]
[g]PGE	DPV	0.05-10	15	[137]
Activated-SPCE	SWV	0.06-50	5.1	This Work

[a] *poly(3,4-ethylenedioxythiophene) modified glassy carbon electrode;* [b] *electrochemically reduced graphene oxide (ER-GO) modified glassy carbon electrodes;* [c] *multiwall carbon nanotubes modified glassy carbon electrodes;* [d] *single wall carbon nanotubes modified glassy carbon electrodes;* [e] *palygorskite (Pal) nanorods onto carboxyl functionalized graphene nanosheets modified glassy carbon electrodes;* [f] *carbon nanoparticle/chitosan modified glassy carbon electrode;* [g] *pencil graphite electrodes*

5.1.12. Repeatability, Reproducibility and Stability of the Modified Electrode

To investigate the repeatability of the electrochemical responses of the activated-SPCE for 20 µM of NA in BRB-30% DMF (pH 7.50), several consecutive measurements were conducted. The relative standard deviation of ten successive measurements was found to be 4.6%, which indicates good repeatability of the electrode. Similarly, the reproducibility of the method was estimated by comparing the peak current responses of three different modified electrodes prepared following a similar procedure. A RSD of 3.3% was obtained for the peak current response of 20 µM of NA, showing a very good reproducibility of the developed electrode. The stability of the modified electrode was also evaluated by measuring the current response for NA at the activated-SPCE daily for one week. After three weeks the electrode retained 96.8% of its original activity which shows good stability of the modified electrode which rules out the possibility of significant fouling and deactivation of the electrode.

5.1.13. Interference Study

The influence of various potentially interfering substances in the determination 10 μM of NA was studied under the optimum conditions. The potentially interfering substances were among those commonly found with NA in pharmaceutical formulations and/or in biological fluids. The oxidation peak currents of NA were compared before and after addition of the following potential interferents: ascorbic acid, uric acid, glucose, lactose, citric acid, sucrose, starch, *p*-nitrophenol, Mg^{2+}, Ca^{2+}, Fe^{3+}, K^{+}, Na^{+}, Cl^{-}, NO_2^{-}, SO_4^{2-} and NO_3^{-} and results are shown in Table 2. The percent changes in the peak currents was less than 5% for the studied substances except *p*-nitrophenol. This indicates that the electrode exhibited no response to a number of potentially interfering ionic and non-ionic excipients usually used in the production of the pharmaceutical formulations or are present in biological fluids. According to the result obtained only *p*-nitrophenol showed significant interference, even at equimolar concentrations. This can be attributed to the redox potential of *p*-ntrophenol which overlaps with that of NA as proved by a magnified peak at the redox potential of NA. Thus, the separation of *p*-nitrophenol is recommended prior to the electrochemical determination of NA. In general, the activated-SPCE has good selectivity and can be used for the determination of NA without significant interferences.

Table 2. Effect of interferents on the determination of NA at activated-SPCE under the optimum conditions, (average of three determinations)

Interferent	Concentration (µM)	Change in peak current response (%)
Ascorbic acid	1000	2.01
Uric acid	1000	3.23
D-Glucose	1000	3.01
Lactose	1000	2.95
Sucrose	1000	1.23
Starch	1000	0.96
Citric acid	1000	0.88
Mg^{2+}	1000	1.23
Ca^{2+}	1000	2.01
Fe^{3+}	1000	3.22
Na^{+}	1000	2.68
K^{+}	1000	2.49
Cl^{-}	1000	3.35
NO_3^{-}	1000	2.68
SO_4^{2-}	1000	4.22
NO_2^{-}	1000	1.26

5.1.14. Analytical Application

To investigate the practical applicability of the developed method, the determination of NA was carried out in vegetable and urine samples. The preparation of these samples was presented in the experimental section 4.4.2 and 4.4.3. The voltammetric measurements were carried out in using BRB 30% DMF solution pH 7.5 for both samples. The voltammogram did not show any electrochemical response at the peak potential where NA was reduced. This indicates that NA was not available in all the samples. As shown in Table 3, the obtained results analyzed by standard addition method are in good agreement with the spiked concentrations, and the RSDs of six determinations are all below 4%, demonstrating the utility of this sensor for determination of NA in these samples. To verify the accuracy of the developed method, recoveries in the range of

97-106% and 94-107% were obtained for the vegetable extracts and urine sample, respectively. The recovery result points out that the effect of the sample matrix is not significant, and hence the activated-SPCE has excellent potential to be used in real sample analysis.

Table 3. Recovery results of the determination of NA in vegetable and urine sample at activated-SPCE

Real sample	**Added (µM)**	**Obtained (µM)**	**Recovery (%)**
Vegetable	-	-	
	5.0	4.86	97.2
	12.0	12.4	103
	20	21.1	106
Urine	-	-	
	5.0	4.71	94.2
	12.0	12.6	105
	20	21.3	107

5.2. Square Wave Voltammetric Determination of Chloramphenicol at Activated-SPCE

5.2.1. Background

Chloramphenicol (CAP) is an effective antibiotic against both Gram-negative and Gram-positive bacteria. It is used mainly to avoid infections in small wounds, as well as to treat many diseases including cystic fibrosis, conjunctivitis, cholera, typhoid fever, plague, and ear and skin infection [138]. However the usage CAP can be a cause to bone marrow, gray baby syndrome and hematopoietic toxicity. Though, its application is limited in United States for infection treatment it is highly, employed in developing countries due to its low cost [139]. The main waste water sources sewage, discharge from treatment plants and septic systems contains different type pollutants, like pharmaceuticals, cosmetics, hormones, and other various organic wastes [140]. The major group of micropollutants that are growing widely and of concern is antibiotics. They are chemotherapeutic compounds used in animal husbandry and in human health for preventing or treating infections, as growth promoters and sometimes used as food preservatives. The antibiotics have gained more attention not only to their biological activity but also due to the possibility to cause the development of resistance genes in bacteria of the environment that reduce the long-term effectiveness of these compounds [141]. Public apprehension regarding the use of CAP in animals and humans has led to the development of analytical methods for its detection in milk [142, 143], honey [144-146] urine [147-149] and pharmaceutical products [150, 151].

A number of analytical techniques like solid-phase extraction based on molecularly imprinted polymer [152], capillary electrophoresis [153], fluorescence [154], ultra-high pressure liquid chromatography tandem mass spectrometry [155-156], liquid chromatography with tandem mass spectrometry [157-158], high performance liquid chromatography [159] and gas chromatography [160] have been reported for determination of CAP in pure form or in combination with other drugs. Analyses of low concentration of drugs like CAP in biological samples such as blood, serum, urine, and so forth, often required determination methods that have low detection limits and applicable to small samples. Electrochemical techniques are powerful and versatile analytical techniques that offer high sensitivity, accuracy, and precision as well as wide linear dynamic range, with relatively low-cost instrumentation. After the development of more

sensitive pulse methods, electroanalytical techniques are more regularly used for the drug analysis in their dosage forms and especially in biological samples. Moreover, electroanalytical techniques can easily solve many problems of pharmaceutical interest with a high degree of accuracy, precision, sensitivity, and selectivity [161].

The main concern in health care is the proper medication dosage in pharmaceutical formulations and in physiological fluids. Therefore qualitative and quantitative data are highly required for pharmaceutical products in order to check for appropriate drug content and to detect any counterfeit or industrial production error [1]. One of the main challenges that analytical chemists face is developing a method suited to perform rapid 'in-situ' analyses for sensitive and accurate determination. As the demand for real time monitoring of analytical samples increases, both practical and economic interests have driven the development of screen printing technology. The development on screen-printing technology and the serial production of disposable low-cost electrodes for the electrochemical determination of a wide range of substances is widely growing. The printing technology combines easy use and portability with simple and inexpensive analytical methods. It can be applied for in-situ analysis and with its improved analyte detection, as has been shown over the past several years [20-21]. The screen printing technology provides manufacturing large numbers of electrodes in a reproducible, low-cost, and disposable format. The possibility to incorporate chemically functionalized material gave an enormous advantage for SPEs [21].

In this work, the electrochemical oxidation–reduction behavior of CAP on electrochemically activated-SPCE investigated. The introduction of edge plane carbonyl groups on the activated-SPCE was found to act more or less like an edge plane graphite electrode or CNT [162].

The research on carbon nanotubes and graphene has enriched the scope of SPEs in electro-analysis. The improved electrocatalytic properties of CNT towards several target analytes were attributed to the defect/edge plane-like sites [30]. The electrochemical activation of screen printed carbon electrodes helps to overcome the variation in the carbon inks used in the printing process [163]. Based on flexibility and robustness of the SPCE a simple and facile alternative method for the determination of CAP sample and spiked milk sample was established in this study. This new sensing system possesses the following advantages. Firstly, it is more sensitive

and also it exhibits low cost and operational simplicity since there is no complicated modification of the electrode surface before detection.

5.2.2. Electrochemical Activation of SPCE

The electrochemically activated-SPCE electrode was prepared according to the procedure described in 5.1.2.

5.2.3. Electrochemical Behavior of CAP

Figure 21 shows the characteristic cyclic voltammograms of 50 μM CAP in 0.10 M phosphate buffer (pH 6.50) recorded at bare SPCE, and activated-SPCE in the potential range of 0.2 to −1.0 V. Upon scanning from positive to negative potentials, a well-defined cathodic peak (F_1) at −0.59 V is observed. When the scan direction is changed, one additional peak is obtained: an anodic peak (F_2) at −0.069 V and a cathodic peak (S_1) at −0.036 V (second cycle), was observed. The cathodic peak (S_1) and the anodic peak (F_2) are reversible. The peak at −0.59 V (F_1) could be assigned to the irreversible reduction of the nitro group of CAP to phenylhydroxylamine, which is due to four electrons and four protons transfer mechanism, whereas the anodic peak (F_2) indicates the oxidation of hydroxylamine to the nitroso group derivative and the cathodic peak (S_1) represents the reduction of the nitroso group derivative to hydroxylamine. This redox process follows a two electron and two proton transfer mechanism Scheme 7 [95]. As shown in Figure 21, no obvious electrochemical response for CAP was observed at the bare SPCE. On the contrary, a well-defined peak of CAP was observed at about −0.032 V for the activated-SPCE indicating its high electrocatalytic activity.

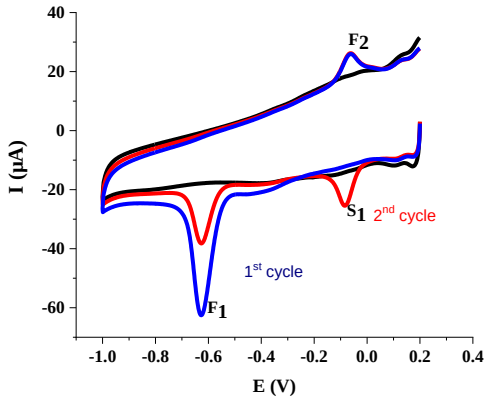

Figure 21. Cyclic voltammograms of 50 µM CAP at bare SPCE (I) and at activated-SPCE (II) in 0.1 M PBS for two consecutive cycles (pH 6.50) at scan rate of 100 mV s^{-1}

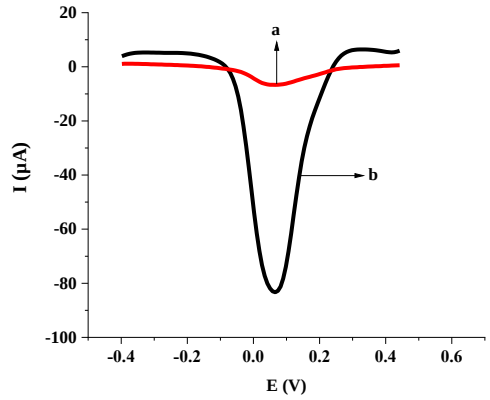

Figure 22. SWVs of 50 µM CAP in 0.1 M of phosphate buffer (pH 6.50) at bare SPCE (a) and Activated-SPCE (b)

The mechanism of the redox reaction of CAP can be described as follows. The well-defined cathodic peak (F_1) at −0.608 V for the activated-SPCE corresponds to the direct reduction of the nitro group to phenyl hydroxylamine, due to a four electron and four proton transfer mechanism. During the reverse scan, one anodic peak (F_2) at −0.067 V and one cathodic peak (S_1) at −0.081 V were obtained (observed in the second run only). The anodic peak indicates the oxidation of hydroxylamine to the nitroso group derivative, whereas the cathodic peak represents the reduction of the nitroso group derivative to hydroxylamine. This redox process follows two electrons and two protons transfer mechanism [164]. It is to be noted that the peak current of the reduction process at −0.608 V is higher than the oxidation peak current at −0.069 V and the

reduction peak current at −0.081 V, indicating the reduction of CAP at the Activated-SPCE shows greater tendency to form hydroxylamine under neutral conditions. As scheme 7 shows, the Activated-SPCE displayed higher peak currents than that of the bare electrode. For the bare SPCE, a very low peak current was observed and this is an indication of the poor electrocatalytic activity of it towards CAP detection.

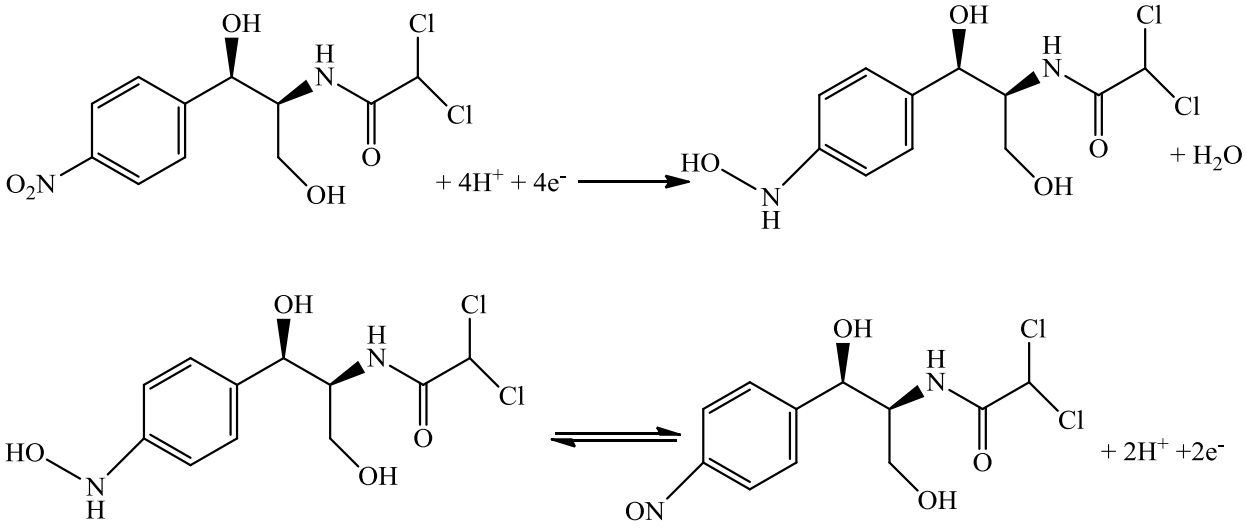

Scheme 7. Electrochemical reaction mechanism for the reduction of CAP on the activated-SPCE

5.2.4. The Effect of pH

The voltammetric response of CAP varied according to the supporting electrolytes used. Alkaline, acidic and neutral supporting electrolytes were used to measure the current response for 50 µM CAP. It was found that neutral media is appropriate for electrochemical determination of CAP at the activated-SPCE; thus, Britton-Robinson, citrate, citrate-phosphate and phosphate buffer solution were tested as supporting electrolytes. The results obtained showed that sharp and large peak current was obtained while using phosphate buffer solution as a supporting electrolyte and thus it was selected as the appropriate solvent for further study.

The effect of pH on the voltammetric signals for CAP oxidation was investigated in 0.1 M PBS in the pH range 4.0 to 8.0 using cyclic voltammetry. It was noted that the current response and the peak potential of CAP significantly changed with increasing pH from 4.0 to 8.0 which shows that the oxidation of CAP is pH dependent. As shown in Figure 23, the oxidation peak current of

CAP increased with increasing pH from 4.0 to 6.5 and then a gradual decrease in current was observed from 6.50 to 8.00 so pH 6.50 was selected for further analysis. A decrease in the peak current response for CAP with increasing pH revealed that the detection of CAP at the activated-SPCE is feasible only in a neutral medium. The relationship between the reduction peak potential and pH is depicted in Figure 23. A negative shift in the peak potential of CAP was noted when the pH of the electrolyte solution increases. The linear regression equation obtained from the cathodic peak potential vs. pH plot is $E_{pc}(V) = -0.05153pH - 0.25276$; $R^2 = 0.99534$. The slope value from the linear graph 51.55 mV pH^{-1} indicates that CAP reduction at the surface of activated-SPCE involves the transfer of equal number of protons and electrons [165].

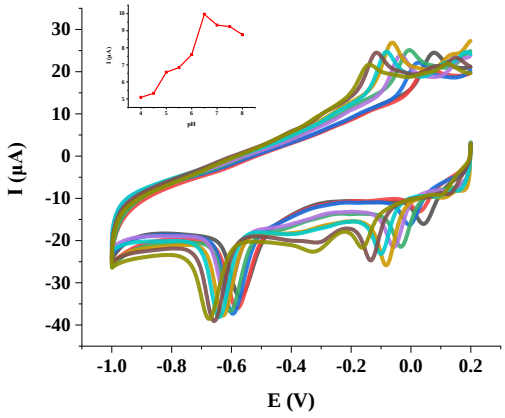

Figure 23. CVs of 50 μM CAP at different pH values (4.0–8.0) at activated-SPCE in 0.1 M PBS (pH 6.50) at scan rate of 100 mV s^{-1}; Inset: The plot of peak currents vs pH

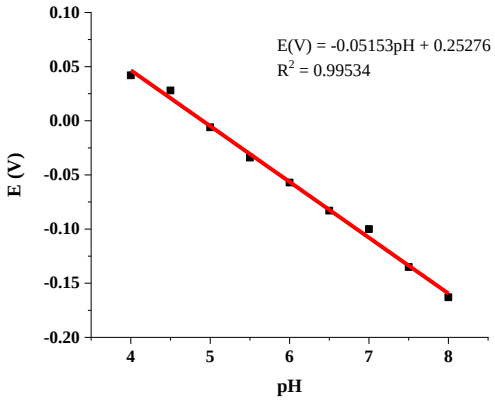

Figure 24. Plot of peak potentials of 50 μM CAP as a function of pH at activated-SPCE in 0.1 M of PBS (pH 6.50) at scan rate of 100 mV s^{-1}

5.2.5. The Effect of Scan Rate

The effect of potential scan rate on the oxidation current of CAP was investigated by cyclic voltammetry Figure 25 in PBS pH 6.5 containing 50 µM CAP. The plot of the oxidation reduction peak current of CAP *vs*. scan rate in the range 50-275 mV s^{-1} Figure 26 is linear with a regression equation of: Ipa (µA) = 0.004675ν (mV s^{-1}) + 2.10347; with R^2 value of 0.99719. Moreover, the study of log I_p vs log ν, with a regression equation: log I (µA) = 0.83171log ν − 0. 84933, R^2 = 0.9919 gives the slope value of 0.83171which is closer to 1. Additionally, the peak potential slightly shifted to the positive direction with increasing scan rates. This result suggests that the electrochemical oxidation of CAP at the surface of activated-SPCE is predominantly an adsorption controlled process [166].

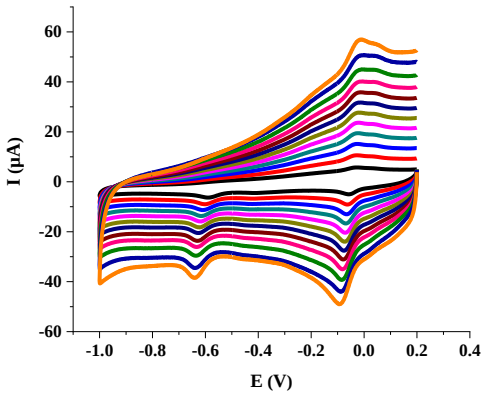

Figure 25. CVs of 50 µM of CAP at activated-SPCE at scan rates of 50–275 mV s^{-1} in PBS pH 6.50

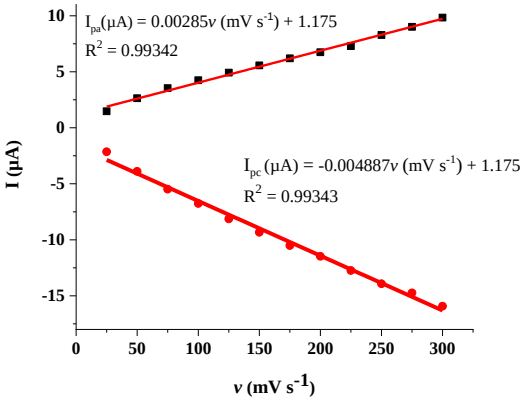

Figure 26. Anodic and cathodic peak current of CAP vs scan rate

5.2.6. The Effect of Accumulation Potential and Time

The sensitivity of the sensor is undoubtedly improved by optimizing accumulation parameters; potential and time. The effect of varying the accumulation potential on the reduction current of CAP was studied in the range 0.0 to −1.0 V with a difference of 0.1 V at an accumulation time of 15 s using SWV. The current response increased up to −0.8 V and decreased after −0.8 V Figure 27 (I). Therefore, the accumulation potential of −0.8 V was chosen as an optimum potential for further measurements.

The effect of accumulation time on the reduction peak current for 50 μM CAP was also investigated in the range 15–115 s with a difference of 15 s by SWV, and the results as illustrated in Figure 27 (II). The peak current increased with increasing accumulation time till it reach 60 s and then a current plateau was observed as a result of surface saturation. Therefore, 60 s was chosen as the optimal accumulation time for the determination of CAP.

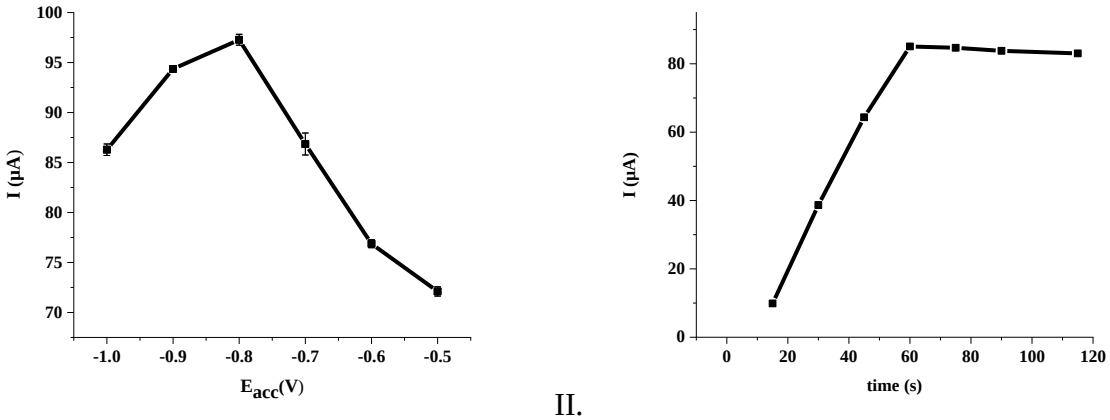

I. II.

Figure 27. (I) Effects of accumulation potential and **(II)** accumulation time on the peak current of 50 μM CAP in PBS (pH 6.5).

5.2.7. Optimization of SWV Parameters for CAP Determination

Square wave parameters were evaluated in order to obtain the highest signal for CAP determination. The dependence of the peak current on SW parameters was studied in the range of: step potential (1–15 mV); amplitude (10–120 mV) and frequency (10–100 Hz) by keeping two of these parameters at constant value while measuring the other. By considering the optimum signal and good square wave voltammetric peak shape for CAP, the optimized parameters were 8 mV step potential; 90 mV amplitude and 30 Hz frequency.

5.2.8. Determination of CAP by Square Wave Voltammetric Technique

The determination of CAP was performed under the optimized conditions using square-wave voltammetry. Figure 28 shows the SW voltammograms with increasing concentration of CAP in 0.1 M PBS (pH 6.5) using activated-SPCE as the working electrode. The peak current versus concentration plot for CAP is linear in the range of 0.05 to 100 μM, Figure 29. The linear relationship gave the regression equation: Ip(μA) = −1.68[CAP](μM) − 3.6 and R^2 = 0.99517. The limit of detection (LoD, $3s_b/m$) and limit of quantification (LoQ, $10s_b/m$), were found to be 0.02 and 0.067 μM, respectively; where s_b is the standard deviation of the blank measurements (n = 6) and m is the slope of the analytical calibration curve [167].

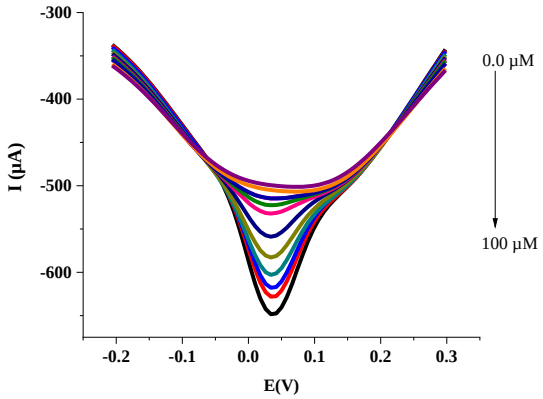

Figure 28. SWVs for varying concentrations of CAP: 0.0, 0.05, 0.5, 5.0, 7.5, 15, 30, 45, 65, 80 and 100 µM in 0.1 M PBS pH 6.50 at activated-SPCE

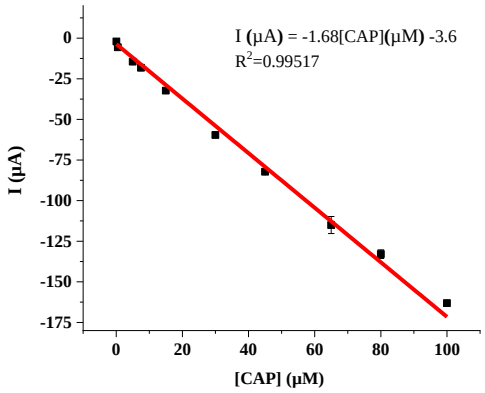

Figure 29. The plot of peak current *vs*. CAP concentration

Table 4 presents the analytical performance of different modified electrodes and techniques that have been previously reported in the literature for the determination of CAP. The performance of the present sensor is superior to most of the previous sensors reported in the literature in terms of sensitivity and linear dynamic range (Table 4), which can be attributed to the presence of oxygen functionality at the surface of the sensor. Besides, the modification of the present sensor is very simple and does not require much time.

Table 4. Comparison of the performance of the proposed method with other electrochemical sensors used for the determination of CAP

Electrodes	Method	Linear Range (µM)	LoD (µM)	Reference
[a]Fe_3O_4/GCE	SWV	0.09-47	0.009	[168]
[b]Gr/CuPc/GCE	DPV	0.01- 20	0.027	[164]
[c]MWCNT–CTAB–PDPA/GCE	DPSV	0.01- 10	0.002	[95]
[d]EPC/GCE	SWV	0.01-1 and 1-4	0.0029	[169]
[e]GO/ZnO/GCE	DPV	0.2–7.2	0.01	[170]
[f]Z-800/rGO/GCE	DPV	1-180	0.25	[171]
[g]MoS2‑IL/GO/GCE	DPV	0.1-400	0.047	[172]
[h] rGO/PdNPs/GCE	DPV	0.05-100	50	[173]
[i]Mn_2O_3 TNS/SPCE	DPV	0.015-1.28 & 1.35-566.3	4.26	[174]
Activated-SPCE	SWV	0.05-100	0.02	This Work

[a]Fe_3O_4 nanoparticles, [b]Graphene/Copper Phthalocyanine Nanocompositse, [c] multi-walled carbon nanotube–cetyltrimethylammonium bromide–poly(diphenylamine), [d]exfoliated porous carbon, [e] graphene oxide hierarchical zinc oxide nanocomposite, [f]zeolitic imidazolate framework reduced graphene oxide, [g] de-layered molybdenum disulfide/graphene oxide nanocomposites, [h] palladium nanoparticles decorated reduced graphene oxide, [I] manganese(III) oxide tiny nanostructures screen printed carbon electrodes.

* The LoQ which 0.067µM is above the lower calibration curve.

5.2.9. Repeatability, Reproducibility and Stability of the Modified Electrodes

The repeatability of the activated-SPCE was investigated by measuring the SWV signals in 0.1 M PBS solution (pH 6.50) containing 50 µM CAP. The relative standard deviation (RSD) of the peak currents obtained for the same electrode after five consecutive measurements was 1.37%. On the other hand, the reproducibility of activated-SPCE was examined by comparing the responses of three different screen printed carbon electrodes prepared following the same experimental procedure. The RSD of the peak currents between three different electrodes measured independently was found to be 3.6%. The stability of the sensor was examined after keeping it in an open air for 15 days and the peak current retained 95.3% of its initial value. The

results show that the developed modified screen printed electrode provided excellent repeatability, reproducibility, and stability towards the electro-oxidation of CAP.

5.2.10. Interference Study

Selectivity of a sensor plays an important role in the determination of analytes in various samples. The influence of various potentially interfering substances in the determination 50 μM of CAP was studied under the optimum conditions. Oxidation peak currents of CAP were compared before and after addition of the following potential interferents: ascorbic acid, lactose, urea, D-glucose, glycine, *p*-nitro phenol, Zn^{2+}, Ca^{2+}, Mg^{2+}, K^{+}, Na^{+}, Cl^{-} and NO_3^{-} and the results are shown in Table 5. The percent changes in the peak currents were less than 5% for all the studied substances except that of *p*-nitrophenol. This indicates that the electrode exhibited no response to a number of potentially interfering ionic and non-ionic excipients usually used in the production of the pharmaceutical formulations or are present in biological fluids. The interference of *p*-nitrophenol can be attributed due to the overlap of the redox potential of it with that of chloramphenicol as proved by a magnified peak at the redox potential of CAP. Thus, the separation of *p*-nitrophenol is recommended prior to the electrochemical determination of chloramphenicol. In general, the activated-SPCE has good selectivity and can be used for the determination of CAP without significant interferences.

Table 5. Interference effect of some foreign species on the peak current response of 50 µM CAP at activated-SPCE

Interferents	Concentration (µM)	Signal Change (%)
ascorbic acid	5000	2.36
Lactose	5000	2.33
Urea	5000	3.25
D-glucose	5000	4.12
Glycine	5000	1.25
Zn^{2+}	5000	2.36
Ca^{2+}	5000	2.33
Mg^{2+}	5000	3.69
K^{+}	5000	1.05
Na^{+}	5000	0.92
Cl^{-}	5000	1.23
NO_3^{-}	5000	0.92

5.2.11. Analytical Application

The practical application of the developed sensor was demonstrated by determining CAP-eye drop in the commercial pharmaceutical tablet formulation and milk samples. The experimentally detected values and the labeled values were compared, Table 6. It was found that the result obtained using the proposed sensor is in good agreement with the labeled values with RSD ≤ 3%. Therefore, it is recommended that the proposed sensor can be utilized successfully for the determination of CAP in pharmaceutical preparations. Moreover, the accuracy and reliability of the proposed method was checked by spiking the pharmaceutical tablet formulations and milk samples with appropriate quantity of the standard CAP and calculating the percent recovery values. The milk samples were prepared according to the procedure described section 4.4.1 and standard addition method was used for the assay of CAP in the milk samples. The results are shown in Table 7. As can be seen from the table, the recovery results lie between 93% and 105%, indicating that the effect of the sample matrix is not significant and hence the activated-SPCE has excellent potential to be used in real sample analysis.

Table 6. The recovery of CAP spiked in CAP-eye drop sample (n = 3)

Added (μM)	Found (μM)	Recovery (%)
0	15.1	-
10	26.2	104

Table 7. Detection of CAP in milk products (n = 3)

Added (μM)	Found (μM)	Recovery (%)
10	9.34	93.6
20	20.5	102
50	51.6	103

5.3. Square Wave Voltammetric Determination of Nicotine at Electrografted Screen Printed Carbon Electrode

5.3.1. Background

Nicotine, 3-(1-methyl-2-pyrrolidinyl) pyridine, is an alkaloid abundantly found in the nightshade family of plants called *Nicotiana tabacum* L., Solanaceae. It is the major ingredient of tobacco [175]. Nicotine intoxication is rarely seen because the doses of nicotine found in most commercially available products are quite low. However, its toxicity has been reported with oral ingestion of liquid nicotine that is used in electronic cigarettes as these liquids can contain lethal doses of nicotine if ingested excessively [176]. However intake of nicotine from the commercially available cigarettes produces stimulant effects, such as increased heart rate and blood pressure, arousal, and reduction of anxiety. At high doses, nicotine can produce bradycardia, hypotension, and depressed mental status due to ganglionic blockade [177]. Tobacco addiction produces devastating health consequences, including premature death in half of lifelong smokers. Mortality from smoking is such that half of the deaths occur in middle age [178]. Apart from its harmful effects, relevant research analysis have been made to find out its medicinal values, especially in the cardiovascular, respiratory disorder in lung cancer and age related disease like Alzheimer and Parkinson diseases [179]. Substantial evidence indicates adverse effects of smoking on COVID-19 including predisposition to the virus infection, severity of progression, and mortality. However, there is a meta-analysis report that concludes that active smoking is not associated with severity of coronavirus disease, although this contention has been challenged. Still, some studies claim to have found a lower incidence of hospitalized COVID-19 patients among smokers [180].

The determination of nicotine is an important issue for the tobacco industry, since the quality of the product can be determined by its nicotine content. The nicotine content of tobacco varies with tobacco type, but the normal nicotine level range goes from 1% to 3% [181]. Therefore, its determination is important in medicine, toxicology and tobacco industry. Over the past two decades, several analytical techniques including high-performance liquid chromatography [182-184], gas chromatography-mass spectrometry [185-187], high performance capillary electrophoresis [188], capillary electrophoresis [189], capillary electrophoresis coupled with electrochemluminescence [190] and spectrophotometry [191, 192] were used for its

determination. In addition to the requirement of hi-tech and expensive instrumentation the above mentioned analytical methods possess huge disadvantages due to the loss of significant amount of analyte during the tedious sample preparation in extraction, purification and prolonged analysis time. Detection of biological molecules using electrochemically modified electrodes has also attracted great interest in sensor applications since this method combines chemical recognition layer and the benefits of electrochemical methods (such as selectivity, sensitivity and speed) [193]. The main challenge for the electrochemical nicotine sensors is that the oxidation of nicotine occurs at a very positive potential, which outrange the potential window of typical working electrodes. Effectively decreasing the over potential with improved current is required for the oxidation of nicotine with enhanced analytical performance of the sensors. In this work, this is achieved by using carbon based materials electrografted using *para*-aminobenzene sulfonic acid (*p*-ABSA) on an activated-SPCE.

Electrografting (spontaneous or through reduction) of diazonium salts provide highly reactive aryl radicals that bind very strongly to substrate surfaces through covalent bonds to give composite materials as shown in Scheme 8 [194]. The covalent modification of carbon surfaces by electrografting was performed with the oxidation of primary amines and the reduction of aryldiazonium cations, which allows the attachment of organic moieties on carbon surfaces through N-C and C-C bonds, respectively. Even though these electrografting methods have their inherent advantages and limitations, all of them represent an extensive library for the functionalization of carbon surfaces with a wide diversity of organic groups [195]. The advantage of an electrografted layer (complete monolayer or submonolayer) of aryl groups is it results in a very strongly attached and extremely stable electrode, and due to this stability [196]. Several attempts have been made to construct electrochemical sensors or biosensors by grafting on SPCEs for trace uranium analysis [197], electrografted carboxylic function containing group SPCEs for trace metal analysis [198], hydrogen peroxide biosensor based on electrografted organic film [199] and electrochemical immunosensor for milk allergen β-lactoglobulin based on electrografting of organic film on graphene modified SPCEs [200].

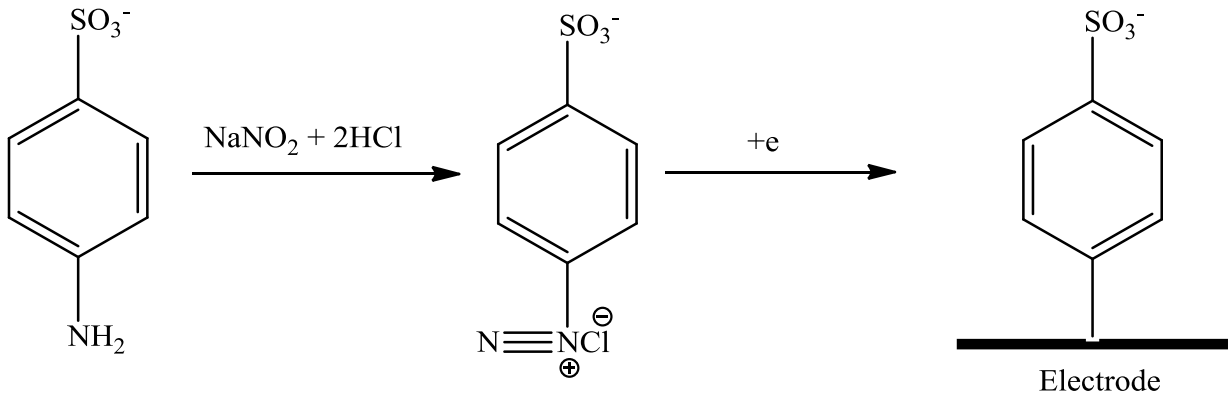

Scheme 8. Electrografting of *p*-ABSA

Even though the exact oxidation mechanism of nicotine has not been determined up to now, according to a hypothesis proposed its oxidation mechanism in alkaline solutions at boron-doped diamond electrode involves the formation of methanol and substitution of the CH_3 by OH in the tertiary nitrogen of pyrrolidine ring with two electron transition scheme 9 [201-202].In this work, the electrochemical oxidation–reduction behavior of nicotine were studied on *p*-ABSA grafted screen printed carbon electrode (SPCE) after treating the bare SPCE using 0.5 M KOH. The introduction of sulfonic acid group to the conductive SPCE was found to be an effective sensor for the electrochemical determination of nicotine.

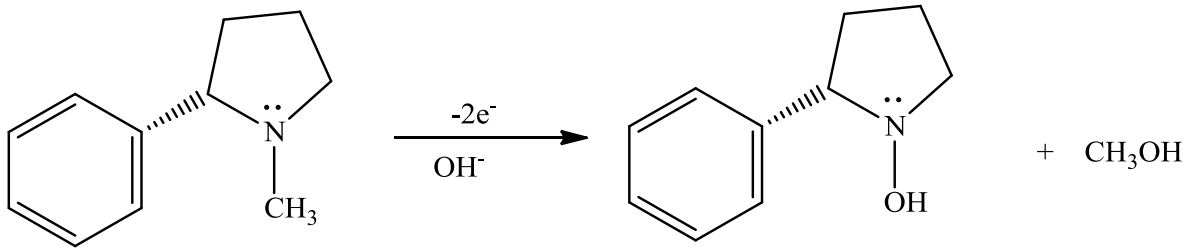

Scheme 9. Suggested mechanism for the reaction of nicotine in alkaline media

5.3.2. Electrografting of *p*-Aminobenzene Sulfonic Acid

Prior to modification, SPCE was subjected to an electrochemical activation according to the procedure 4.7.1. This process helps to expose the conductive cite of the screen printed carbon electrode surface which is covered by polymer binder used in the electrode [203]. Then the electrode surface modification was carried out in the diazotation mixture using the method as described in [204] with slight modification. The sample solution was prepared according to

procedure 4.7.2. The the diazonium cation generated by in-situ reaction was dropped into the surface of the electrodes covering the whole area. Thereafter the electrochemical grafting was performed by linear sweep voltammetry by cycling in the potential range 0.0 to −1.0 V for 15 cycles. After modification, the electrode was rinsed with distilled water and used without any further treatment.

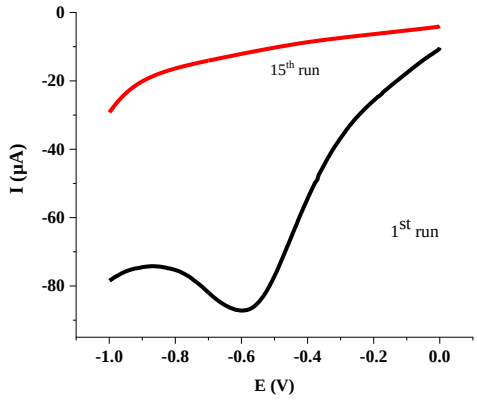

Figure 30. Linear sweep voltammogram for the in-situ generated *p*-ABSA in the diazotation mixture (10 mM $NaNO_2$ + 5 mM *p*-PABSA in 0.5 M HCl) in SPCE with the potential range of 0.0 to −1.0 at a scan rate of 100 mV s^{-1}

5.3.3. Electrochemical Characterization of *p*-ABSA Modified Electrode

Cylic voltammetry using ferri/ferrocyanide solution is a useful tool to monitor the behavior of modified electrode because electron transfer could take place either through the barrier or through the defects in the barrier. Therefore, this tool was used to investigate the blocking behavior and to confirm the electrochemical modifications of the electrode surface [205].

Cyclic voltammograms for bare SPCE and *p*-ABSA/SPCE are shown in Figure 31. The characteristic anodic and cathodic peak potentials were observed in the case of the bare SPCE. The redox peak shape for *p*-ABSA modified electrode declined, illustrating the successful covalent attachment of *p*-ABSA with electrode surface that hinders the diffusion of the probe towards the electrode surface. The negatively charged terminal sulfonic acid group (SO_3^-) acts as an electrostatic barrier that repels $[Fe(CN)_6]^{4-/3-}$ anions and lowers the ability of the redox probe to access the layer and retards the electron transfer kinetics between the redox probe and the electrode.

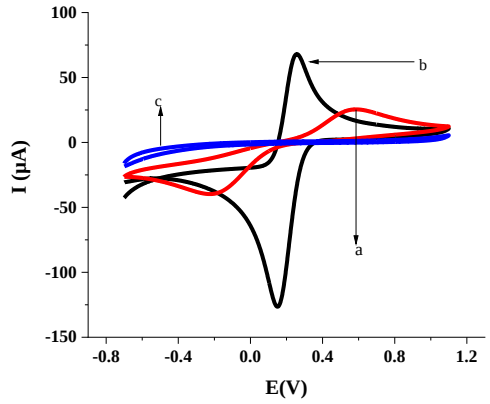

Figure 31. Cyclic voltammograms of 5 mM $[Fe(CN)_6]^{4-/3-}$ at scan rate of 100 mV s^{-1} for; bare (a), activated-SPCE (b), and *p*-ABSA grafted SPCE (c)

5.3.4. Electrochemical Impedance Spectroscopy

Electrochemical impedance spectroscopy can also provide detailed information on the charge transfer ability of the modified electrode. Faradic impedance spectra are shown in Figure 32 for the bare, activated-SPCE and *p*-ABSA grafted SPCE. The results were very similar to those obtained with CV shown in Figure 31. The semicircle diameter of the Nyquist plot of the activated-SPCE and bare SPCE was described in 5.1.5. After modified with *p*-ABSA, R_{ct} increased, which was reflected by the appearance of substantial increase in the semicircular part of the spectrum, indicating that the *p*-ABSA successfully attaches on the SPCE surface and hindered the charge transfer.

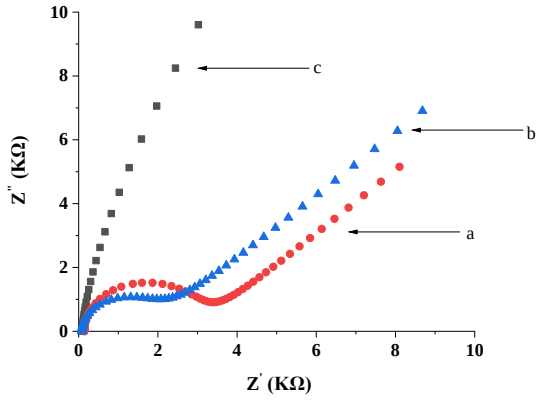

Figure 32. Nyquist plots of 5 mM $[Fe(CN)_6]^{4-/3-}$ at; (a) bare SPCE (b) activated-SPCE (c) *p*-ABSA grafted SPCE

Compared with both the bare SPCE and activated-SPCE, the *p*-ABSA grafted SPCE showed a larger R_{ct} after modification with *p*-ABSA. The results indicate that *p*-ABSA plays a role similar to a non-conductive layer and makes the electron transfer more difficult. The R_{ct} of the *p*-ABSA grafted SPCE increases dramatically with increase of pH, due to the inhibition of the electron transfer. It is possible that the full deprotonation of sulfonic acid groups causes some surface structure change on the *p*-ABSA film as pH increases which completely block the electrode surface [206-207].

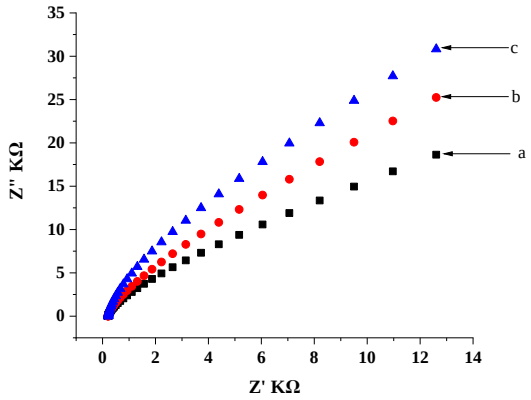

Figure 33. Nyquist plots of 5 mM $[Fe(CN)_6]^{4-/3-}$ in *p*-ABSA/SPCE at a) pH 3.5 b) pH 5.5 and c) pH 7

5.3.5. Surface Characterization

The FTIR spectrums were recorded for the bare SPCE and *p*-ABSA/SPCE. Figure 34 shows the FTIR spectrum of bare, activated-SPCE and *p*-ABSA grafted SPCE. The most intense and broad peaks occur in the range of 3320-3500 cm^{-1} attributed to O-H stretching vibrations of hydroxyl groups on the surface of the SPCE. The relative intensity of the O-H stretching band for the activated-SPCE has decreased as compared to the *p*-ABSA grafted SPCE, which indicates that C–OH still exists, but in lower proportion. The formation of GO like structure is confirmed by the appearance of the bands for C=O stretching vibrations of the carbonyl group of GO at ~1737 cm^{-1} [208].

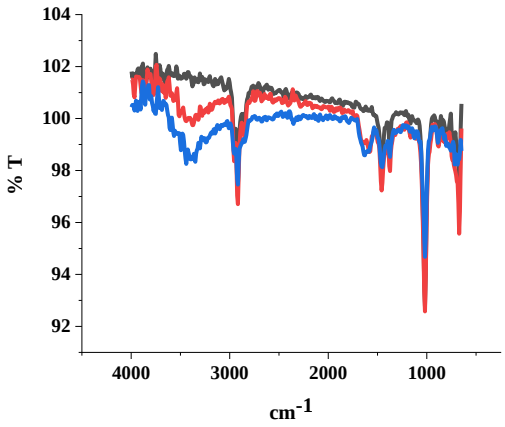

Figure 34. FTIR spectrum of bare SPCE (a) and *p*-ABSA/SPCE (b)

The covalent attachment of *p*-ABSA was also confirmed by UV-Vis spectroscopic analysis, Figure 35. The spectral band of *p*-ABSA is observed at 250 nm [209].

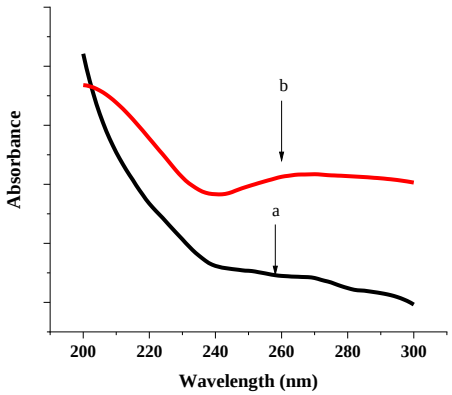

Figure 35. UV spectrum of bare SPCE (a) and *p*-ABSA/SPCE (b)

The high-resolution SEM image Figure 36 (I) shows that the carbon surface is covered with a high content of graphite particles. The SEM images shown in Figure 36 (II) reveal the morphological changes of the bare SPCE surface caused by the activation. The surface of pristine SPCE is smooth and flat. But the electrochemical activation leads to the deterioration of carbon surface. Thus, the rough and porous surface of the SPCE was observed after the activation. The SPCE activated in alkaline media exhibits several dents with various forms as shown in Figure 36 (II). The dents are presumably formed via carbon dissolution in alkaline media revealing an oxidized carbon surface. And the high-resolution SEM shows that the *p*-ABSA grafted SPCE is highly dispersed and can be identified Figure 36 (III).

I. 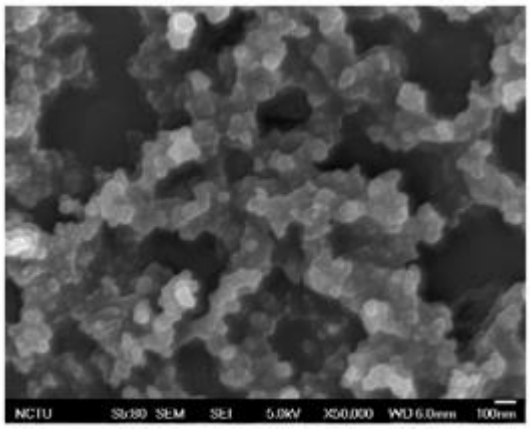 II. 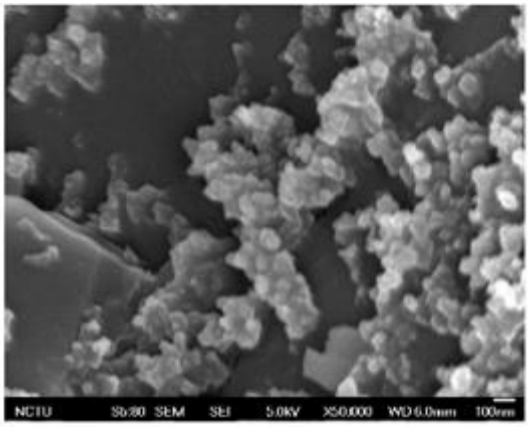

III. 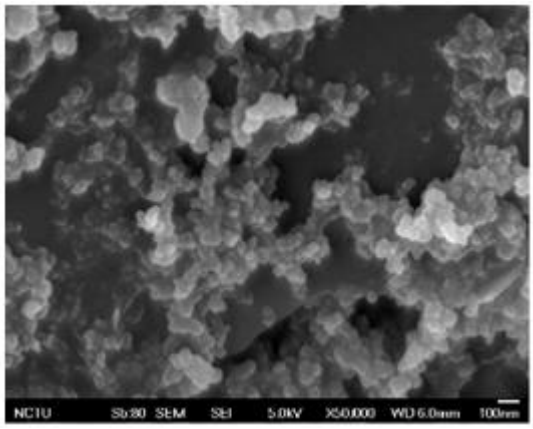

Figure 36. SEM images of pristine SPCE **(I)** activated-SPCE **(II)** and *p*-ABSA/SPCE **(III)**

5.3.6. Electrochemical Behavior of NIC at *p*-ABSA/SPCE

In order to determine the electrochemical behavior of the bare SPCE and the modified SPCE, towards 100 µM nicotine CV was performed in BRB solution (pH = 8). The obtained CV and SWV are depicted in Figure 37 and 38, the voltammograms show irreversible oxidation peaks for nicotine. At the bare SPCE, no clear oxidation peak was observed. Moreover a higher current is observed at *p*-ABSA/SPCE at a positive potential + 0.896 V, which indicates the present modified electrode has high electrocatalytic activity towards nicotine compared with the bare SPCE.

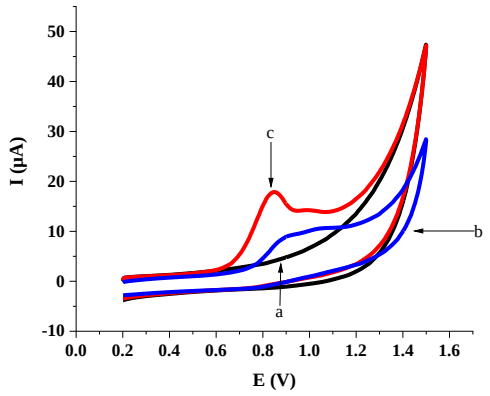

Figure 37. The characteristic cyclic voltammograms of NIC in BRB solution pH 8 recorded in 0 μM NIC (a) 100 μM bare SPCE (b) and 100 μM *p*-ABSA/SPCE (c) in the potential range of 0.2 to 1.4 V at a scan rate of 100 mV s^{-1}

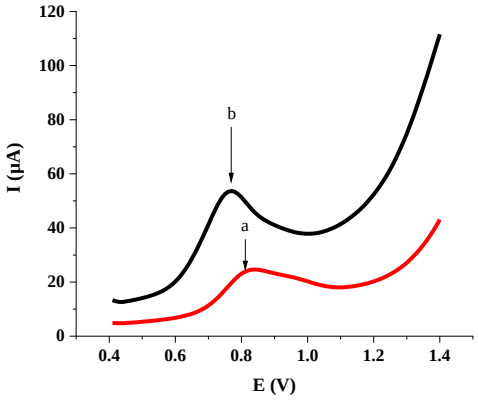

Figure 38. SWVs of 100 μM NIC in 0.1 M of BRB solution (pH 8.0) at bare SPCE (a) and *p*-ABSA/SPCE (b)

The electrochemical responses of *p*-ABSA/SPCE for nicotine was also studied in different buffer medium phosphate buffer (PB), Britton-Robinson (BR), Tris/Borate/EDTA (TBE) and Tris/Acetate/EDTA (TAE) solution but a higher and sharp anodic peak was achieved using BRB solution. Hence, BRB was selected because it gave almost two times higher peak current than the other three buffer solution. So all the electrochemical measurement were carried out in BRB solution at pH = 8.0 Figure 39.

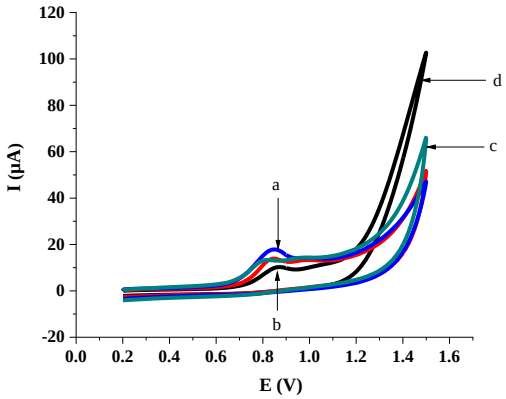

Figure 39. Cyclic voltammograms of 100 µM NIC in BRB (a), PB (b), TBE (c) and in TAB (d) solution recorded at *p*-ABSA/SPCE in the potential range of 0.2 to 1.4 V at a scan rate of 100 mV s^{-1}

5.3.7. The Effect of Scan Rate

The influence of scan rate on the peak potentials and currents of 100 µM nicotine on the *p*-ABSA/SPCE was examined using CV in BRB solution (pH 8.0) by varying the scan rates from 50 to 200 mV s^{-1}. An irreversible oxidation peak of nicotine was observed during the anodic scan from 0.2 to 1.4 V at all scan rates while no peak was observed in the absence of nicotine at *p*-ABSA/SPCE Figure 40.

The effect of potential scan rate on the peak current and the peak potential of nicotine was evaluated. The positive shifts in the peak potential together with the absence of cathodic wave confirmed the irreversibility of the oxidation process. The logarithm of peak current versus logarithm of scan rate gave a straight line with a slope of 0.352 (correlation coefficient 0.995), close to the theoretical value of 0.5, which is expected for an ideal reaction of solution species [210], so in this case the process had a diffusive component. The linear relationship existing between peak current and the square root of the scan rate with a slope of 0.834 (correlation coefficient 0.99783), showed that the oxidation process is predominantly diffusion-controlled in the whole scan rate range studied.

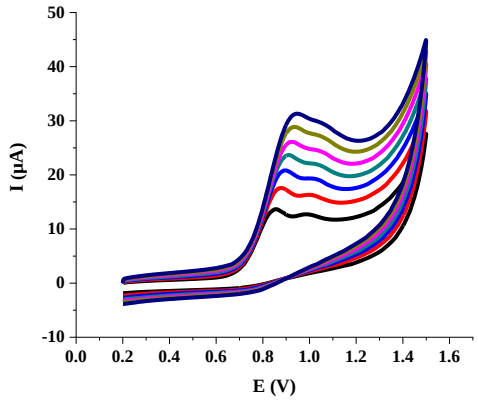

Figure 40. CVs of 100 μM NIC at *p*-ABSA/SPCE in BRB solution (pH 8.0) at a different scan rates (0.05-0.200 V s^{-1})

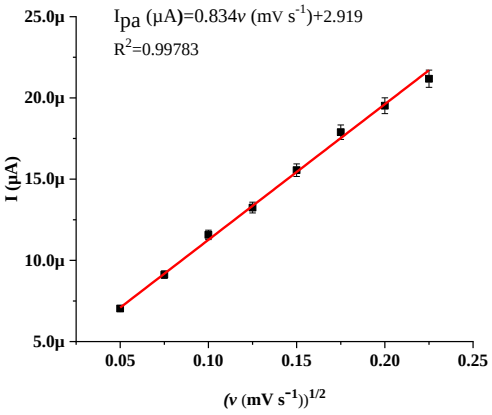

Figure 41. The linear plot of cathodic peak current response for nicotine *vs.* square root of scan rate

5.3.8. The Effect of pH

Nicotine is a weak, diacidic base with two pK_a values, pK_{a1} = 8.02 and pK_{a2} = 3.12 which are the monoprotonated Scheme 10 (a) and diprotonated Scheme 10 (c) form. At pH ≥ 9.0, the unprotonated Scheme 10 (b) free base form of nicotine predominates in the supporting electrolytes. The change in protonation of the acid-base functions in the pyrrolidine moiety at pH 7.0-8.0 close to pK_{a1} forms the monoprotonated form and diprotonated form predominated at pH 2.0-2.7 [211- 212] as shown in Scheme 10.

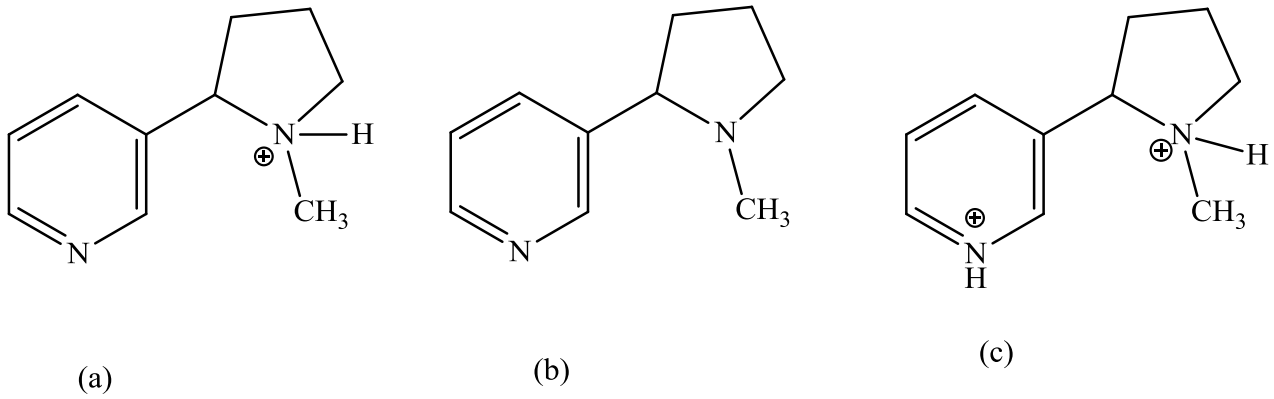

(a) (b) (c)

Scheme 10. Three different forms of nicotine: monoprotonated form (a), free base (b) and diprotonated form (c)

As a result, the pH value for the measurement system has influence on the current response for nicotine. Figure 42 shows the electrochemical signal of the *p*-ABSA/SPCE as a function of the pH value. The current signal reaches the maximum at pH 8, which is chosen as the optimum condition for the subsequent experiments. Under the optimal pH condition, nicotine exists in the monoprotonated pyrrolidine Scheme 10 (a) nitrogen form that electrostatically interacts with the negative charge surface of the sulfonic acid group in the *p*-ABSA modified electrodes. It is worth noting that at a lower pH value, some electrochemically active sites could be occupied by the positive charges on the nitrogen atoms in the pyridine ring, which would lead to less effective adsorption for nicotine oxidation. Meanwhile, the surface charge densities of *p*-ABSA sheets can be modulated by the pH value of the supporting electrolytes. A lower pH value may cause less negative charges in *p*-ABSA with lower adsorption ability. Therefore, we chose pH 8.0 as the optimal pH condition. When the solution pH was lower than 5.5, the CV oxidation peak current for nicotine was smaller and poorly shaped, as reported previously. Hence, we examined the pH effect from pH 5.5 to 9.0 Figure 42. The oxidation peak potential of nicotine negatively shifted gradually along with the increase in pH, and almost leveled off at pH higher than 8, which agrees well with the literature [195].

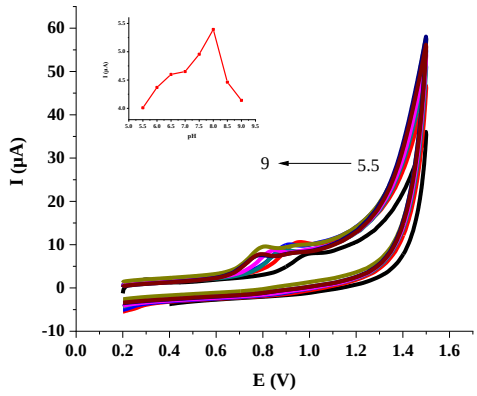

Figure 42. CVs of 100 μM NIC at different pH values (5.5–9.0) at *p*-ABSA)/SPCE in BRB solution at scan rate of 100 mV s^{-1} Inset: The plot of peak currents vs pH

The plot of peak potential as a function of pH Figure 43 gave a linear relationship with regression equation: E (V) = −0.05362pH + 1.279 (R^2 = 0.9962). The value for the slope is close to 0.05362, this indicates that an equal number of electrons and protons are involved in the electrode reaction [213]. Though the exact mechanism for the electrochemical oxidation of NIC is unknown, the proposed mechanism at BDD electrode in alkaline media which involves methanol formation and substitution of CH_3 by OH at the tertiary nitrogen of pyrrolidine ring with two electrons and two protons transfer [214] may presumably be the possible mechanism at the *p*-ABSA modified SPCE.

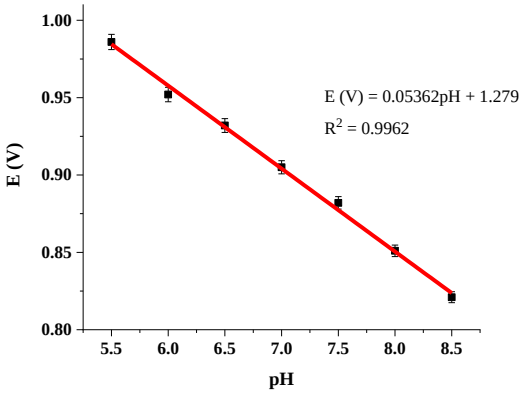

Figure 43. Plot of peak potentials of 100 μM NIC as a function of pH at *p*-ABSA in BRB solution at scan rate of 100 mV s^{-1}

5.3.9. Optimization of SWV Parameters for NIC Determination

For a higher signal and more sensitive determination of NIC at the modified electrode, square wave voltammetry (SWV) technique was employed. A well resolved anodic peak was obtained for NIC in BRB (pH 8.0). So the effects of SW parameters (frequency, amplitude and step potential) on the current response were investigated by varying their values. Results showed an increase in peak current with increasing SW frequency, amplitude and step potential. But the optimum values were chosen considering the anodic peak shape and the magnitude of peak current response. Therefore, the optimum parameters selected for subsequent measurements were step potential of 11 mV, SW amplitude of 60 mV and frequency of 40 Hz.

5.3.10. The Effect of Accumulation Potential and Time

The effect of accumulation potential on the response for 100 µM nicotine was investigated between –0.5 and +0.5 V. Varying the accumulation potential with a 15 s accumulation time, the peak current increased with increase in the potential starting from −0.5 V, and reached maximum at 0.1 V Figure 44 (I). At potentials higher than 0.1 V, a decrease of current was observed. Therefore, 0.1 V was chosen as the optimum accumulation potential.

Since accumulation time also has a great influence on the peak current, the accumulation time was studied between 15 and 75 s with an accumulation potential of 0.1 V. Figure 44 (II) shows that the peak current increases, and then reaches a plateau around 45 s. The results suggested that the amount of nicotine adsorbed at the surface *p*-ABSA/SPCE reach saturation when accumulation time reached 30 s. Considering both sensitivity and work efficiency, 45 s accumulation time was employed for the determination of nicotine.

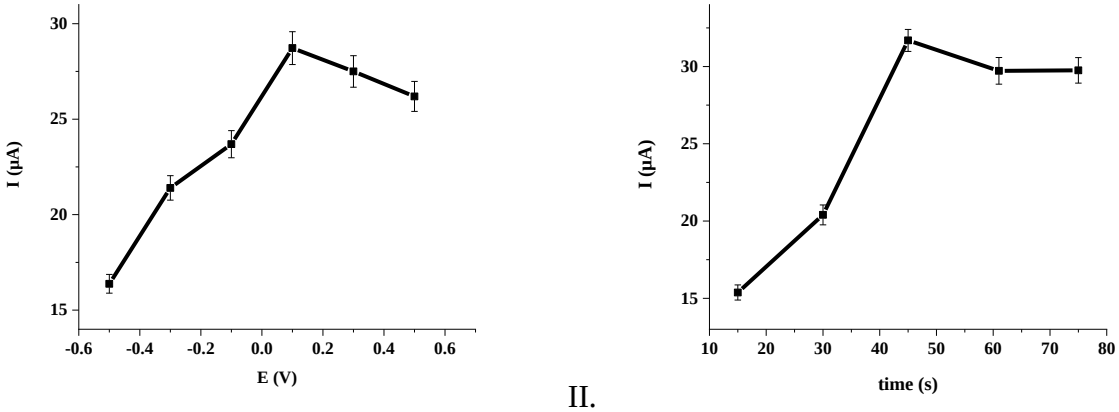

I. II.

Figure 44. (I) Effects of accumulation potential and **(II)** accumulation time (B) on the peak current of 100 µM NIC in BRB solution (pH 8.0)

5.3.11. Determination of NIC by Square Wave Voltammetric Technique

The determination of NIC was performed under the optimized conditions using square-wave voltammetry. Figure 45 shows the SW voltammograms of NIC for varying the concentrations of NIC in BRB solution (pH 8.0) using *p*-ABSA/SPCE as the working electrode. The peak current versus concentration plot for NIC is linear in the range of 0.5 to 300 µM. The linear relationship gave the regression equation: Ip (µA) = 0.1747 (µM) + 5.3198 and R^2 = 0.999. The limit of detection (LoD, $3s_b/m$) and limit of quantification (LoQ, $10s_b/m$) were found to be 0.35 µM and 1.14 µM, respectively; where s_b is the standard deviation of the blank measurements (n = 6) and m is the slope of the analytical calibration curve [165].

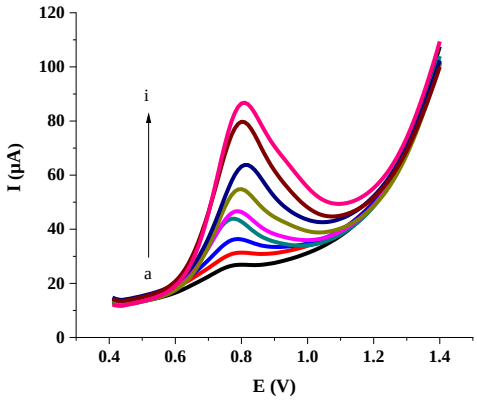

Figure 45. SWVs for varying concentrations of NIC: 0.5, 10, 25, 50, 100, 150, 200, 260 and 300 µM in BRB solution pH 8.0 at *p*-ABSA/SPCE

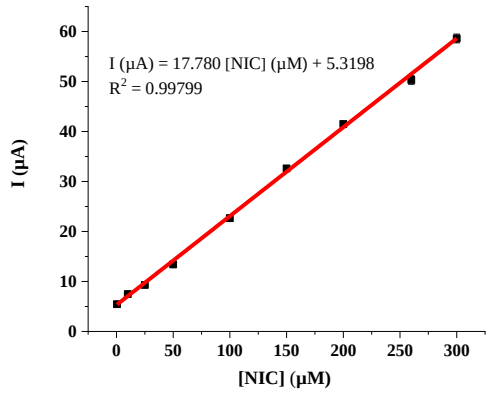

Figure 46. The plot of peak current *vs*. NIC concentrations

Table 8 presents the analytical performance (detection limit and linear range) of different modified electrodes and techniques that have been previously reported in the literature for the detection of NIC. The performance of the present sensor is superior to most of the previous sensors reported in the literature in terms of sensitivity and linear dynamic range (Table 8), which can be attributed to the functionalities created on the surface of the electrode.

Table 8. Comparison of the performance of the proposed method with other electrochemical sensors used for the determination of NIC

Electrodes	Method	Linear Range (μM)	LoD (μM)	Reference
[a]CPE	SWV	50-500, 50-1000	6.1, 3.2	[215]
[b]TiO_2 /PEDOT/ITOE	AMP	0-5000	4.9	[216]
[c]PdHCF/GO/GCE	AMP	8-240	1.208	[217]
[d]BDDE	DPV	0.2-2.47	0.061	[218]
[e]PDDA-RGO/Au/GCE	DPV	0.5 -300	0.12	[219]
[f]p-(ARS)-GR/SPCE	DPV	30-1000	4.6	[220]
[g]EA/GCE	SWV	1-200	0.7	[221]
[h]MWCNT/GCE	DPV	31-1900	9.3	[222]
[i]bAuNPs	DPV	20-2000	2.3	[223]
p-ABSA/SPCE	SWV	0.5-300	0.35	This Work

[a] carbon paste electrodes, [b] titanium oxide/poly(3,4-ethylenedioxythiophene)/Indium/tin oxide electrode, [c] Palladium hexacyanoferrate incorporated Graphene oxide modified glassy carbon Electrode, [d] Boron-doped diamond electrode, [e] poly(diallyldimethylammonium chloride) functionalized reduced graphene oxide–gold nanoparticle modified glassy carbon electrode, [f] poly (alizarin red S) modified graphene/screen printed carbon electrode, [g] Electrochemically activated glassy carbon electrodes, [h] Multi-walled carbon nanotube modified glassy carbon electrode, [i] biosynthesized gold nanoparticles modified Pencil graphite electrode.

* The LoQ which 1.14 μM is above the lower calibration curve.

5.3.12. Repeatability, Reproducibility and Stability of the Modified Electrodes

The repeatability of the *p*-ABSA/SPCE was investigated by measuring the SWV signals for 100 μM NIC in BRB solution (pH 8.0). The relative standard deviation (RSD) of the peak currents obtained for the same electrode after fifteen consecutive measurements was 2.4%. On the other hand, the reproducibility of the modified electrode was examined by comparing the responses of three different electrodes prepared following the same experimental procedure. The RSD of the peak currents between three different electrodes measured was found to be 2.5%. The stability of the sensor was examined after keeping it in an open air for 15 days and the peak current was retained 95.6% of its initial value. The results show that the developed modified screen printed

electrode provided excellent repeatability, reproducibility, and stability towards the electro-oxidation of NIC.

5.3.13. Interference Study

Selectivity of the sensor plays an important role in the determination of analyte in various samples. Possible interference in the detection of nicotine using *p*-ABSA/SPCE was investigated by adding various organic compounds and ions in BRB solution pH 8 containing 100 µM of nicotine. The analyzed common ions Fe^{3+}, Mg^{2+}, Ca^{2+}, K^{+}, Na^{+} and NH_4^{+} and uric acid and glucose had no noticeable effect (<5% for all species) on the current responses of the 100 µM nicotine with fifty fold concentration. Hence, it can be concluded that these species do not significantly interfere in the determination of nicotine, and the modified electrode had good selectivity for the determination of nicotine in the presence of the common interfering species. Though the interfering substances commonly exist in human urine and cigarette samples the determination of nicotine is not affected by their presence.

Table 9. Interference effect of some foreign species on the peak current response of 100 µM NIC at pABSA/SPCE

Interferents	Concentration (µM)	Signal Change (%)
Uric acid	5000	3.26
D-Glucose	5000	2.59
Fe^{3+}	5000	2.19
Ca^{2+}	5000	4.36
Mg^{2+}	5000	4.21
K^{+}	5000	0.98
Na^{+}	5000	0.89
NH_4^{+}	5000	1.02

5.3.14. Analytical Application

In order to study the practical applications of the *p*-ABSA/SPCE, two different real samples cigarette and urine were taken. The real samples were prepared according to procedure 4.5.2 and

4.4.2. The most commonly used nicotine analysis method required complex extraction procedures. However, recent studies have shown that ultrasonication of the sample is an alternative technique for extracting nicotine instead of using expensive and environmentally harmful organic solvents. The collapse of the bubbles created in the sonication of solutions results in the generation of high local energy and contact between the solvent and the solute, and can thus highly increase the sample extraction efficiency [94]. The sample preparation procedure used in this study was used according to procedure [224] with a slight modification. In brief, the ultrasonic extraction time of 3 hr were chosen instead of 1 hr in order to achieve a quantitative recovery of nicotine into aqueous solution. Then the real samples were prepared by diluting 100 µL of the cigarette sample in to 50 mL and the urine samples with BRB solution pH 8. Recoveries of the samples were conducted by adding the standard volume of nicotine solution to the real samples. The obtained recovery results of cigarette and urine samples are presented in Table 10. The recovery data of the present study clearly shows that accurate detection of nicotine in cigarette and urine samples is achieved.

Table 10. Determination of nicotine levels in urine samples using *p*-ABSA/SPCE (n = 3)

Sample	Added (µM)	Found (µM)	Recovery (%)
Urine	0	0	
	15	15.9	106
	35	33.8	95.7
	65	67.9	104

Table 11. Determination of nicotine levels in Cigarette sample using *p*-ABSA/SPCE (n = 3)

Sample	Detected (µM)	Added (µM)	Found (µM)	Recovery (%)
Cigarette	4	56	58.8	97.8
		156	165	103

5.4. A chemical Sensor Based on PEDOT and Electrografted *p*-Aminobenzene Sulfonic Acid Diazonium Salt for Sensitive Determination of Brucine in Aqueous Media

5.4.1. Background

Brucine is an alkaloid which is isostructural to strychnine with methoxy groups, rather than hydrogen, at the 9- and 10-positions of the aromatic ring Scheme 11 [225, 226]. It exists mainly in the seeds of *Strychnos nux-vomica* L (Loganiaceae) and used as a traditional medicinal herb native to East India, Burma, Thailand, China, and Northern Australia. Its main efficacies include pain relief, reduction of swelling, improve microcirculation, and inhibit platelet aggregation. However, it is possible for the medicinal doses of it to generate a toxic effect on the nutritious canal; it blocks neuromuscular conduction, shows curare action, and blocks neural cell sodium current. Thus, development of a simple, rapid, and accurate method for brucine is of importance [227, 228].

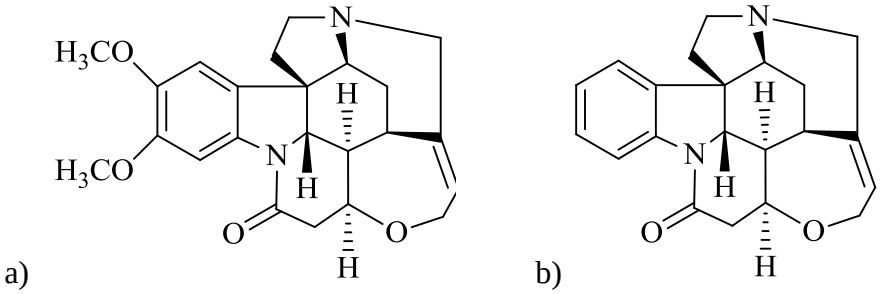

Scheme 11. Chemical structure of a) brucine and b) strychnine

At present a number of analytical methods have been reported for the determination of brucine including high performance liquid chromatography [229], capillary zone electrophoresis [230], thin layer chromatography [231], liquid chromatography-electrospray ionization-mass spectrometry [232], ultra-performance liquid chromatography-tandem mass spectrometry [233], liquid chromatography-electrospray/ion-trap mass spectrometry [234] and gas chromatography-mass spectrometry [235]. However, an electrochemical sensor has advantages due to its simple measurement procedure, short response time, and sufficient sensitivity and selectivity [236]. Electrochemical sensors are smaller devices that can be transferred and manipulated easily. They can be used easily for onsite analysis to meet the quality set. They can also provide relevant

information on a process to make decision [237]. Nowadays, screen-printing technology has been utilized in environmental, medical and industrial applications. The integrated graphite screen printed electrode comprising three electrode configuration in one strip offers simple, low-cost and sensitive real-time detection of an analyte in a microliter volume without any pretreatment [238]. Screen printed electrode also offers other general advantages such as mass production of miniaturized, inexpensive and robust electrodes from different materials in diverse geometries and multiplexed formats [239]. In general, SPCE have three main advantages over other electrode. The first advantage is controlling the area, the thickness, and composition of the electrode. The second advantage is the validation of experimental results is easy due to the presence of many replicate printed electrodes. The final one is the chemical or polymer used for the modification can be incorporated with the graphite ink prior to printing [23]. In order to establish electrochemical sensors with a higher performance, modifications of the electrode surface should be carried out. Modification of the electrode by electrocatalytic materials has been proposed to attain high sensitivity [240]. Electrografting using diazonium salt reduction is among the most common modification methods that have been widely studied on different carbon electrodes. This method turned out to be a simple, fast and versatile way for surface modification by way of covalent attachment of an organic layer to a conductive substrate [241]. Grafting diazonium salt is a general method of surface modification used, and it can be done electrochemically by LSV to in-situ generated diazonium salts [242]. The formation of a poly(3,4-ethylenedioxythiophene)(PEDOT) layer attached to the surface of the thienyl-modified glassy carbon electrode (GCE) via electrografting, using an electrochemical polymerization process was investigated. A better redox peak was achieved as compared to the classical polymer film on a bare electrode, thus indicating enhanced electron transfer ability attributed to ordered and uniform structure [243]. In our case, PEDOT film surface was attached to that of *p*-ABSA grafted SPCE and better redox peak to that of PEDOT film on SPCE was achieved.

Literature survey unveils that few electrochemical methods have been reported earlier for the determination of brucine using chemically modified glassy carbon electrode based sensors poly-(DL-aspartic acid)-modified GCE [244], poly-(Alizarin Red S) modified GCE [94], Surface-imprinted polymer grafted with water compatible external layer via reversible addition fragmentation chain transfer (RAFT) precipitation polymerization [245], carbon nanotubes nafion composite modified GCE with high sensitivity were also reported [246]. All the above

methods used GCE, but our method used the cheap screen printed carbon electrode with higher reproducibility and comparable sensitivity this give an advantage to incorporate the modifier during printing.

5.4.2. Electrode Preparation

Prior to surface modification, the screen printed carbon electrode (SPCE) was activated with 0.5 M KOH solution. In brief, 0.5 M KOH was drop casted onto the SPCE surface covering whole area of the reference, counter and working electrode, and then the potential was cycled by linear sweep voltammetry (LSV) for 10 cycles in the potential range of −1.5 to 1.0 V at a scan rate of 100 mV s^{-1}. After activating the SPCE the electrode modification was done by two straightforward steps. First, the activated-SPCE surface was modified by electrochemical reduction of diazonium radical generated in-situ by LSV [247] as described in procedure 4.6.2. The potential was swept between the potential range of 0.0 and −1.0 V at scan rate of 100 mV s^{-1} for 15 cycles (the optimum) Figure 29. This process allows the diazonium salt to be reduced and directly deposited on the substrate without a requirement to isolate the salt. The reduction of the diazonium species was via one electron process leading to the formation of *p*-sulfonic acid radicals that are covalently attached to the surface of the carbon in the screen printed electrode [242]. The electrode systems obtained hereafter will be denoted as *p*-ABSA modified screen printed carbon electrode (*p*-ABSA/SPCE). Before the polymerization of EDOT, the grafted electrode was cleaned by deionized water and flushed with nitrogen for drying. Finally, the PEDOT film was deposited onto the modified surface by cycling (10 cycles optimum) 10 mM EDOT in an aqueous solution containing 0.05 M sodium dodecyl sulfate (SDS) + 0.1 M $LiClO_4$ in the potential range of 0.4-1.5 V at a scan rate of 100 mV s^{-1} [248]. The electrode systems thus obtained hereafter will be denoted as PEDOT/*p*-ABSA/SPCE.

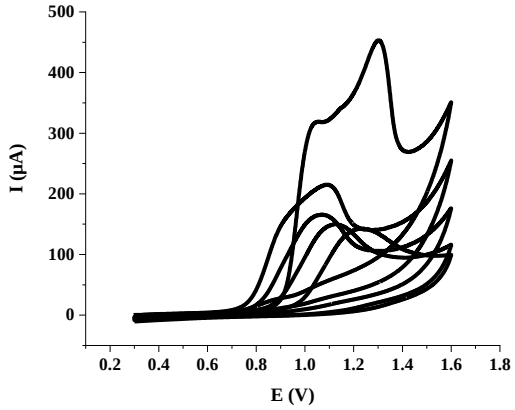

Figure 47. Cyclic voltammogram of 10 mM EDOT in an aqueous solution of 0.05 M SDS and 0.1 M LiClO4 on the *p*-ABSA/SPCE at a scan rate of 100 mV s^{-1}

5.4.3. Surface Characterization

FTIR spectroscopy is often used to determine functional group formation on modified electrodes. Indeed, the various changes in the FTIR spectra of the electrodes exhibit the attachment of a new functional group on the electrode surface after each modification step. The FTIR spectra of bare SPCE, activated-SPCE, *p*-ABSA/SPCE and PEDOT/*p*-ABSA/SPCE are shown in Figure 48. For the activated-SPCE, the broad peak at 3371 cm^{-1} which corresponds to O-H stretching, and the small peak around 1575 cm^{-1} shows the formation of hydroxyl group during and carbonyl group on the electrode surface during the electrochemical activation. The FTIR spectrum of *p*-ABSA/SPCE has a broader peak at 3371 cm^{-1}, and this is by the increase in O-H stretching of the sulfonic acid group due to the grafting of *p*-ABSA. An additional medium intensity peak at 642 cm^{-1} is due to symmetric in-plane deformation of the sulfonate anion and those bands connected with aromatic ring vibration were observed in the whole spectral range, i.e. (CH) is in the range 2354 cm^{-1} [249]. From the PEDOT/*p*-ABSA/SPCE FTIR spectrum the bands at approximately 1109, 1168 and 1254 cm^{-1} are due to the C-O-C bending vibration in ethylenedioxy group. While the bands at 873 and 800 cm^{-1} are the characteristic bands of stretching vibrations of the C-S-C bond in thiophene ring, thus the FTIR spectra of the electrode suggests the successful formation of the designed fictional groups [250].

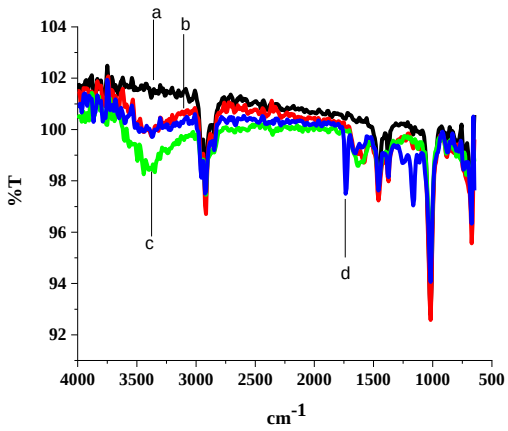

Figure 48. FTIR spectra of bare SPCE (a), activated-SPCE (b), *p*-ABSA/SPCE (c) and PEDOT/*p*-ABSA/SPCE (d)

The PEDOT/*p*-ABSA/SPCE shows a characteristic UV-Vis peak at approximately 400 to 700 nm. This peak at approximately 400 to 700 can be ascribed to the π-π* transitions of the thiophene ring [249].

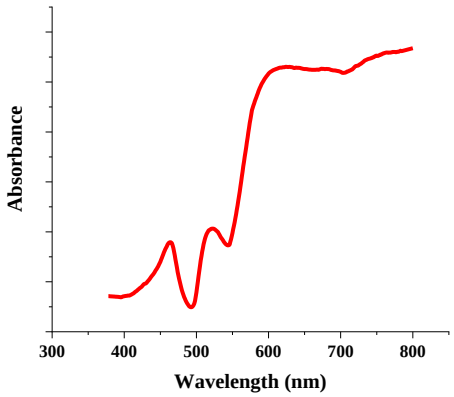

Figure 49. UV-Vis spectra of PEDOT/*p*-ABSA/SPCE

The high-resolution SEM image Figure 50 (I) shows that the carbon surface is covered with high content of graphite particles. However, the KOH treated SPCE is characterized by a higher microporous structure of flake shape with non-uniform distribution, along with cavities Figure 50 (II). The SEM further shows that the *p*-ABSA/SPCE is highly dispersed and can be discernible Figure 50 (III). The surface area of the PEDOT/*p*-ABSA/SPCE should be greater

than the area of the unmodified SPE due to its rough nanostructure Figure (IV), which could be used to promote the electron transfer reaction and enhance the detection signal.

I. 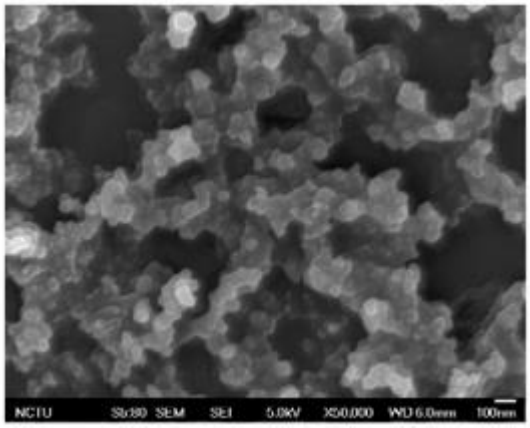 II. 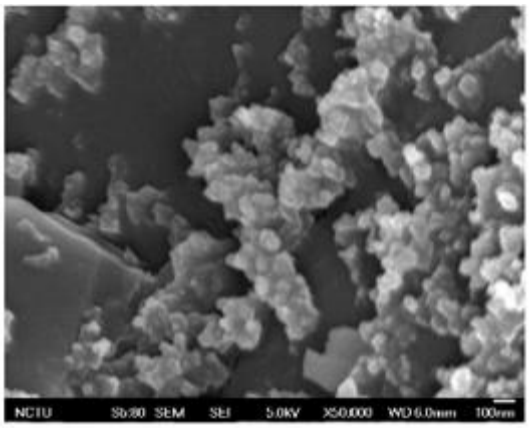

III. 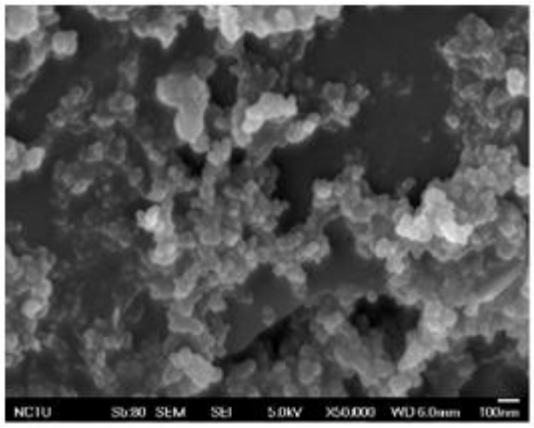 IV. 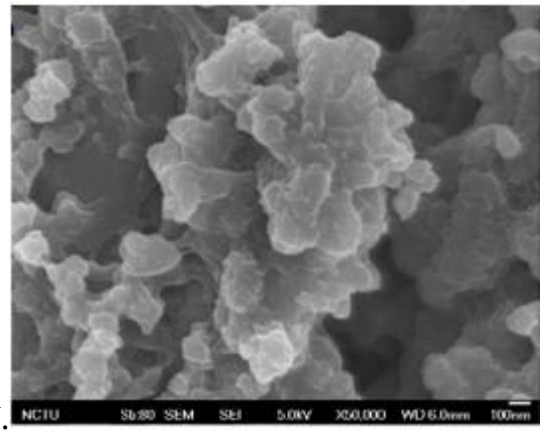

Figure 50. SEM images of bare SPCE **(I),** activated-SPCE **(II)**, *p*-ABSA/TSPCE **(III)** and PEDOT/*p*-ABSA/TSPCE **(IV)**

5.4.4. Estimation of the Electroactive Surface Area

In order to confirm whether the modification of the bare screen printed carbon electrode has brought an improvement in the electrochemical properties and thus the electrical conductivity, the electroactive surface area of the bare SPCE was compared with that of PEDOT/*p*-ABSA/SPCE by cyclic voltammetry using 1.0 mM $K_3Fe(CN)_6$ in 0.5 M KCl as a redox probe at different scan rates. The electro-active surface areas were estimated according to Randles-Sevcik equation Equation 1 and the diffusion coefficient of $[Fe(CN)_6]^{3-}$ was taken to be 7.60×10^{-6} cm^2s^{-1}[251]. The peak currents of the $K_3Fe(CN)_6$ were proportional to the square root of the scan rate. From the slope of the plot of Ip vs $v^{1/2}$, using equation 1, the effective surface area of the

bare SPCE was calculated to be 3.07–3.08 mm^2 and, for PEDOT/*p*-ABSA/SPCE, the surface area was 5.0-5.23 mm^2. Thus, the electroactive surface area, which measures the efficiency of the exposed surface to the catalytic reaction, of PEDOT/*p*-ABSA/SPCE increased by about 1.7 times compared to the bare SPCE, which is an evidence for improved conductivity of PEDOT/*p*-ABSA/SPCE film. This is also confirmed by running CV of the $Fe(CN)_6]^{4-/3-}$ redox the result in Figure 51 shows that PEDOT/*p*-ABSA/SPCE has better conductivity than the other electrodes.

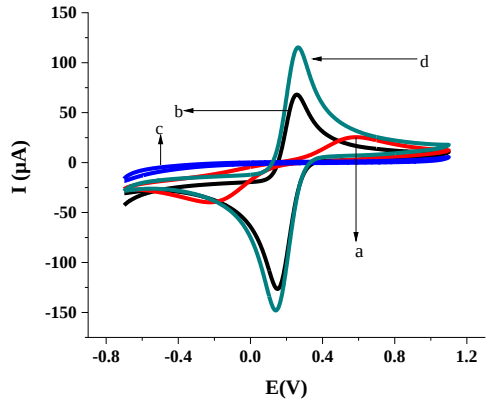

Figure 51. Cyclic voltammograms recorded at bare SPCE (a), activated-SPCE (b), *p*-ABSA/SPCE (c) and PEDOT/*p*-ABSA/SPCE (b) for a solution of 1 mM $[Fe(CN)_6]^{4-/3-}$ in 0.1 M KCl at a scan rate of 100 mV s^{-1}

5.4.5. Electrochemical Impedance Analysis of PEDOT/*p*-ABSA/SPCE

Electrochemical impedance spectroscopy (EIS) is an efficient tool for studying the interface properties of surface-modified electrodes. The diameter of the semicircle portion of the Nyquist plot of EIS is equivalent to the charge transfer resistance (R_{ct}) [252]. Figure 52 shows the Nyquist plot of different modified electrodes in 5 mM $[Fe(CN)_6]^{4-/3-}$ containing 0.1 M KCl solution. The R_{ct} values are in the order of: *p*-ABSA/SPCE (c) > bare SPCE (a)> activated-SPCE (b) > PEDOT/*p*-ABSA/SPCE (d). The highest R_{ct} value at the *p*-ABSA/SPCE (curve b) shows a large electron transfer resistance (R_{ct}) value because of the presence of excessive negative moieties, which produce an insulating behavior and obstructed its electrochemical characteristics [206]. But the PEDOT/*p*-ABSA/SPCE has the smallest electron transfer resistance 128 Ω compared to the activated-SPCE and bare SPCE which are 462 and 501.6 Ω, respectively

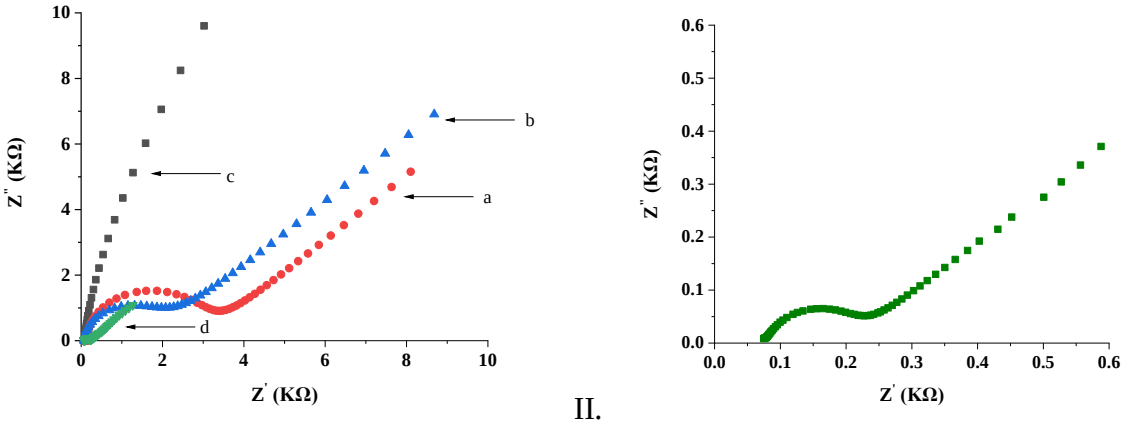

Figure 52. **(I)** Electrochemical impedance spectroscopy Nyquist diagrams recorded in a solution of 10 mM $[Fe(CN)_6]^{4-/3-}$ in 0.1 M KCl bare SPCE (a), activated-SPCE (b), *p*-ABSA/SPCE (c) and PEDOT/*p*-ABSA/SPCE (d) **(II)** Nyquist diagrams of PEDOT/*p*-ABSA/SPCE

5.4.6. Electrochemical Behavior of Brucine

The electrochemical activity of the electrode was evaluated using cyclic voltammetry in 0.2 M acetate buffer solution pH 4.0, in the presence and in the absence of 10 µM brucine Figure 53 for two consecutive cycles. Addition of brucine causes a large oxidation peak current at a potential around 0.5 V with well-defined irreversible peaks lower potential at the PEDOT/*p*-ABSA/SPCE. The mechanism for the electrochemical reaction of brucine is as shown in Scheme 12. The peak at around 500 mV resulted from the irreversible oxidation of brucine to dicarbonyl-strychnine. Then a pair of quasi-reversible redox peaks were obtained, which occurred at the dicarbonyl-strychnine [244]. From the mechanism given the pair of the quasi-reversible redox peaks becomes higher at lower pH but the oxidation of brucine dicarbonyl-strychnine is pH independent.

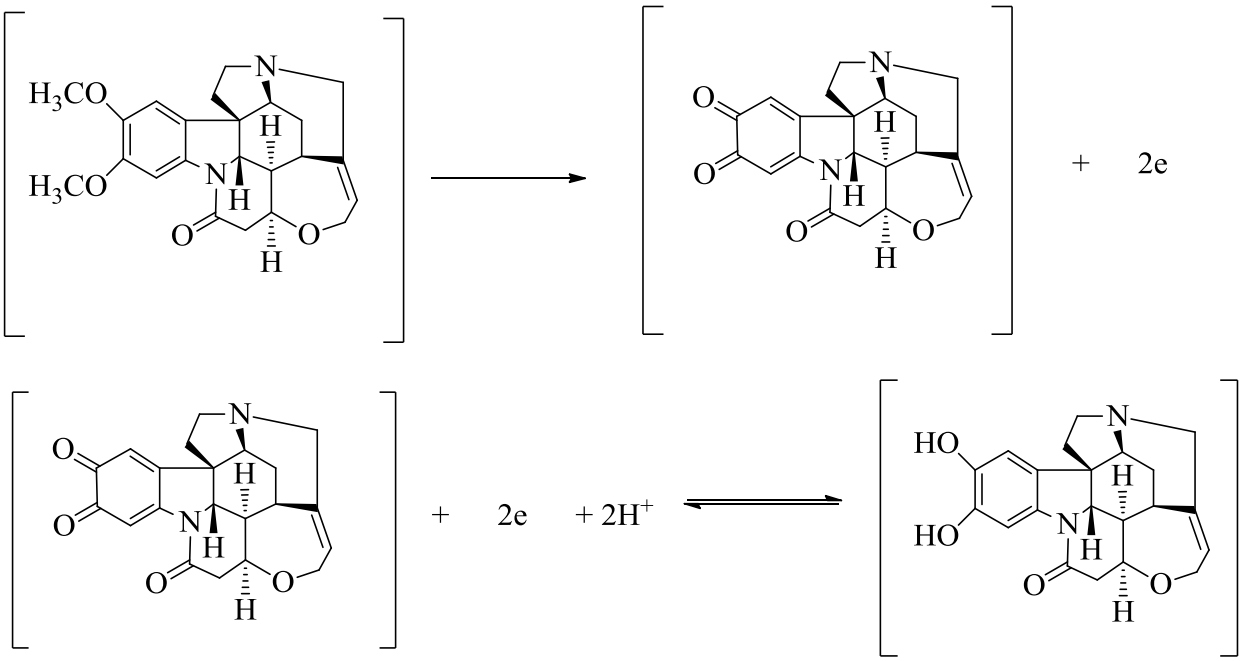

Scheme 12. Mechanism for the oxidation of brucine

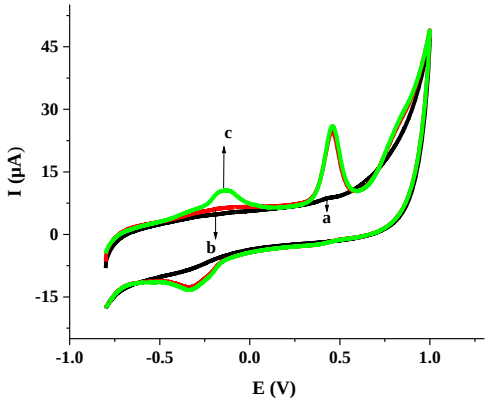

Figure 53. Cyclic voltammograms of 10 µM brucine in ABS of pH 4.0 at PEDOT/*p*-ABSA/SPCE for 0.0 µM brucine (a), 10 µM brucine first cycle (b), and second cycle (c) in the potential range of −0.80-0.80 V at scan rate of 100 mv s^{-1}

Figure 54 compared cyclic voltammograms of 10 µM of brucine ABS (pH = 4.0) at the activated-SPCE (curve a), *p*-ABSA/SPCE (curve b), PEDOT/SPCE (curve c) and PEDOT/*p*-ABSA/SPCE (curve d). In order to explain all phenomena thoroughly, each scan was performed twice. Both the bare and activated-SPCE do not exhibit any peak for BRU but the *p*-ABSA/SPCE gave an irreversible anodic peak with Ep = 0.682 mV in the first cycle and very

small reversible peaks appeared in the second cycle. However, at the PEDOT/SPCE and PEDOT/*p*-ABSA/SPCE exhibited an irreversible anodic peak with E_{pa} = 0.613 mV and E_{pa} = 0.458 mV, respectively. A very sharp and higher anodic peak current with low E_{pa} was obtained at PEDOT/*p*-ABSA/SPCE. Therefor PEDOT/*p*-ABSA modified SPCE was selected for the determination of BRU.

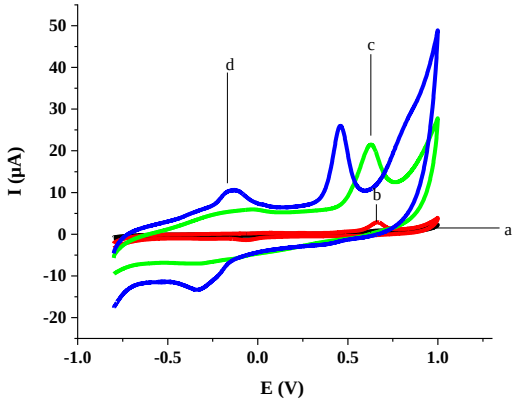

Figure 54. Cyclic voltammograms of 10 µM brucine in ABS of pH 4.0 at activated-SPCE (a), *p*-ABSA/SPCE (b), PEDOT/SPCE (c) and PEDOT/*p*-ABSA/SPCE (d) in the potential range of −0.80 to 0.80 V at scan rate of 100 mV s^{-1}

5.4.7. The Effect of pH

Britton-Robinson buffer, acetate buffer, citrate buffer, phosphate buffer and H_2SO_4 were examined for the determination of brucine; but the optimum results were obtained with acetate buffer and thus selected for further experiments.

The effect of pH on the voltammetric signals for brucine oxidation was investigated in 0.20 M acetate buffer solution (ABS) in the pH range 3.0 to 6.0 using cyclic voltammetry. It was noted that the current response and the peak potential of BRU significantly changed with increasing pH from 3.0 to 6.0 which shows that the oxidation of BRU is pH dependent. As shown in Figure 55, the oxidation peak current of BRU increased with increasing pH from 3.0 to 4.0 and then a gradual decrease in pH was observed from 5.0 to 6.0. A decrease in the peak current response for BRU with increasing pH revealed that the detection of BRU at the PEDOT/*p*-ABSA/SPCE electrode is feasible only in an acidic medium. The oxidation peak current

response obtained at pH 4.0 is comparable with that of 4.5, but pH 4.5 was selected for further study.

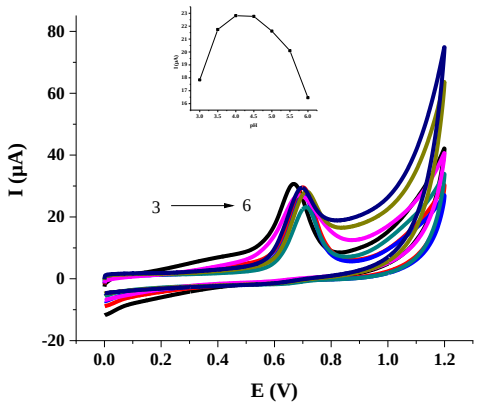

Figure 55. Cyclic voltammograms of 10 µM brucine at the PEDOT/*p*-ABSA/SPCE at different pH (3-6) using 0.20 M ABS at scan rate was 100 mV s^{-1}. Inset: The plot of peak currents vs pH

The oxidation peak potential of BRU was also affected by a change in pH as shown in Figure 55. The peak potential shifted positively with increase in pH value from 3.0 to 5.5. This result suggests the involvement of protons in the electrode process. A linear relationship was observed between the oxidation peak potential and the pH with a regression equation of: E(V) = 0.05063pH + 0.49783, R^2 = 0.99713 Figure 56. A slope of 50 suggests that the electrode process involves the transfer of equal number of protons and electrons.

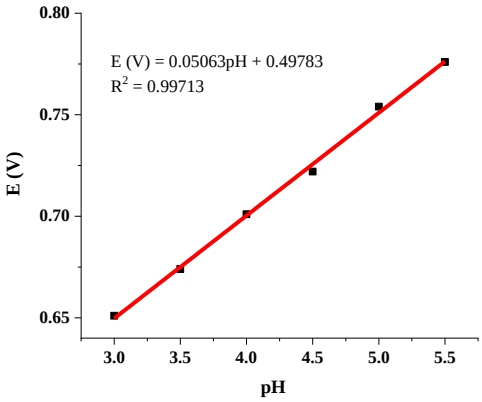

Figure 56. Plot of peak potentials of 10 µM Bru as a function of pH at PEDOT/*p*-ABSA/SPCE in 0.20 M of acetate buffer at scan rate of 100 mV s^{-1}

5.4.8. The Effect of Scan Rate

The effect of potential scan rate on the oxidation current of BRU was investigated by cyclic voltammetry Figure 57 in acetate buffer pH 4.0 containing 10 µM BRU. The plot of the oxidation peak current of brucine *vs* scan rate in the range 30-400 mV s^{-1} Figure 58 is linear with a regression equation: I_{pa} (µA) = 0.0909*v* (V s^{-1}) + 2.908; with R^2 = 0.997. This result shows that the first scan reaction of BRU was adsorption controlled. Furthermore, with increase in the scan rate, the potential shifted to more positive values, which confirms the irreversible electrochemical oxidation of brucine at PEDOT/*p*-ABSA/SPCE. The linear relationship between the logarithm of peak current and the logarithm of the scan rate can be expressed using the regression equation: log (I_{pa} (µA)) = 0.834log*v* − 6.587 (R^2 = 0.998) with a slope close to 1 further confirms the reaction of BRU in the PEDOT/*p*-ABSA/SPCE is adsorption controlled electrode process.

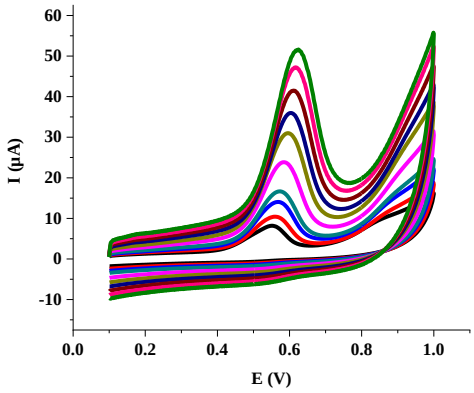

Figure 57. Cyclic voltammograms of 10 µM brucine at the scan rates: 30, 60, 80, 100, 150, 200, 250, 300, 350 and 400 mV s^{-1}

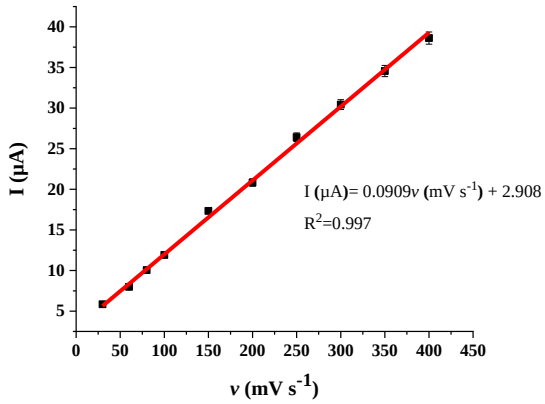

Figure 58. Plot of I_p *vs* scan rate for at PEDOT/*p*-ABSA/SPCE in 0.2 M ABS pH 4

5.4.9. The Effect of Accumulation Potential and Time

Since the oxidation of brucine at the surface of PEDOT/*p*-ABSA/SPCE is an adsorption controlled process, the effect of accumulation potential and time were studied using SWV. The effect of accumulation potential was studied by varying the accumulation potential from −500 to 300 mV with intervals of 100 mV with 60 s accumulation time. However, the peak current response of 10 μM brucine was almost unchanged, indicating that the accumulation potential has no significant effect on the oxidation peak current of brucine at the prepared electrode. Thus, an open circuit accumulation was employed for subsequent measurements.

The effect of accumulation time was also studied in the range of 0 to 240 s at an open circuit accumulation potential with a 30 s difference. The peak current increased with accumulation time from 0 to 60 s and reached a maximum value around 210 s, Figure 59. Upon increasing the accumulation time beyond 210 s the oxidation peak current of brucine remains almost constant. Therefore, an open circuit accumulation time of 210 s was employed for subsequent study in this work.

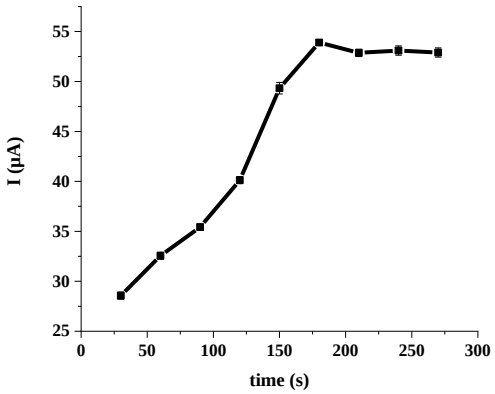

Figure 59. Effect of accumulation time on the oxidation peak current of 10 μM brucine at PEDOT/*p*-ABSA/SPCE

5.4.10. Optimization of SWV Parameters for BRU Determination

For sensitive and lower detection limit, a square wave voltammetry (SWV), technique was selected for the detection of brucine at PEDOT/*p*-ABSA/SPCE. A well-defined peak at 569 mV was observed due to the reduction of brucine. The SWV parameters step, amplitude and frequency were optimized before any analytical measurements. The effect of step potential on the reduction current of brucine was studied over the range 1 -15 mV by fixing the amplitude and frequency at 40 mV and 15 Hz, respectively. The peak current increased significantly up to 7 mV with the best shape for the peak. The influence of amplitude on the reduction current of 10 μM brucine was also investigated in the range 10-100 mV, the peak current was found to increase with increasing amplitude and reached maximum at 40 mV and then decreased. Thus, 40 mV was fixed as the working amplitude in the detection of brucine. In addition, the influence of square wave frequency on the peak current was also evaluated at the optimized step potential and amplitude. The frequency was varied in the range between10 and 100 Hz with a difference of 10 Hz, the peak currents reached maximum at 50 Hz and gradually decreased thereafter. Hence, for further electrochemical investigation, a step potential of 7 mV, amplitude of 40 mV and 50 Hz frequency were selected as the optimal values.

5.4.11. Determination of BRU by Square Wave Voltammetric Technique

Calibration was performed on PEDOT/*p*-ABSA/SPCE for the determination of brucine using the following SWV conditions–frequency: 50 Hz; step potential: 7 mV; pulse amplitude: 40 mV in

0.1 M ABS (pH 4. 0). The prepared sensor offered well-defined concentration dependence. Figure 60 presents SW voltammograms obtained by successive additions of brucine over the 0.03–5.0 µM concentration range. The peak current at a potential of +0.84V increased proportionally with the brucine concentration Figure 61 to yield a highly linear calibration plot, I(µA) = 7.912 [BRU](µM) + 0.922 (correlation coefficient, 0.9984). The limit of detection (LoD, $3s_b/m$) and limit of quantification (LoQ, $10s_b/m$) were calculated as 0.012 µM and 0.042 µM, respectively; where s_b is the standard deviation of the blank and m is the slope of the calibration curve.

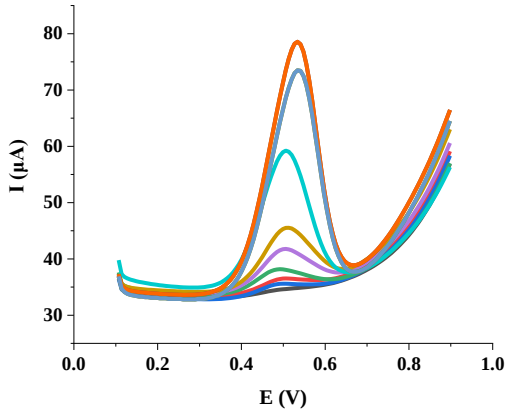

Figure 60. Square wave voltammograms for varying concentrations of brucine 0.03µM, 0.075 µM, 0.1 µM, 0.35 µM, 0.6 µM, 0.9 µM, 1.6 µM, 2.8 µM and 5 µM in ACB pH 4.0

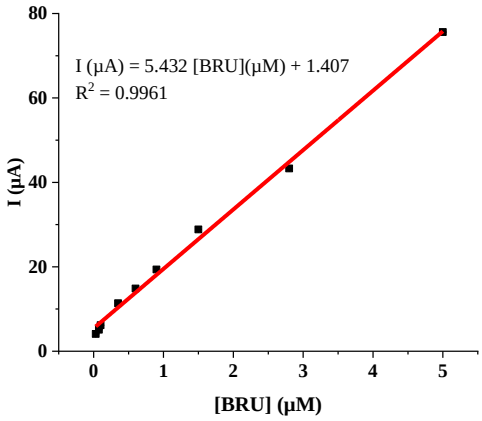

Figure 61. The plot of peak current vs brucine concentrations

Table 11 presents the analytical parameters (detection limit and linear range of the analytical curve) of different modified electrodes and techniques that have been previously reported in the

literature for the detection of brucine. The performance of the present sensor is superior to most of the previous sensors reported in the literature in terms of sensitivity and linear dynamic range (Table 12), which can be attributed to the synergic effect of the sensor. Besides, the modification of the present sensor is very simple and does not require much time.

Table 12. Comparison of the performance of the proposed method with other electrochemical sensors used for the determination of BRU

Electrodes	Method	Linear Range (µM)	LoD (nM)	Reference
[a] Brucine-poPD/SWNTs/GCE	LSV	0.62-12	210	[253]
[b] Poly(alizarin red S)/GCE	SWV	0.01- 1	5	[93]
[c]AMP SAMs/Au	SWV	0.4-200	60	[254]
[d]poly(DL -aspartic acid)/GCE	DPV	0.05-90	3	[244]
[e]MWNTs-modified GCE	SWV	1-100	20	[255]
[f]C-Ni/GCE	DPV	0.047-240	14	[256]
PEDOT/*p*-ABSA/SPCE	SWV	0.03-5	12	This work

[a] *molecularly imprinted poly-o-phenylenediamine Single wall carbon nanotube modified glassy carbon electrodes;* [b] *Poly(alizarin red S) modified glassy carbon electrodes;* [c] *4-amino-2-mercaptopyrimidine self-assembled monolayer gold electrode;* [d] *poly(DL -aspartic acid) modified glassy carbon electrode;* [e] *Multiwall carbon nanotube modified glassy carbon electrodes;* [f] *magnetic carbon-coated nickel nanoparticles modified glassy carbon electrodes*

* The LoQ which 0.042 µM is above the lower calibration curve.

5.4.12. Repeatability, Reproducibility and Stability of the Modified Electrode

The repeatability of the PEDOT/*p*-ABSA/SPCE was evaluated with repeated current responses (n = 20) with the same electrode for 3.0 µM brucine in ABS pH 4 solution and the relative standard deviation (RSD) of the peak current was calculated to be 4.7%, which demonstrates that good reproducibility of the method. The electrode to electrode reproducibility was investigated with four different electrodes for their responses for 3.0 µM brucine .The relative standard deviation of the current responses was found to be 4.1%. From these values it is possible to conclude that using single electrode modification is better throughout the experiment. The stability of the sensor was examined after keeping the electrode in an open air for three weeks

and the peak current retained 96% of its initial value. This indicates that the modified electrode has good stability.

5.4.13. Interference Study

In order to verify the selectivity of the developed electrode PEDOT/*p*-ABSA/SPCE, potentially interfering substances were added to a 3 µM brucine at 1:1, 1:10 and 1:100 concentration ratios using the optimized conditions. The results show that Ca^{2+}, Zn^{2+}, Al^{3+}, K^{+}, Na^{2+}, NO_3^{-}, Cl^{-}, SO_4^{2-}, uric acid, ascorbic acid and tyramine did not significantly interfere with the quantification of brucine at 100-fold excess but Mg^{2+} interfere with the determination of brucine even in 1:1 ratio table 12.

Table 13. Interference effect of some foreign species on the peak current response of brucine at PEDOT/*p*-ABSA/SPCE

Interferent	Concentration (µM)	Response change (%)
Ca^{2+}	30	3.34
Zn^{2+}	30	4.25
Al^{3+}	30	2.13
Na^{+}	30	1.67
K^{+}	30	1.73
NO_3^{-}	30	3.96
Cl^{-},	30	2.78
SO_4^{2-}	30	2.75
Uric Acid	30	3.69
Ascorbic acid	30	4.52
Tyramine	30	2.38

5.4.14. Analytical Application

The proposed methods were applied to the determination of the drug in spiked tap water samples. Blanks were previously analyzed using the modified SPCE, and no amounts of the tested drug were detectable. In order to evaluate the accuracy of the method for the determination of brucine,

recovery measurements were performed by fortifying samples with brucine standard. Table 13 shows the recoveries were from 96.6% to107%. These results demonstrate the reported protocol provides accurate results.

Table 14. Determination of Brucine in water sample using standard (n = 3)

Sample	Added (μM)	Found (μM)	Recovery (%)
Water	0	-	-
	0.3	0.29	96.6
	1	1.03	103
	2	2.14	107

6. Conclusion

In this study different types of chemically modified screen printed carbon electrodes were used for the electrochemical determination of niclosamide, chloramphenicol, nicotine and brucine in biological fluid and pharmaceutical formulations.

Three different methods were used for modifying the bare screen printed carbon electrodes. The first modifying method was simple and fast techniques used to prepare activated-SPCE using alkaline solution. The second modifying method is to prepare *p*-ABSA modified SPCE (*p*-ABSA/SPCE) by the covalent attachment of *p*-ABSA on the activated-SPCE surface by grafting it electrochemically, and the final electrode was prepared by electropolymerization of EDOT in to *p*-ABSA grafted SPCE. Different characterization techniques such as SEM, UV-Vis spectroscopy, FTIR and EIS were used to confirm the modification and study the change in the surface morphological structure of the prepared electrodes. Among all electrodes, PEDOT/*p*-ABSA/SPCE exhibited highest electroactive surface area with better conductivity to $[Fe(CN)_6]^{4-/3-}$ redox probe. The entire prepared electrode demonstrated excellent reproducibility, good stability and selectivity towards possible interfering substances.

A sensor for niclosamide was prepared by electrochemical activation of SPCE using KOH by LSV. The activated-SPCE exhibited an excellent electrocatalytic activity with a significant enhancement of the peak current of niclosamide as compared to the bare electrode. The developed sensor was successfully applied for the determination of niclosamide in vegetable and urine samples. A good recovery result with a high selectivity towards possible coexisting species was obtained.

An activated-SPCE was prepared in a similar way used for the electrochemical determination of chloramphenicol and it showed a better electrocatalytic activity towards the determination of the drug. Compared with earlier reported electrochemical determination method of the drug, low detection limit was obtained at the activated-SPCE. This low detection limit indicates that the electrochemical sensor is suitable for trace analysis. In addition, the method was also successfully applied for the detection of chloramphenicol in pharmaceutical products and milk samples.

The *p*-ABSA modified SPCE was prepared by electrografting using an in-situ generated diazonium salt. The covalently attached *p*-ABSA modified SPCE that has negatively charged surface in alkaline media exhibited an excellent electrochemical activity towards cationic analyte. Nicotine was determined at *p*-ABSA grafted SPCE because the protonated form of it is attracted by negatively charged surface of *p*-ABSA. The *p*-ABSA grafted SPCE shows an enhancement in the peak current and shifts of the peak potential towards the negative in the nicotine oxidation. Besides, the low detection limit, wider linear range, high selectivity and stability of the sensor, make determination of nicotine possible with this electrode. Moreover, the electrode was also utilized successfully for the analysis of nicotine in urine and cigarette samples.

A new and sensitive electrochemical sensor for the determination of brucine is reported based on PEDOT/*p*-ABSA/SPCE. The PEDOT/*p*-ABSA modified SPCE was prepared by two successive steps first the *p*-ABSA was covalently attached using LSV from the in-situ generated diazonium ion then PEDOT was electropolymerized to *p*-ABSA grafted SPCE using a mixture containing EDOT in $LiClO_4$ with SDS by CV. The electrode showed reproducible measurements, better selectivity and good recovery for the determination of brucine in water sample. The electrode prepared has higher conductivity towards $[Fe(CN)_6]^{4-/3-}$ redox probe.

7. References

1. Govindhan, M., Adhikari, B.-R., and Chen, A. (2014) Nanomaterials-based electrochemical detection of chemical contaminants. *RSC Advances, 4*, 63741–63760.

2. Hayat, A., and Marty, J. (2014) Disposable screen printed electrochemical sensors: Tools for environmental monitoring. *Sensors*, *14*, 10432–10453.

3. Aljabali, A. A. A., Berardi, A., and Evans, D. J. (2018). Nature's nanoparticles: Using viruses as nanomedicines and for bioimaging. *Fundamentals of Nanoparticles*, 29–50.

4. Švancara, I., and Kalcher, K. (2014). Introduction to electroanalysis of environmental samples. *Environmental Analysis by Electrochemical Sensors and Biosensors*, 3–21.

5. Hulanicki, A., Glab, S., and Ingman, F. (1991) Chemical sensors: definitions and classification. *Pure and Applied Chemistry*, *63*, 1247-1250.

6. Myasoedov, B. F. (1992) Chemical sensors (review). *Bulletin of the Russian Academy of sciences, 41***,** 383–387.

7. Bi, H., and Han, X. (2019). Chemical sensors for environmental pollutant determination. *Chemical, Gas, and Biosensors for Internet of Things and Related Applications*, 147–160.

8. Cristea, C., Hârceagă, V., and Săndulescu, R. (2014) Electrochemical sensor and biosensors. *Nanostructure Science and Technology*, *1*, 155-165.

9. Power, C. A., and Morri, A. (2013) Electrochemistry. *Electroanalytical Sensor Technology*, 141-178.

10. Kimmel, D. W., Leblanc, G., Meschievitz, M. E., and Cliffel, D. E. (2011) Electrochemical sensors and biosensors. *Analytical Chemistry*, *84*, 685-707.

11. Rahman, M., Kumar, P., Park, D.-S., and Shim, Y.-B. (2008) Electrochemical sensors based on organic conjugated polymers. *Sensors*, *8*, 118-141.

12. Ozkan, S. A., Kauffmann, J.-M., and Zuman, P. (2015) Electrochemical biosensors for drug analysis. *Monographs in Electrochemistry*, 141-186.

13. Farghaly, O. A., Abdel, H., and Abd-Alhakeem, H. (2014) Analytical application using modern electrochemical techniques. *International Journal of Electrochemical Sciences, 9*, 3287-3318.

14. Grieshaber, D., MacKenzie, R., Vörös, J., and Reimhult, E. (2008). Electrochemical biosensors - Sensor principles and architectures. *Sensors, 8*(3), 1400–1458.

15. Chen, A., and Shah, B. (2013) Electrochemical sensing and biosensing based on square wave voltammetry. *Analytical Methods, 5*, 2158-2173.

16. Zhang, X.-E., Men, D., and Wei, H. (2013). Nanowire biosensors. *Encyclopedia of Biophysics*, 1691–1693.

17. Li, G., and Miao, P. (2012) Theoretical background of electrochemical analysis. *Springer Briefs in Molecular Science Electrochemical Analysis of Proteins and Cells*, 5-181.

18. Komorsky-Lovrić, Š. (2009) Working electrodes. *Electroanalytical Methods*, 273-290.

19. Shaowei, C. (2007) Practical electrochemical cells: Handbook of Electrochemistry, *Elsevier*, 33-57.

20. Couto, R., Lima, J., and Quinaz, M. (2016) Recent developments, characteristics and potential applications of screen-printed electrodes in pharmaceutical and biological analysis. *Talanta, 146*, 801-814.

21. Richard, C. A., Philip N. B., and Jacek, L. (2015) Electrochemistry at highly oriented pyrolytic graphite (HOPG): Toward a new perspective. *Advances in Electrochemical Sciences and Engineering Electrochemistry of Carbon Electrodes*, 31-82.

22. Beitollahi, H., Mohammadi, S. Z., Safaei, M., and Tajik, S. (2020) Applications of electrochemical sensors and biosensors based on modified screen-printed electrodes: a review. *Analytical Methods*, *12*, 1547-1560.

23. Mohamed, H. M. (2016) Screen-printed disposable electrodes: Pharmaceutical applications and recent developments. *Trends in Analytical Chemistry, 82*, 1-11.

24. Karolina, P., Jan, D., Marcela, J., Hana, D., Jiří, B. (2011) Utilization of unmodified screen-printed carbon electrode in electroanalysis of organic compounds (an over view). *Sensing in Electroanalysis*, *6*, 129-138.

25. Fletcher, S. (2015) Screen-printed carbon electrodes. *Advances in Electrochemical Sciences and Engineering Electrochemistry of Carbon Electrodes*, 425-444.

26. Ciucu, A. A. (2014) Chemically modified electrodes in biosensing. *Journal of Biosensensor and Bioelectronics, 5*, 2155-6210.

27. Zen, J.-M., Senthil, K. A., and Tsai, D.-M. (2003). Recent updates of chemically modified electrodes in analytical chemistry. *Electroanalysis, 15*(13), 1073–1087.

28. Compton, G. R., and Tanner, .E. L, (2018) How can electrode surface modification benefit electroanalysis? *Electroanalysis*, *30*, 1336-1341.

29. Wanga, J., Pedreroa, M., Sakslund, H., Hammerichb, O., and Pingarronc, J. (1990) Electrochemical activation of screen-printed carbon strips. *Analyst, 121*, 345-350.

30. Lakshmanakumar, M., Sethuraman, S., Rajan, K. S., Krishnan, U. M., and Rayappan, J. B., (2020) Activation of edge plane pyrolytic graphite in screen printed carbon electrodes on OHP sheet, Whatman paper and textile substrates. *Journal of Applied Electrochemistry, 50*, 559-567.

31. Richard, L. M. (2008) Advanced carbon electrode materials for molecular electrochemistry. *Chemical Reviews*, *108*, 2646-2687.

32. Pesquero, N. C., Gongora-Rubio, M. R., and Yamanaka, H. (2013). A novel LTCC electrochemical cell construction and characterization: A detection compartment for portable devices. *The Analyst*, *138*(15), 4298.

33. Kozak, J., Tyszczuk-Rotko, K., Wójciak, M., and Sowa, I. (2021). Electrochemically activated screen-printed carbon sensor modified with anionic surfactant (aSPCE/SDS) for

simultaneous determination of paracetamol, diclofenac and tramadol. *Materials*, *14*(13), 3581.

34. Kumar, A., and Jena, H. M. (2016). Preparation and characterization of high surface area activated carbon from fox nut (*Euryale ferox*) shell by chemical activation with H_3PO_4. *Results in Physics*, *6*, 651–658.
35. Nazemi, Z., Shams, E., and Amini, M. K. (2010) Covalent modification of glassy carbon electrode by nile blue: Preparation, electrochemistry and electrocatalysis. *Electrochimica Acta*, *55*, 7246-7253.
36. Paloma, Y., Susana, C., and José, M.P. (2018) Integrated affinity biosensing platforms on screen-printed electrodes electrografted with diazonium salts. *Sensors*, *18(2)*, 675.
37. Allongue, P., Delamar, M., Desbat, B., Fagebaume, O., Hitmi, R., Pinson, J., and Savéant, J.-M. (1997) Covalent modification of carbon Surfaces by aryl radicals generated from the electrochemical reduction of diazonium salts. *Journal of the American Chemical Society*, *119(1)*, 201–207.
38. Menanteau, T., Dias, M., Levillain, E., Downard, A. J., and Breton, T. (2016) Electrografting via diazonium chemistry: The key role of the aryl substituent in the layer growth mechanism. *The Journal of Physical Chemistry C*, *120(8)*, 4423–4429.
39. Qiu, Z., Yu, J., Yan, P., Wang, Z., Wan, Q., and Yang, N. (2016) Electrochemical grafting of graphene nano platelets with aryl diazonium salts. *ACS Applied Materials & Interfaces*, *8*, 28291-28298.
40. Salehzadeh, H., Nematollahi, D., Khakyzadeh, V., Mokhtari, B., and Henderson, L. C. (2014) General approach for electrochemical functionalization of glassy carbon surface by in situ generation of diazonium ion under acidic and non-acidic condition with a cascade protocol. *Electrochimica Acta*, *139*, 270-280.
41. Awuzie, C. (2017) Conducting polymers. *Materials Today: Proceedings*, *4*, 5721-5726.
42. Inzelt, G. (2012) Conducting polymers a new era in electrochemistry. *Monographs in Electrochemistry*, 149-171.

43. Tsakova, V. (2013) Conductive polymer-based materials for medical electroanalytic applications. Applications of electrochemistry in medicine: Modern aspects of electrochemistry, *Springer*, *56*, 283-342.

44. Ates, M. (2013) A review study of (bio)sensor systems based on conducting polymers. *Materials Science and Engineering: C*, *33*, 1853-1859.

45. Yoon, H. (2013) Current trends in sensors based on conducting polymer nanomaterials. *Nanomaterials*, *3*, 524-549.

46. Gerard, M. (2002) Application of conducting polymers to biosensors. *Biosensors and Bioelectronics*, *17*, 345-359.

47. Le, T.-H., Kim, Y., and Yoon, H. (2017) Electrical and electrochemical properties of conducting polymers. *Polymers*, *9*, 150.

48. Li, Y. (2015) Conducting polymers. *Lecture Notes in Chemistry*, 23-50.

49. Chandrasekhar, P. (1999) Basics of conducting polymers (CPs). *Conducting polymers, Fundamentals and applications*, 3-22.

50. Prathish, K. P., Carvalho, R. C., and Brett, C. M. (2014) Highly sensitive poly(3,4-ethylenedioxythiophene) modified electrodes by electropolymerisation in deep eutectic solvents. *Electrochemistry Communications*, *44*, 8-11.

51. Wang, Y. (2009) Research progress on a novel conductive polymer–poly(3,4-ethylenedioxythiophene) (PEDOT). *Journal of Physics: Conference Series*, *152*, 012023.

52. Yue, Y., and Zhang, B. (2015) Organic Semiconductors, Conductors, and Superconductors. *Lecture Notes in Chemistry*, 1-22.

53. Hui, Y., Bian, C., Xia, S., Tong, J., and Wang, J. (2018) Synthesis and electrochemical sensing application of poly(3,4-ethylenedioxythiophene)-based materials: A review. *Analytica Chimica Acta*, *1022*, 1-19.

54. Mantione, D., Agua, I.D., Sanchez-Sanchez, A., and Mecerreyes, D. (2017) Poly(3,4-ethylenedioxythiophene) (PEDOT) derivatives: innovative conductive polymers for bioelectronics. *Polymers*, *9*(*354)*, 1-21.

55. Lyutov, V., Gruia, V., Efimov, I., Bund, A., and Tsakova, V. (2016). An acoustic impedance study of PEDOT layers obtained in aqueous solution. *Electrochimica Acta*, *190*, 285–293.

56. Seo, K. I., and Chung, I. J. (2000). Reaction analysis of 3,4-ethylenedioxythiophene with potassium persulfate in aqueous solution by using a calorimeter. *Polymer*, *41*(12), 4491–4499.

57. Kwon, G., Kim, S.-H., Kim, D., Lee, K., Jeon, Y., Park, C.-S., and You, J. (2021). Vapor phase polymerization for electronically conductive nanopaper based on bacterial cellulose/poly(3,4-ethylenedioxythiophene). *Carbohydrate Polymers*, *257*, 117658.

58. Jung, F., Thurn, M., Krollik, K., Gao, G. F., Hering, I., Eilebrecht, E., Emara, Y., Weiler, M., Günday-Türeli, N., Türeli, E., Parnham, M. J., and Wacker, M. G. (2021) Predicting the environmental emissions arising from conventional and nanotechnology-related pharmaceutical drug products. *Environmental Research*, *192*, 1-31.

59. Xin, X., Huang, G., and Zhang, B. (2021) Review of aquatic toxicity of pharmaceuticals and personal care products to algae. *Journal of Hazardous Materials*, *410*, 1-18.

60. Dixit, V. A. (2019). A simple model to solve a complex drug toxicity problem. *Toxicology Research*, *8*(2), 157–171.

61. Olender, D., Żwawiak, J., and Zaprutko, L. (2018) Multidirectional efficacy of biologically active nitro compounds included in medicines. *Pharmaceuticals*, *11*(2), 1-22.

62. Nepali, K., Lee, H.-Y., and Liou, J.-P. (2018) Nitro-group-containing drugs. *Journal of Medicinal Chemistry*, *62*(6), 2851–2893.

63. Matsuura, H. N., and Fett-Neto, A. G. (2015) Plant alkaloids: Main features, toxicity, and mechanisms of action. *Plant Toxins*, 1–15.

64. Rezaei, B., and Irannejad, N. (2019). Electrochemical detection techniques in biosensor applications. *Electrochemical Biosensors*, 11–43.

65. Arya, S. K., Singh, S. P., and Malhotra, B. D. (2008) Electrochemical techniques in biosensors. *Handbook of Biosensors and Biochips*, 1-37.

66. Ozkan, S. A., Kauffmann, J.-M., and Zuman, P. (2015) Electroanalytical techniques most frequently used in drug analysis. *Monographs in Electrochemistry*, 45-81.

67. Brownson, D. A. C., and Banks, C. E. (2014) Interpreting electrochemistry. *The Handbook of Graphene Electrochemistry*, 23-77.

68. Elgrishi, N., Rountree, K. J., Mccarthy, B. D., Rountree, E. S., Eisenhart, T. T., and Dempsey, J. L. (2017) A practical beginner's guide to cyclic voltammetry. *Journal of Chemical Education*, *95*, 197-206.

69. Bruno, G. P., and Oliver J. C. (2012) Introduction to electrochemistry. *Power ultrasound in electrochemistry*, 1–21.

70. Zanello, P. (2007) Voltammetric techniques. *Inorganic electrochemistry: Theory, practice and application*, 49-136.

71. Mirceski, V., Skrzypek, S., and Stojanov, L. (2018) Square-wave voltammetry. *ChemTexts*, *4:17*, 1-14.

72. Lovrić, M. (2009) Square-wave voltammetry. *Electroanalytical Methods*, 121–145.

73. Mirceski, V., Gulaboski, R., Lovric, M., Bogeski, I., Kappl, R., and Hoth, M. (2013) Square-wave voltammetry: A review on the recent progress. *Electroanalysis*, *25*, 2411-2422.

74. Suni, I. I. (2008) Impedance methods for electrochemical sensors using nanomaterials. *Trends in Analytical Chemistry*, *27*, 604-611.

75. Macdonald, J. R., and Johnson, W. B. (2005) Fundamentals of impedance spectroscopy. *Impedance Spectroscopy*, 1–26.

76. Randviir, E. P., and Banks, C. E. (2013) Electrochemical impedance spectroscopy: an overview of bioanalytical applications. *Analytical Methods*, *5*, 1098.

77. Chang, B.-Y., and Park, S.-M. (2010) Electrochemical Impedance Spectroscopy. *Annual Review of Analytical Chemistry*, *3*, 207-–229.

78. Muralidharan, V. (1997) Warburg impedance - basics revisited. *Anti-Corrosion Methods and Materials*, *44*, 26-29.

79. Sacco, A. (2017) Electrochemical impedance spectroscopy: Fundamentals and application in dye-sensitized solar cells. *Renewable and Sustainable Energy Reviews*, *79*, 814-829.

80. Theophanides, T. (2012) Introduction to Infrared Spectroscopy. *Infrared Spectroscopy - Materials Science, Engineering and Technology*, 1-11.

81. Stahl, D. C., and Tilotta, D. C. Infrared spectroscopic detection for SPME. *RSC Chromatography Monographs Applications of Solid Phase Microextraction*, 625-637.

82. Griffiths, P., and Haseth, J. A. Fourier Transform Raman Spectrometry. *Fourier Transform Infrared Spectrometry*, 375–393.

83. Mahesar, S. A., Lucarini, M., Durazzo, A., Santini, A., Lampe, A. I., and Kiefer, J. (2019) Application of infrared spectroscopy for functional compounds evaluation in olive oil: A current snapshot. *Journal of Spectroscopy*, 1-11.

84. Zhang, C. (2007) UV-Visible and infrared spectroscopic methods in environmental analysis. *Fundamentals of Environmental Sampling and Analysis*, 190–219.

85. Skoog, D. A., Crouch, S. R., Holler, F. J., and West, D. M. (2014) Instruments for optical spectrometry. *Fundamentals of Analytical Chemistry*, 683-721.

86. Khandpur, R. S. (2015) Colorimetres and Spectrophotometers (Visible – Ultraviolet) *Handbook of analytical instruments*, 32-95.

87. Michler, G. H. (2008) Scanning electron microscopy (SEM). *Electron Microscopy of Polymers*, 87–120.

88. Zhou, W., Apkarian, R., Wang, Z.L., and Joy, D. (2006) Fundamentals of scanning electron microscopy (SEM). *Scanning Microscopy for Nanotechnology*, 1-40.

89. Leonard, D. N., Chandler, G. W., and Seraphin, S. (2012). Scanning electron microscopy. *Characterization of Materials*, 1721-1736.

90. Azad, M., and Avin, A., Scanning electron microscopy (SEM): A review, *Proceedings of 2018 International Conference on Hydraulics and Pneumatics*, 77-85.

91. Boiko, D. A., Pentsak, E. O., Cherepanova, V. A., and Ananikov, V. P. (2020) Electron microscopy dataset for the recognition of nanoscale ordering effects and location of nanoparticles. *Scientific Data 7*, 101. Ni, C. (2013). Scanning electron microscopy (SEM). *Encyclopedia of Tribology*, 2977–2982.

92. Kor, K., and Zarei, K. (2014) Electrochemical determination of chloramphenicol on glassy carbon electrode modified with multi-walled carbon nanotube–cetyltrimethylammonium bromide–poly(diphenylamine). *Journal of Electroanalytical Chemistry*, *733*, 39–46.

93. Hua, Q. T., Ruecha, N., Hiruta, Y., and Citterio, D. (2019). Disposable electrochemical biosensor based on surface-modified screen-printed electrodes for organophosphorus pesticide analysis. *Analytical Methods*, *11*(27), 3439–3445.

94. Mümin, Y., Filik, H., Aydar, S., and Avan, A.A. (2016) Electrochemical determination of brucine in urine with a poly(alizarin red s)-modified glassy carbon electrode. *Analytical Letters*, *49*, 2716-2727.

95. Geto, A., Amare, M., Tessema, M., and Admassie, S. (2012) Voltammetric determination of nicotine at poly(4-amino-3-hydroxynaphthalene sulfonic acid)- modified glassy carbon electrode. *Electroanalysis*, *24*, 659–665.

96. Breton, T., and Bélanger, D. (2008). Modification of carbon electrode with aryl groups having an aliphatic amine by electrochemical reduction of in situ generated diazonium cations. *Langmuir*, *24*(16), 8711–8718.

97. Gruia, V.-T., Ispas, A., Efimov, I., and Bund, A. (2020). Cation exchange behavior during the redox switching of poly (3,4-ethylenedioxythiophene) films. *Journal of Solid State Electrochemistry*, *24(11-12)*, 3231–3244.

98. Bowling, R., Packard, R. T., and McCreery, R. L. (1989). Mechanism of electrochemical activation of carbon electrodes: Role of graphite lattice defects. *Langmuir*, *5*(3), 683–688.

99. Vliet, S.M., Dasgupta, S., Sparks, N.R., Kirkwood, J.S., Vollaro, A., Hur, M., Nieden, N.I.Z., and Volz, D.C. (2019) Maternal-to-zygotic transition as a potential target for niclosamide during early embryogenesis. *Toxicology and Applied Pharmacology, 380,* 1-9.

100. Taylor, D. (2015). The pharmaceutical industry and the future of drug development. *Issues in Environmental Science and Technology*, 1–33.

101. Kartalović, B., Pucarević, M., Marković, Z., Stanković, M., Novakov, N., Pelić, M., and Ćirković, M. (2017) Determination of niclosamide and its metabolites in liver and muscles of common carp (*Cyprinus carpio*) fingerlings. *Acta Scientiae Veterinariae, 45:1490*, 1-6.

102. Yao, Y., Zhang, L., Duan, X., Xu, J., Zhou, W., and Wen, Y. (2014) Differential pulse striping voltammetric determination of molluscicide niclosamide using three different carbon nanomaterials modified electrodes. *Electrochimica Acta, 127*, 86-94.

103. Molero, L., Faundez, M., Valle, M.A.D., Río, R.D., and Armijo, F. (2013) Electrochemistry of methimazole on fluorine-doped tin oxide electrodes and its square-wave voltammetric determination in pharmaceutical formulations. *Electrochimica Acta, 88*, 871-876.

104. Martinez Calatayud, J. (2005). Spectrophotometry pharmaceutical applications. *Encyclopedia of Analytical Science*, 373–383.

105. Daabees, H. G. (2000) Selective differential spectrophotometric methods for determination of niclosamide and drotaverine hydrochloride. *Analytical Letters*, *33*, 639-656.

106. Onur, F., and Tekin, N. (1994) Spectrophotometric determination of niclosamide and thiabendazole in tablets. *Analytical Letters*, *27*, 2291-2301.

107. El-Hay, S. S. A., and Belal, F. F. (2018) Development of a micelle-enhanced high-throughput fluorometric method for determination of niclosamide using a microplate reader. *Luminescence*, *34*, 48-54.

108. Cirkovic, M., Kartalovic, B., Novakov, N., Pelic, M., Djordjevic, V., Radosavljevic, V., and Aleksic, N. (2015) Distribution of niclosamide residues in meat and internal organs of common carp. *Procedia Food Science*, *5*, 54-56.

109. Paghadar, C., and Vadia, N. (2019) Development and validation of stability indicating RP-HPLC and HPTLC for determination of niclosamide in bulk and in synthetic mixture. *Arabian Journal of Chemistry*, *12*, 1803-1814.

110. Doran, G., and Stevens, M.M. (2014) Simultaneous determination of niclosamide and its degradates in water by LC-MS/MS. *Analytical Methods*, *6*, 6871-6877.

111. Jiang, H., Zhang, Y., Chen, X., Lv, J., and Zou, J. (2013) Simultaneous determination of pentachlorophenol, niclosamide and fenpropathrin in fishpond water using an LC-MS/MS method for forensic investigation. *Analytical Methods*, *5*, 111-115.

112. Shen, L., Li, Z., and He, P. (2010) Electrochemical behavior of β2-agonists at graphite nanosheet modified electrodes. *Electrochemistry Communications*, *12*, 876-881.

113. Gowda, J.I., Buddanavar, A.T., and Nandibewoor, S.T. (2015) Fabrication of multiwalled carbon nanotube-surfactant modified sensor for the direct determination of toxic drug 4-aminoantipyrine. *Journal of Pharmaceutical Analysis*, *5*, 231-238.

114. Talib, N., Salam, F., and Sulaiman, Y. (2018) Development of highly sensitive immunosensor for clenbuterol detection by using poly(3,4-ethylenedioxythiophene)/ graphene oxide modified screen-printed carbon electrode. *Sensors*, *18*, 4324.

115. Kassa, A., and Amare, M. (2019) Electrochemical determination of paracetamol, rutin and sulfonamide in pharmaceutical formulations by using glassy carbon electrode – A Review. *Cogent Chemistry*, *5*, 1681607.

116. Huangfu, C., Fu, L., Li, Y., Li, X., Du, H., and Ye, J. (2013) Sensitive stripping determination of cadmium(II) and lead(II) on disposable graphene modified screen-printed electrode. *Electroanalysis*, *25*, 2238-2243.

117. Alagarsamy, P. (2017) A disposable single-use electrochemical sensor for detection of resorcinol based on electrochemically activated screen printed carbon electrode in hair dyes. *International Journal of Electrochemical Science*, 6842-6852.

118. Yang, T.-H., Hung, C.-L., Ke, J.-H., and Zen, J.-M. (2008) An electrochemically preanodized screen-printed carbon electrode for achieving direct electron transfer to glucose oxidase. *Electrochemistry Communications*, *10*, 1094-1097.

119. González-Sánchez, M., Gómez-Monedero, B., Agrisuelas, J., Iniesta, J., and Valero, E. (2019) Electrochemical performance of activated screen printed carbon electrodes for hydrogen peroxide and phenol derivatives sensing. *Journal of Electroanalytical Chemistry*, *839*, 75-82.

120. Pan, D., Rong, S., Zhang, G., Zhang, Y., Zhou, Q., Liu, F., Li, M., Chang, D., and Pan, H. (2015) Amperometric determination of dopamine using activated screen-printed carbon electrodes. *Electrochemistry*, *83*, 725-729.

121. Chapados, C., and Max, J.J.(2004) Infrared spectroscopy of aqueous carboxylic acids: Comparison between different acids and their salts. *Journal of Physical Chemistry A*, *108*, 3324 -3337.

122. Takahama, S., Johnson, A., and Russell, L. M. (2013) Quantification of carboxylic and carbonyl functional groups in organic aerosol infrared absorbance spectra. *Aerosol Science and Technology*, *47*, 310-325.

123. Hosu, I., Constantinescu-Aruxandei, D., Jecu, M.-L., Oancea, F., and Doni, M. B. (2016) Peroxynitrite sensor based on a screen printed carbon electrode modified with a poly(2,6-dihydroxynaphthalene) film. *Sensors*, *16*, 1975.

124. Gamero-Quijano, A., Huerta, F., Salinas-Torres, D., Morallón, E., and Montilla, F. (2013) Electrocatalytic performance of SiO_2-SWCNT nanocomposites prepared by electroassisted deposition. *Electrocatalysis*, *4*, 259-266.

125. Athar, M.M., and Zaib, M. (2015) Electrochemical evaluation of phanerocheaete chrysosporium based carbon paste electrode with potassium ferricyanide redox System. *International Journal of Electrochemical Science*, *10*, 6690-6702.

126. Flowers, P. A., and Strickland, J. C. (2010). Easily constructed microscale spectroelectrochemical cell. *Spectroscopy Letters*, *43*(7-8), 528–533.

127. Zanoni, B.V. M., Rosa, V. L. I., Pesquero, R. C., and Stradiotto, R. N.(1997) Electrochemical behavior of a nitrobenzenesulfonyl derivative of aniline in aqueous solution. *Journal of the Brazilian Chemical Society, 8(3),* 223-227.

128. Elqudaby, H. M., Hendawy, H. A. M., Souaya, E. R., Mohamed, G. G., and Eldin, G. M. G. (2016) Utility of activated glassy carbon and pencil graphite electrodes for voltammetric determination of nalbuphine hydrochloride in pharmaceutical and biological fluids. *International Journal of Electrochemistry*, *2016*, 1-9.

129. Rezaei, B., and Damiri, S. (2008) Voltammetric behavior of multi-walled carbon nanotubes modified electrode-hexacyanoferrate(II) electrocatalyst system as a sensor for determination of captopril. *Sensors and Actuators B: Chemical*, *134*, 324-331.

130. Saglikoglu, G., and Yilmaz, S. (2015) Voltammetric sensitive determination of metronidazole at poly(*p*-aminobenzene sulfonic acid)-modified glassy carbon electrode. *Russian Journal of Electrochemistry*, *51*, 862-866.

131. Ghalkhani, M., and Shahrokhian, S. (2010) Application of carbon nanoparticle/chitosan modified electrode for the square-wave adsorptive anodic striping voltammetric determination of niclosamide. *Electrochemistry Communications*, *12*, 66-69.

132. Mehretie, S., Admassie, S., Tessema, M., and Solomon, T. (2012) Electrochemical study of niclosamide at poly(3,4-ethylenedioxythiophene) modified glassy carbon electrode. *Sensors and Actuators B: Chemical*, *168*, 97-102.

133. Yao, Y., Zhang, L., Duan, X., Xu, Z., Zhou,W., and Wen, Y., (2014) Differential pulse striping voltammetric determination of molluscicide niclosamide using three different carbon nanomaterials modified electrodes. *Electrochimica Acta*, *127*, 86-94.

134. Lopes, C. B., de Assis dos Santos Silva, F., Lima, P. R., de Freitas, J. D., Sousa, J., Kubota, L. T., and Goulart, M. O. (2015). Electrocatalytic activity of activated niclosamide on multi-walled carbon nanotubes glassy carbon electrode toward NADH oxidation. *Journal of Solid State Electrochemistry*, *19*(9), 2819–2829.

135. Yao, Y., Zhang, L., Duan, X., Xu, J., Zhou, W., and Wen, Y. (2014). Differential pulse stripping voltammetric determination of molluscicide niclosamide using three different carbon Nanomaterials modified electrodes. *Electrochimica Acta*, *127*, 86–94.

136. Zhang, Z., Yao, Y., Xu, J., Wen, Y., Zhang, J., and Ding, W. (2017) Nanohybrid sensor based on carboxyl functionalized graphene dispersed palygorskite for voltammetric determination of niclosamide. *Applied Clay Science*, *143*, 57–66.

137. Dede, E., Sağlam, Ö., and Dilgin, Y. (2014). Sensitive voltammetric determination of niclosamide at a disposable pencil graphite electrode. *Electrochimica Acta*, *127*, 20–26.

138. Bansode, W.F, Singh, K. R., and Shukla, P.(2011) Chloramphenicol Toxicity: A Review. *Journal of Medicine and Medical Sciences*, *2(13)*, 1313-1316.

139. Scholar, E. (2007). Chloramphenicol. *xPharm: The Comprehensive Pharmacology Reference*, 1–7.

140. Elliott, S. M., Erickson, M. L., Krall, A. L., and Adams, B. A. (2018). Concentrations of pharmaceuticals and other micropollutants in groundwater downgradient from large on-site wastewater discharges. *Plos one*, *13*(11), 1-17.

141. Roberts, C. M, (2000) Antibiotic toxicity, interactions and resistance development. *Periodontology 2000*, *28*, 280-297.

142. Wu, X., Tian, X., Xu, L., Li, J., Li, X., and Wang, Y. (2017) Determination of aflatoxin M1 and chloramphenicol in milk based on background fluorescence quenching immunochromatographic assay. *BioMed Research International*, *2017*, 1-7.

143. Rejtharová, M., and Rejthar, L. (2009) Determination of chloramphenicol in urine, feed water, milk and honey samples using molecular imprinted polymer clean-up. *Journal of Chromatography A, 1216*, 8246-8253.

144. Kawano, S.-I., Hao, H.-Y., Hashi, Y., and Lin, J.-M. (2015) Analysis of chloramphenicol in honey by on-line pretreatment liquid chromatography–tandem mass spectrometry. *Chinese Chemical Letters*, *26*, 36-38.

145. Barreto, F., Ribeiro, C., Hoff, R. B., and Costa, T. D. (2012) Determination and confirmation of chloramphenicol in honey, fish and prawns by liquid chromatography–tandem mass spectrometry with minimum sample preparation: validation according to 2002/657/EC Directive. *Food Additives & Contaminants: Part A*, *29*, 550-558.

146. Forti, A., Campana, G., Simonella, A., Multari, M., and Scortichini, G. (2005) Determination of chloramphenicol in honey by liquid chromatography–tandem mass spectrometry. *Analytica Chimica Acta*, *529*, 257-263.

147. Aresta, A., Bianchi, D., Calvano, C., and Zambonin, C. (2010) Solid phase microextraction-Liquid chromatography (SPME-LC) determination of chloramphenicol in urine and environmental water samples. *Journal of Pharmaceutical and Biomedical Analysis*, *53*, 440-444.

148. Gantverg, A., Shishani, I., and Hoffman, M. (2003) Determination of chloramphenicol in animal tissues and urine. *Analytica Chimica Acta*, *483*, 125-135.

149. Hormazábal, V., and Yndestad, M. (2001). Simultaneous determination of chloramphenicol and ketoprofen in meat and milk and chloramphenicol in egg, honey, and urine using liquid chromatography-mass spectrometry. *Journal of Liquid Chromatography & Related Technologies*, *24*(16), 2477–2486.

150. Hamoudi, T. A., and Bashir, W. A. (2018) Spectrophotometric Determination of Chloramphenicol in Pharmaceutical Preparations. *Journal of Education and Science*, *27*, 19-35.

151. Monogarova, O.V., Chaplenko, A.A. and Oskolok, K.V. (2020) Identification and quantification of chloramphenicol in medicines by multisensory digital colorimetry. *Moscow University Chemistry Bulletine*, *75***,** 1–7.

152. Xie, Y., Hu, Q., Zhao, M., Cheng, Y., Guo, Y., Qian, H., and Yao, W. (2017) Simultaneous determination of erythromycin, tetracycline, and chloramphenicol residue in raw milk by molecularly imprinted polymer mixed with solid-phase extraction. *Food Analytical Methods*, *11*, 374-381.

153. Blais, B. W., Cunningham, A., and Yamazaki, H. (1994) A novel immunofluorescence capillary electrophoresis assay system for the determination of chloramphenicol in milk. *Food and Agricultural Immunology*, *6*, 409-417.

154. Tsai, H., Hu, H. C., Hsieh, C. C., Lu, Y. H., Chen, C. H., and Fuh, C. B. (2019) Fluorescence studies of the interaction between chloramphenicol and nitrogen-doped graphene quantum dots and determination of chloramphenicol in chicken feed. *Journal of the Chinese Chemical Society*, *67*, 152-159.

155. X.-D., Wu, P.-G., Jiang, W., and Ma, B.-J. (2015) Determination of chloramphenicol, thiamphenicol, and florfenicol in fish muscle by matrix solid-phase dispersion extraction (MSPD) and ultra-high pressure liquid chromatography tandem mass spectrometry. *Food Control*, *52*, 34-38.

156. Zeng, S., Ye, jianzhi, Lin, L., Chen, W., and Yang, C. (2019). Rapid determination of chloramphenicol in tilapia by ultra-high performance liquid chromatography-mass spectrometry. *E3S Web of Conferences*, *78*, 02005.

157. Guy, P.A., Royer, D., Mottier, P., Gremaud, E., Perisset, A., and Stadler, R.H. (2004) Quantitative determination of chloramphenicol in milk powders by isotope dilution liquid chromatography coupled to tandem mass spectrometry. *Journal of Chromatography A*, *1054*, 365-371.

158. Sørensen, L. K., Elbæk, T. H., and Hansen, H. (2003) Determination of chloramphenicol in bovine milk by liquid chromatography/tandem mass spectrometry. *Journal of AOAC International*, *86(4)*, 703-706.

159. Ashton, M. (1989) HPLC determination of chloramphenicol, chloramphenicol monosuccinate and chloramphenicol glucuronide in biological matrices. *Journal of Liquid Chromatography*, *12*, 1719-1732.

160. Li, Y., Liu, X., Zhang, R., ZomPa, D. G., Luo, P., Tang, L., Liu, X., Zhou, Y., and Wen, S. (2018). Analysis of chloramphenicol in drinking water using an evaporation preparative step and isotope dilution liquid chromatography–tandem mass spectrometry. *Acta Chromatographica*, *30*(1), 17–20.

161. Uslu, B., and Ozkan, S. A. (2011). Electroanalytical methods for the determination of pharmaceuticals: A review of recent trends and developments. *Analytical Letters*, *44*(16), 2644–2702.

162. Velický, M., Toth, P. S., Woods, C. R., Novoselov, K. S., and Dryfe, R. A. (2019). Electrochemistry of the basal plane versus edge plane of graphite revisted. *The Journal of Physical Chemistry C*, *123*(18), 11677–11685.

163. Dorledo de Faria, R. A., Messaddeq, Y., Heneine, G. D., and Matencio, T. (2019). Application of screen-printed carbon electrode as an electrochemical transducer in biosensors. *International Journal of Biosensors & Bioelectronics*, *5*(1).

164. Xia, Y.-M., Zhang, W., Li, M.-Y., Xia, M., Zou, L.-J., and Gao, W.-W. (2019) Effective electrochemical determination of chloramphenicol and florfenicol based on graphene/copper phthalocyanine nanocomposites modified glassy carbon electrode. *Journal of The Electrochemical Society*, *166(8)*, B654-B663.

165. S., R., Abraham, P., S., A., and Kumary V., A. (2019). Graphene-palladium composite for the simultaneous electrochemical determination of epinephrine, ascorbic acid and uric acid. *Journal of the Electrochemical Society*, *166*(14).

166. Nady, H., El-Rabiei, M. M., and El-Hafez, G. M. A. (2017). Electrochemical oxidation behavior of some hazardous phenolic compounds in acidic solution. *Egyptian Journal of Petroleum*, *26*(3), 669–678.

167. Desimoni, E., and Brunetti, B. (2014). Data treatment of electrochemical sensors and biosensor. *Environmental analysis by electrochemical sensors and biosensors*, 1137–1151.

168. Giribabu , K., Jang, S.-C., Haldorai, Y. Rethinasabapathy, M., Yeong, O.Y., Rengaraj, A., Han, Y.-H., Cho, W.-S., Roh, C., and Huh, Y.S. (2017) Electrochemical determination of chloramphenicol using a glassy carbon electrode modified with dendrite-like Fe_3O_4 nanoparticles. *Carbon Letters*, *23*, 38–47.

169. Xiao, L., Xu, R., Yuan, Q., and Wang, F. (2017) Highly sensitive electrochemical sensor for chloramphenicol based on MOF derived exfoliated porous carbon. *Talanta*, *167*, 39–43.

170. Sebastian, N., Yu, W.-C., and Balram, D. (2019) Electrochemical detection of an antibiotic drug chloramphenicol based on a graphene oxide/hierarchical zinc oxide nanocomposite. *Inorganic Chemistry Frontiers*, *6*, 82–93.

171. Yuan, Y., Xu, X., Xia, J., Zhang, F., Wang, Z., and Liu, Q. (2019) A hybrid material composed of reduced graphene oxide and porous carbon prepared by carbonization of a zeolitic imidazolate framework (type ZIF-8) for voltammetric determination of chloramphenicol. *Microchimica Acta*, *186*, 191.

172. Sun, T., Pan, H., Mei, Y., Zhang, P., Zeng, D., Liu, X., Rong, S., and Chang, D. (2018) Electrochemical sensor sensitive detection of chloramphenicol based on ionic-liquid-assisted synthesis of de-layered molybdenum disulfide/graphene oxide nanocomposites. *Journal of Applied Electrochemistry*, *49*, 261-270.

173. Yi, W., Li, Z., Dong, C., Li, H.-W., and Li, J. (2019) Electrochemical detection of chloramphenicol using palladium nanoparticles decorated reduced graphene oxide. *Microchemical Journal*, *148*, 774-783.

174. Rajaji, U., Muthumariappan, A., Chen, S.-M., Chen, T.-W., Tseng, T.-W., Wang, K., Qi, D., and Jiang, J. (2019) Facile sonochemical synthesis of porous and hierarchical manganese(III) oxide tiny nanostructures for super sensitive electrocatalytic detection of antibiotic (chloramphenicol) in fresh milk. *Ultrasonics Sonochemistry*, *58*, 104648.

175. Hsia, S.L., Mischel, A.K., and Brody, A.L. (2020) Nicotine. *Absolute Addiction Psychiatry Review*, 105-120. (168)

176. Maessen, G. C., Wijnhoven, A. M., Neijzen, R. L., Paulus, M. C., Heel, D. A., Bomers, B. H., Boersma, L. E., Konya, B., and Heyden, M. A. (2019) Nicotine intoxication by e-cigarette liquids: a study of case reports and pathophysiology. *Clinical Toxicology*, *58(1)*, 1–8.

177. Rahim, S., Rauf, A., Rauf, S., Shah, M. R., and Malik, M. I. (2018) Enhanced electrochemical response of a modified glassy carbon electrode by poly(2-vinlypyridine-b-methyl methacrylate) conjugated gold nanoparticles for detection of nicotine. *RSC Advances, 8*, 35776–35786.

178. Benowitz, N. (2008) Clinical phharmacology of nicotine: Implications for understanding, preventing, and treating tobacco addiction. *Clinical Pharmacology & Therapeutics*, *83*, 531-541.

179. Barreto, G. E., Iarkov, A., and Moran, V. E. (2015). Beneficial effects of nicotine, cotinine and its metabolites as potential agents for parkinson's disease. *Frontiers in Aging Neuroscience*, *6*.

180. Tizabi, Y., Getachew, B., Copeland, R. L., and Aschner, M. (2020) Nicotine and the nicotinic cholinergic system in COVID-19. *The FEBS Journal*, *287*, 3656-3663.

181. Levent, A., Yardim, Y., and Senturk, Z. (2009) Voltammetric behavior of nicotine at pencil graphite electrode and its enhancement determination in the presence of anionic surfactant. *Electrochimica Acta*, *55*, 190-195.

182. Palazzolo, D., Nelson, J. M., and Hudson, Z. (2019) The use of HPLC-PDA in determining nicotine and nicotine-related alkaloids from e-liquids: A comparison of five e-liquid brands purchased locally. *International Journal of Environmental Research and Public Health*, *16*, 3015.

183. Bansal, M., Sharma, M., Bullen, C., and Svirskis, D. (2018) A stability indicating HPLC method to determine actual content and stability of nicotine within electronic cigarette liquids. *International Journal of Environmental Research and Public Health*, *15*, 1737.

184. Pereira, G.R., Marchetti, J.M., and Bentley, M.V.L.B. (2001) A simple and rapid method for nicotine assay by HPLC from cutaneous microdialysis samples. *Analytical Letters*, *34*, 1669-1676.

185. Hossain, A.M., and Salehuddin, S.M. (2013) Analytical determination of nicotine in tobacco leaves by gas chromatography-mass spectrometry. *Arabian Journal of Chemistry*, *6*, 275-278.

186. Pagano, T., Difrancesco, A.G., Smith, S.B., George, J., Wink, G., Rahman, I., and Robinson, R.J. (2015) Determination of nicotine content and delivery in disposable electronic cigarettes available in the United States by gas chromatography-Mass spectrometry. *Nicotine & Tobacco Research*, *18*, 700-707.

187. Lisko, J. G., Stanfill, S. B., Duncan, B. W., and Watson, C. H. (2013). Application of GC-MS/MS for the analysis of tobacco alkaloids in cigarette filler and various tobacco species. *Analytical Chemistry*, *85*(6), 3380–3384.

188. Lu, G.H., and Ralapati, S. (1998) Application of high-performance capillary electrophoresis to the quantitative analysis of nicotine and profiling of other alkaloids in ATF-regulated tobacco products. *Electrophoresis*, *19*, 19–26.

189. Yang, S.S., and Smetena, I. (1995) Evaluation of capillary electrophoresis for the analysis of nicotine and selected minor alkaloids from tobacco. *Chromatographia, 40*, 375-378.

190. Sun, J., Du, H., and You, T. (2011) Determination of nicotine and its metabolite cotinine in urine and cigarette samples by capillary electrophoresis coupled with electrochemiluminescence. *Electrophoresis*, *32*, 2148-2154.

191. Willits, C.O., Swain, M.L., Connelly, J.A., and Brice, B.A. (1950) Spectrophotometric determination of nicotine. *Analytical Chemistry*, *22*, 430-433.

192. Asthana, A., Rastogi, R., Sunita, G., and Gupta, V. K. (2004). A simple spectrophotometric method for the determination of nicotine in environmental samples. *Journal of the Chinese Chemical Society*, *51*(5A), 949–953.

193. Acar, E.T., and Atun, G. (2018) Sensitive determination of nicotine on PolyNiTSPc electrodeposited glassy carbon electrode: Investigation of reaction mechanism. *Electroanalysis*, *30*, 2994–3002.

194. Pinson, J., and Podvorica, F.I. (2020) Surface modification of materials: Electrografting of organic films. *Current Opinion in Electrochemistry*, *24*, 44-48.

195. Ramírez-Chan, D.E., Fragoso-Soriano, R., and González, F.J. (2019) Effect of electrolyte ions on the formation, electroactivity, and rectification properties of films obtained by electrografting. *ChemElectroChem*, *7*, 904-913.

196. Nassef, H.M., Civit, L., Fragoso, A., and O'sullivan, C.K. (2008) Amperometric sensing of ascorbic acid using a disposable screen-printed electrode modified with electrografted o-aminophenol film. *The Analyst*, *133*, 1736.

197. Betelu, S., Vautrin-Ul, C., Ly, J., and Chaussé, A. (2009) Screen-printed electrografted electrode for trace uranium analysis. *Talanta*, *80*, 372-376.

198. Bouden, S., Bellakhal, N., Chaussé, A., and Vautrin-Ul, C. (2014) Performances of carbon-based screen-printed electrodes modified by diazonium salts with various carboxylic functions for trace metal sensors. *Electrochemistry Communications*, *41*, 68-71.

199. Radi, A.-E., Muñoz-Berbel, X., Cortina-Puig, M., and Marty, J.-L. (2009). A third-generation hydrogen peroxide biosensor based on horseradish peroxidase covalently immobilized on electrografted organic film on screen-printed carbon electrode. *Electroanalysis*, *21*(14), 1624–1629.

200. Eissa, S., Tlili, C., L'hocine, L., and Zourob, M. (2012) Electrochemical immunosensor for the milk allergen β-lactoglobulin based on electrografting of organic film on graphene modified screen-printed carbon electrodes. *Biosensors and Bioelectronics*, *38*, 308-313.

201. Suffredini, H.B., Santos, M.C., Souza, D.D., Codognoto, L., Homem-De-Mello, P., Honório, K.M., Silva, A.B.F.D., Machado, S.A.S., and Avaca, L.A. (2005) Electrochemical behavior of nicotine studied by voltammetric techniques at boron-doped diamond electrodes. *Analytical Letters*, *38*, 1587-1599.

202. Li, X., Zhao, H., Shi, L., Zhu, X., Lan, M., Zhang, Q., and Hugh Fan, Z. (2017). Electrochemical sensing of nicotine using screen-printed carbon electrodes modified with nitrogen-doped graphene sheets. *Journal of Electroanalytical Chemistry*, *784*, 77–84.

203. Banks, C.E., Davies, T.J., Wildgoose, G.G., and Compton, R.G. (2005) Electrocatalysis at graphite and carbon nanotube modified electrodes: edge-plane sites and tube ends are the reactive sites. *Chemical Communications*, 829-841.

204. Rocha, D. P., Squissato, A. L., da Silva, S. M., Richter, E. M., and Munoz, R. A. A. (2020). Improved electrochemical detection of metals in biological samples using 3D-

printed electrode: Chemical/electrochemical treatment exposes carbon-black conductive sites. *Electrochimica Acta, 335*, 135688.

205. Hetemi, D., Noël, V., and Pinson, J. (2020). Grafting of diazonium salts on surfaces: Application to biosensors. *Biosensors*, *10(4)*, 1-32.

206. Liu, J., Cheng, L., Liu, B., and Dong, S. (2000) Covalent modification of a glassy carbon surface by 4-aminobenzoic acid and its application in fabrication of a polyoxometalates-consisting monolayer and multilayer films. *Langmuir*, *16*, 7471-7476.

207. Yang, G., Shen, Y., Wang, M., Chen, H., Liu, B., and Dong, S. (2006) Copper hexacyanoferrate multilayer films on glassy carbon electrode modified with 4-aminobenzoic acid in aqueous solution. *Talanta*, *68*, 741-747.

208. Belaabed, B., Lamouri, S., Naar, N., Bourson, P., and Hamady, S. (2010). Polyaniline-doped benzene sulfonic acid/epoxy resin composites: Structural, morphological, thermal and dielectric behaviors. *Polymer Journal*, *42*(7), 546–554.

209. Karimova, N. V., Luo, M., Grassian, V. H., and Gerber, R. B. (2020). Absorption spectra of benzoic acid in water at different pH and in the presence of salts: insights from the integration of experimental data and theoretical cluster models. *Physical Chemistry Chemical Physics*, *22(9)*, 5046–5056.

210. Mersal, G. A., Mostafa, N. Y., and Omar, A.-E. H. (2017). Hydrothermal synthesis and processing of hydrogen titanate nanotubes for nicotine electrochemical sensing. *Materials Research Express*, *4(8)*, 1-10.

211. Ameer, M. A., Fekry, A. M., Azab, S. M., and Shehata, M. (2018). Synthesis of a simply modified electrochemical nicotine sensor based on silver nanoparticles. *Canadian Journal of Chemistry*, *96(8)*, 821–827.

212. Karthika, A., Karuppasamy, P., Selvarajan, S., Suganthi, A., and Rajarajan, M. (2019). Electrochemical sensing of nicotine using $CuWO_4$ decorated reduced graphene oxide immobilized glassy carbon electrode. *Ultrasonics Sonochemistry*, *55*, 196–206.

213. Rosy, and Goyal, R. N. (2014). Estimation of amoxicillin in presence of high concentration of uric acid and other urinary metabolites using an unmodified pyrolytic graphite sensor. *Journal of the Electrochemical Society*, *162*(1), G8-G13.

214. Švorc, Ľ., Stanković, D. M., and Kalcher, K. (2014). Boron-doped diamond electrochemical sensor for sensitive determination of nicotine in tobacco products and anti-smoking pharmaceuticals. *Diamond and Related Materials*, *42*, 1–7.

215. Stočes, M., Švancara, I. (2014) Electrochemical behavior of nicotine at unmodified carbon paste electrode and its determination in a set of refilling liquids for electronic cigarettes, *Electroanalysis*, *26*, 2655-2663.

216. Wu, C.T., Chen, P.Y., Chen, J.G., Suryanarayanan, V., and Ho, K.-C. (2009) Detection of nicotine based on molecularly imprinted TiO_2-modified electrodes, *Analytical Chimica Acta*, *633*, 119-126.

217. Chen, S.-M., Chang, M.-H., and Yang, C.Y. (2016). Amperometric determination of nicotine using a composite of palladium hexacyanoferrate incorporated graphene oxide modified electrode. *International Journal of electrochemical science*, *11*, 2650–2658.

218. Kowalcze, M., and Jakubowska, M. (2020). Voltammetric determination of nicotine in electronic cigarette liquids using a boron-doped diamond electrode (BDDE). *Diamond and Related Materials*, *103*, 107710.

219. Jing, Y., Lin, E., Su, X., Liu, Y., Li, H., Yuan, X., Ping, L., and Fan, Y. (2016). Electrodeposition of Au nanoparticles on poly(diallyldimethylammonium chloride) functionalized reduced graphene oxide sheets for voltammetric determination of nicotine in tobacco products and anti-smoking pharmaceuticals. *RSC Advances*, *6(31)*, 26247–26253.

220. Filik, H., Avan, A., and Aydar, S. (2016). Electrochemical determination of nicotine poly (alizarin red S) modified graphene screen-printed carbon electrode. *Current Nanoscience*, *13(1)*, 92–99.

221. Kassa, H., Geto, A., and Admassie, S. (2013) Voltammetric determination of nicotine in cigarette tobacco at electrochemically activated glassy carbon electrode, *Bulletin of the chemical society of Ethiopia*, *27(3),* 321-328.

222. Xiong, H., Zhao, Y., Liu, P., Zhang, X., and Wang, S. (2009). Electrochemical properties and the determination of nicotine at a multi-walled carbon nanotubes modified glassy carbon electrode. *Microchimica Acta*, *168*, 31–36.

223. Jing, Y., Ning, S., Guan, Y., Cao, M., Li, J., Zhu, L., Zhang, Q., Cheng, C., and Deng, Y. (2020). Electrochemical determination of nicotine in tobacco products based on biosynthesized gold nanoparticles. *Frontiers in Chemistry*, *8*.

224. Li, X., Zhao, H., Shi, L., Zhu, X., Lan, M., Zhang, Q., and Hugh Fan, Z. (2017). Electrochemical sensing of nicotine using screen-printed carbon electrodes modified with nitrogen-doped graphene sheets. *Journal of Electroanalytical Chemistry*, *784*, 77–84.

225. Teske, J., Weller, J.-P., Albrecht, U.-V, and Fieguth, A. (2011) Fatal intoxication due to brucine. *Journal of Analytical Toxicology*, *35*, 248-253. (215)

226. Izawa, K., Amino, Y., Kohmura, M., Ueda, Y., and Kuroda, M. (2010) Human-environment interactions -taste. *Comprehensive Natural Products II*, 631–671.

227. Tang, H.-B., Cai, H.-L., Li, H.-D., Zhang, L.-J., Li, X.-L., Tang, J.-H., and Chen, M.-L. (2013) HPLC–DAD method for comprehensive quality control of semen strychnine. *Pharmaceutical Biology*, *51*, 1378-1383.

228. Xu, X.-L., Shang, Y., and Jiang, J.-G. (2015). Plant species forbidden in health food and their toxic constituents, toxicology and detoxification. *Food and Function*, *7*, 646-664.

229. Guo, J., Meng, H., Li, H.H., and Wang, Q.F. (2016). Determination of strychnine, brucine, strychnine N-oxide, and brucine N-oxide in plasma samples after the oral administration of processed semen strychnine extract by high-performance liquid chromatography with ultrasound-assisted mixed cloud point extraction. *Journal of Separation Science*, *39*(13), 2553–2561.

230. Yin, X. F., Li, Z., Zhang, S. H., Wu, C. X., Wang, C., and Wang, Z. (2011) Determination of strychnine and brucine in traditional Chinese medicine preparations by capillary zone electrophoresis with micelle to solvent stacking. *Chinese Chemical Letters*, *22*, 330-333.

231. Rathi, A., Srivastava, N., Khatoon, S., and Rawat, A. K. S. (2008) TLC determination of strychnine and brucine of *strychnos nux vomica* in ayurveda and homeopathy drugs. *Chromatographia*, *67*, 607-613.

232. Xu, Y., Si, D., and Liu, C. (2009) Determination of strychnine and brucine in rat plasma using liquid chromatography electrospray ionization mass spectrometry. *Journal of Pharmaceutical and Biomedical Analysis*, *49*, 487-491.

233. Liu, Y., Zhu, R., Li, H., Yan, M., and Lei, Y. (2011) Ultra-performance liquid chromatography–tandem mass spectrometric method for the determination of strychnine and brucine in mice plasma. *Journal of Chromatography B*, *879*, 2714-2719.

234. Chen, X., Lai, Y., and Cai, Z. (2012) Simultaneous analysis of strychnine and brucine and their major metabolites by liquid chromatography-electrospray ion trap mass spectrometry. *Journal of Analytical Toxicology*, *36*, 171-176.

235. Marques, E., Gil, F., Proença, P., Monsanto, P., Oliveira, M., Castanheira, A., and Vieira, D. (2000) Analytical method for the determination of strychnine in tissues by gas chromatography/mass spectrometry: Two case reports. *Forensic Science International*, *110*, 145-152.

236. Ostojić, J., Herenda, S., Bešić, Z., Miloš, M., and Galić, B. (2017). Advantages of an electrochemical method compared to the spectrophotometric kinetic study of peroxidase inhibition by boroxine derivative. *Molecules*, *22*(7), 1120.

237. Shetti, N. P., Nayak, D. S., Reddy, K. R., and Aminabhvi, T. M. (2019). Graphene–clay-based hybrid nanostructures for electrochemical sensors and biosensors. *Graphene-based blectrochemical sensors for biomolecules*, 235–274.

238. Can, D., Richard, B., Estefanía, C.-R., Fernández-Abedul, M.T., Merkoçi, A., Manz, A., Urban, G.A., and Güder, F. (2019) Disposable sensors in diagnostics, food, and environmental monitoring. *Advanced Materials*, 1806739.

239. Khorshed, A. A., Khairy, M., Elsafty, S. A., and Banks, C. E. (2019) Disposable screen-printed electrodes modified with uniform iron oxide nanocubes for the simple electrochemical determination of meclizine, an antihistamine drug. *Analytical Methods*, *11*, 282-287.

240. Fletcher, S. (2015). Screen-printed carbon electrodes. *Advances in Electrochemical Sciences and Engineering*, 425–444. (230/23)

241. Yáñez-Sedeñ, P., Campuzano, S., and Pingarrón, J. M. (2018). Integrated affinity biosensing platforms on screen-printed electrodes electrografted with diazonium salts. *Sensors, 18(675),* 1–21.

242. Diarisso, A., Fall, M., and Raouafi, N. (2018) Elaboration of a chemical sensor based on polyaniline and sulfanilic acid diazonium salt for highly sensitive detection nitrite ions in acidified aqueous media. *Environmental Science: Water Research & Technology, 4 (7),* 1024-1034.

243. Blacha, A., Koscielniak, P., Sitarz, M., Szuber, J., and Zak, J. (2012) Pedot brushes electrochemically synthesized on thienyl-modified glassy carbon surfaces. *Electrochimica Acta*, *62*, 441-446.

244. Liu, J., Yang, L., Zhang, K., Li, K., Wu, X., and Ye, B. (2013) The detailed electrochemical character of brucine at a poly(aspartic acid)-modified electrode and its sensitive determination. *Analytical Methods*, *5*, 2712-2719.

245. Zhao, L., Zhao, F., and Zeng, B. (2011) Preparation of surface-imprinted polymer grafted with water-compatible external layer via RAFT precipitation polymerization for highly selective and sensitive electrochemical determination of brucine. *Biosensors and Bioelectronics*, *60*, 71-76.

246. Savalia, R., and Chatterjee, S. (2017) Sensitive detection of brucine an anti-metastatic drug for hepatocellular carcinoma at carbon nanotubes-nafion composite based biosensor. *Biosensors and Bioelectronics*, *98*, 371-377.

247. Gautier, C., López, I., and Breton, T. (2021). A post-functionalization toolbox for diazonium (electro)-grafted surfaces: review of the coupling methods. *Materials Advances*, *2(9)*, 2773-2810.

248. Sakmeche, N., Aeiyach, S., Aaron, J.-J., Jouini, M., Lacroix, J.C., and Lacaze, P.-C. (1999) Improvement of the electrosynthesis and physicochemical properties of poly(3,4-Ethylenedioxythiophene) using a sodium dodecyl sulfate micellar aqueous medium. *Langmuir*, *15*, 2566-2574.(238)

249. Swiderski, G., Kalinowskaa, M., Swisłockaa, R., and Lewandowski, W. (2011) Spectroscopic (FT-IR, FT-Raman and ^{1}H and ^{13}C NMR) and theoretical in MP2/6-311++G(d,p) and B3LYP/6-311++G(d,p) levels study of benzenesulfonic acid and alkali metal benzenesulfonates. *Spectrochimica Acta Part A*, *100*, 41-50.

250. Zhao, Q., Jamal, R., Zhang, L., Wang, M., and Abdiryim, T. (2014). The structure and properties of PEDOT synthesized by template-free solution method. *Nanoscale Research Letters*, *9(1)*, 557-557.

251. Levin, O. V., Karushev, M. P., Timonov, A. M., Alekseeva, E. V., Zhang, S., and Malev, V. V. (2013). Charge transfer processes on electrodes modified by polymer films of metal complexes with schiff bases. *Electrochimica Acta*, *109*, 153–161.

252. Levin, O. V., Karushev, M. P., Timonov, A. M., Alekseeva, E. V., Zhang, S., and Malev, V. V. (2013). Charge transfer processes onelectrodes modified by polymer films of metal complexes with schiff bases. *Electrochimica Acta*, *109*, 153–161.

253. Liu, P., Zhang, X., Xu, W., Guo, C., and Wang, S. (2012) Electrochemical sensor for the determination of brucine in human serum based on molecularly imprinted poly-o-phenylenediamine/SWNTs composite film. *Sensors and Actuators B: Chemical*, *163*, 84-89.

254. Zhang, X.-H., Wang, S.-F., and Sun, N.-J. (2004) Direct determination of brucine by square wave voltammetry on 4-amino-2-mercaptopyrimidine self-assembled monolayer gold electrode. *Bioelectrochemistry*, *65*, 41-46.

255. Wang, S., and Xu, Q. (2005) Square wave voltammetry determination of brucine at multiwall carbon nanotube-modified glassy carbon electrodes. *Analytical Letters, 38*, 657-671.

256. Wang, S., Xie, F., and Hu, R. (2006) Electrochemical study of brucine on an electrode modified with magnetic carbon-coated nickel nanoparticles. *Analytical and Bioanalytical Chemistry*, *387*, 933-939.

8. List of Publications

1. **Tesfu Hailu**, Yaw-Kuen Li, Merid Tessema; Electrochemical Determination of Chloramphenicol in Milk and Eye-drop Using Easily Activated Screen Printed Carbon Electrode, *Iranian Journal of Analytical Chemistry*, **2021,** 8(1), 93-101.
2. **Tesfu Hailu**, Yaw-Kuen Li, Merid Tessema; Simple, Fast and Cheap Electrochemical Detection of Niclosamide Using Activated Screen Printed Carbon Electrode, *International Journal of Scientific Research in Chemical Sciences*, **2021,** 8(2), 26-35.
3. **Tesfu Hailu**, Yaw-Kuen Li, Merid Tessema; Electrochemical Determination of Nicotine in Cigarette, and Urine Using para-Aminobenzene Sulfonic Acid Grafted Screen Printed Carbon Electrode, **Submitted manuscript**
4. **Tesfu Hailu**, Yaw-Kuen Li, Merid Tessema; Electrochemical Determination of Brucine Using Highly Conductive PEDOT Film Covered *p*-ABSA grafted SPCE, **Ready for Submission**